ABSTRACT

Title of Document:	THE IMPACT OF THERMAL IMAGING CAMERA DISPLAY QUALITY ON FIRE FIGHTER TASK PERFORMANCE
	Justin Lawrence Rowe, Master of Science, 2008
Directed By:	Associate Professor Dr. Frederick W. Mowrer, Department of Fire Protection Engineering

Thermal imaging cameras (TIC) have become a vital fire fighting tool for the first responder community but there are currently no standardized quality control regulations. The purpose of the study was to understand the impact of TIC display image quality on a fire fighter's ability to perform a hazard recognition task. Test subjects were asked to identify a fire hazard by observing infrared images. The image matrix considered the interactions of several image characteristics including contrast, brightness, spatial resolution, and noise. The results were used to create a model function to predict the effect of image quality on user performance. This model was recommended to be incorporated in image quality test methods in development at the National Institute of Standards and Technology. These recommendations will also be provided to the National Fire Protection Association for use in an upcoming standard on fire fighting TIC.

THE IMPACT OF THERMAL IMAGING CAMERA DISPLAY QUALITY ON
FIRE FIGHTER TASK PERFORMANCE.

By

Justin Lawrence Rowe

Thesis submitted to the Faculty of the Graduate School of the
University of Maryland, College Park, in partial fulfillment
of the requirements for the degree of
Master of Science
2008

Advisory Committee:
Associate Professor Dr. Frederick W. Mowrer, Chair
Professor Dr. James A. Milke
Assistant Professor Dr. Peter B. Sunderland

Acknowledgements

Table of Contents

List of Tables

List of Figures

Chapter 1: TIC Overview

1.1 Introduction to TIC for First Responders

Thermal imaging cameras (TIC)[1] are becoming an integral tool to the first responder community, particularly firefighters, law enforcement officers, and hazardous material personnel, by enhancing visibility in operating conditions such as harsh structural fire scenarios and in situations where the only indication of a material is surface temperature and/or differences in emissivity (e.g. hazardous gas or liquid materials). In particular, fire fighters applying TIC for search and rescue, structural navigation, hose stream directing, locating hot spots during overhaul, and fire size-up operations among others. TIC are improving first responder's ability to effectively perform their jobs by decreasing response time in hazardous situations and thus improving safety and reducing overall fire losses.

Currently, there are no standards or performance regulations TIC for fire fighting, as there are for other first responder equipment such as clothing, helmets, SCBA apparatus, and PASS devices. Adoption of standardized TIC performance testing methods will benefit first responders by providing objective test results to compare the different camera models and technologies for deciding the most cost effective purchase while still providing adequate performance. Standardized test methods also provide a way for TIC manufacturers to evaluate existing cameras and drive the development of newer technologies to create better fire fighting tools.

---

[1] TIC is used as an acronym for both the singular and plural forms of thermal imaging camera(s), whichever form is applicable to the context of the sentence.

1. 2 TIC Background

1.2.1 Basic Function

Handheld TIC take advantage of infrared (IR) radiative heat transfer by focusing the net

radiation from an object whether emitted or reflected onto the thermal detector array

inducing an increase in material temperature which triggers a proportional signal output.

Radiation is transmitted through the atmosphere in the form of electromagnetic waves at

specific frequencies. The intensity of the radiation at each frequency is a function of the

temperature and surface properties. As the temperature of an object increases, the

wavelength of peak intensity decreases as described by Planck's formula in Equation1-1

(Theory of Thermography 2007).

$$W_{\lambda b} = \frac{2\pi hc^2}{\lambda^5 \left(e^{hc/\lambda kT} - 1 \right)}$$
1-1

where $W_{\lambda b}$ is the blackbody spectral radiant emittance at wavelength λ, c is 3 x 10^8 m/s

(speed of light), h is 6.6 x 10^{-34}, k is 1.4 x 10^{-23} (Boltzmann's constant), T is the absolute

temperature (K) of a blackbody, and λ is the wavelength (μm).

By integrating Planck's formula in Equation 1-1 over all frequencies, the total radiant

emittance of a blackbody becomes the Stefan-Boltzmann Law shown in Equation1-2.

$$W_b = \sigma T^4$$
1-2

Real objects almost never act as a perfect blackbody over an extended range of

wavelengths and therefore the emissivity of a surface is used to describe the ratio of the

spectral radiant power from the object to that from a blackbody at the same temperature

and wavelength (Theory of Thermography 2007). The radiant emittance of real world

objects is shown in the modified Stefan-Boltzmann Law shown in Equation 1-3 to account for the emissivity of a surface.

$$W = \varepsilon \sigma T^4 \qquad \qquad 1\text{-}3$$

where ε is the emissivity.

TIC detect radiation in the IR spectral band of the electromagnetic spectrum because there is a high transmittance of IR waves through fire related atmospheres. TIC designed for the fire service are tailored to focus on the 8-14 µm wavelengths because within this range, IR waves are less susceptible to diffraction or scattering from water vapor or particulates in the atmosphere as shown in Figure 1- 1.
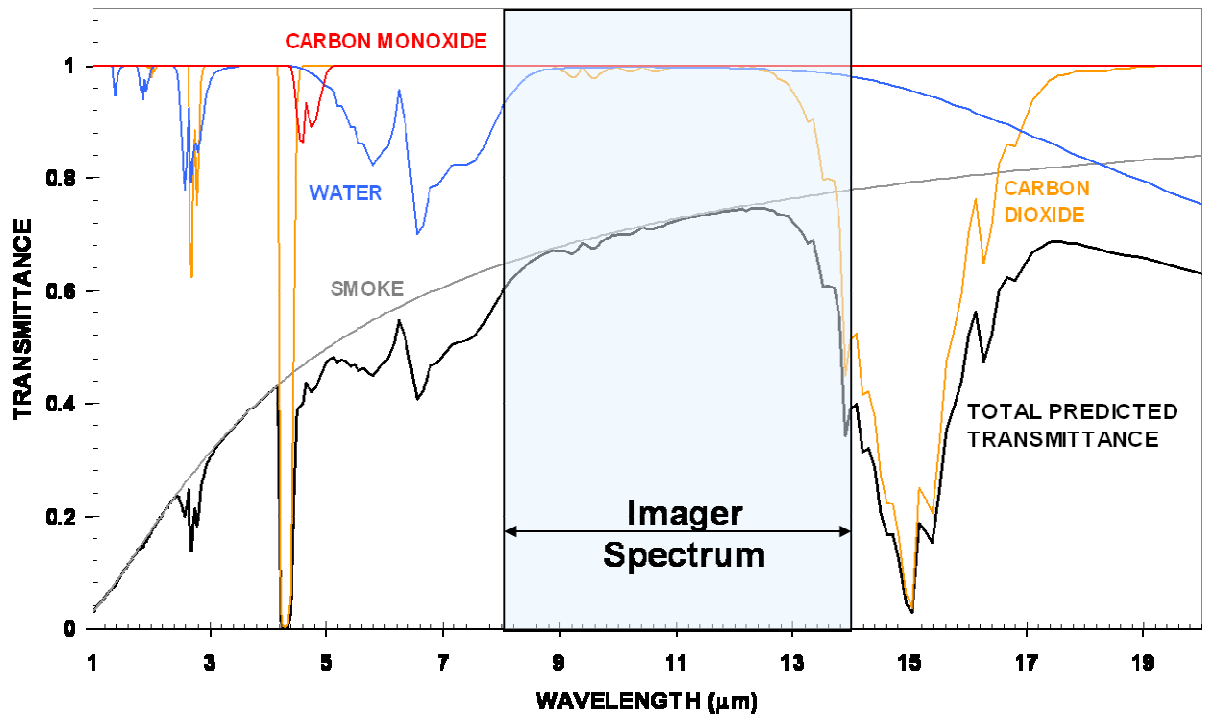
Figure 1- 1 Transmissivity of common combustion products as a function of wavelength for a one meter pathlength (Grosshandler 1993)

IR waves transmit extremely well through carbon monoxide, carbon dioxide and water and relatively well through smoke. The transmittance at the near visible band, less than 1 μm, is almost completely blocked by smoke which illustrates the ineffectiveness of the human eye and other visual optical systems in smoky combustion environments and emphasizes the need for TIC in the fire service.

Incident radiative transfer onto the detector array is not the only important form of heat transfer. The radiative heat lost from the detector pixels to the surroundings acts to cool the detector pixel, increasing the response time of the TIC. Heat loss also occurs through conduction. Each detector pixel is attached to a substrate by supporting legs. Heat is lost through conduction from the detector pixel down the supporting leg to the substrate. In some detector designs such as the hybrid layout discussed in more detail in the following sections, conduction also occurs when heat transfers from one detector pixel to a neighboring pixel. This process, known as thermal spreading, is critical to avoid when designing thermal arrays because it affects the resolution [Kruse 1997].

1.2.1.1 Infrared Optics

TIC for the fire service are designed with IR optics to focus the radiation onto an array of thermal detectors. The IR optics are similar to that of any optical system except for the materials used for the lens and optic focal lengths. A standard transparent lens transmits electromagnetic waves in the visual spectrum but not at the IR wavelengths so TIC use materials that transmit well in the 8-14 μm wavelengths, such as Zinc Selenide and Germanium. The optics of TIC also have a wide field of view (FOV) and a far focusing

distance. Fire fighters need the ability to see a wide FOV to survey a scene more rapidly. Typically, TIC for the fire service are designed with a FOV between 40-60º. The focusing distance ranges from 1 m out to infinity with no manual focusing options. The FOV and minimum 1 m focal length makes the TIC hard to perform testing in a bench scale lab because large targets and ample space are required to fill the FOV of the camera's with thermal targets and measuring equipment. Finally, the optics are designed to avoid narcissus and glare. Narcissus occurs when there is a reflection in the optic components in which the detectors *see* themselves (Holst 1998). Coatings are applied to the optics to avoid internal reflections.

1.2.1.2 Detector Designs

The development of uncooled IR imaging arrays in the 1980's offered a substantial advantage over cooled IR detectors in that they did not have be cryogenically cooled. TIC could therefore be produced at low cost and designed to be lightweight to be used for countless applications for the military and civilian sectors, including fire fighting. Handheld TIC utilize IR arrays that operate using thermal detectors because they do not require cooling systems and large power supplies (Dinaburg 2007).

Thermal IR detectors utilize a sensitive material that has some measureable property that changes dramatically with temperature. The most common detection mechanisms used for handheld TIC are the resistive microbolometer and pyroelectric detectors (Holst 2000). The microbolometer detectors utilize a material with a temperature-dependent resistance to measure a change in resistance of each detector pixel due to the absorption of the IR radiation (Kruse 1997). The two most common materials used in

5

microbolometers are vanadium oxide (VOx) and amorphous silicon. Both of these materials have high temperature coefficients of resistance (TCR), one of the most important properties in determining the voltage response of a detector because the TCR is directly proportional to the voltage response (Muralt 2001).

Pyroelectric detectors utilize the ability of certain materials to change in polarization due to a change in temperature or otherwise known as the pyroelectric effect. When a material is heated (or cooled) positive and negative charges migrate to opposite faces of the sensor creating polarization. The change in surface charge is measured during the transient temperature change resulting from the incoming radiation. Because pyroelectric detectors measure transient temperature changes, they require a chopper to continuously reference the temperature of each pixel to ambient. The detectors are usually made from materials that have very low thermal mass so the temperature change is rapid (Tsai and Young 2003). The most common material used in TIC is a ferroelectric material called barium strontium titanate (BST). Ferroelectric materials offer an additional advantage because with the application of an external electric field, the pyroelectric coefficient is increased. The pyroelectric coefficient is directly proportional to the change in charge of the material. This phenomenon is known as the field-enhanced pyroelectric effect (Muralt 2001).

In either type of detector design, the detector array is attached to a readout integration circuit (ROIC) which functions to read in and format the detector's signal output. Due to the sensitivity of the thermal detector's response to small temperature changes and the heat transfer physics, thermal isolation is critical to the quality of the TIC. Because of the

importance of thermal isolation the primary methods for attaching the thermal detector array to the ROIC will be discussed.

The support structure provides three main functions; mechanical support, and a thermal and electrically conducting path. One of the most important aspects of the design of the supporting structure is to minimize the thermal conductance of the supporting legs that are attached to the detector pixels to increase response time. The detector pixels must also be thermally isolated to avoid thermal spreading. The two main approaches for providing the support are the monolithic and hybrid design. In the hybrid approach the detector pixel layer is separated from a silicon substrate layer which typically incorporates the ROIC. The two layers are joined by a bump bond at two supporting legs which provides the mechanical support as well as the high electrical conduction and low thermal conduction. The monolithic approach is to have the sensor and electronic elements on the same layer.

There are advantages and disadvantages to both types of support structures. The monolithic design sacrifices image quality for a relatively lower cost to manufacture than the hybrid design. Because the detector pixel, supporting structure, and read-out electronics are on the same layer, the detector pixels must be placed farther away from each other. The layout is beneficial to minimize thermal spreading because the substrate acts as a heat sink. However, this also produces a poor fill factor. The two layer hybrid design typically use a laser scribed technique to separate the detector pixels creating a better fill factor and image quality but at a greater cost to manufacturer.

1.2.2 Applications for Fire Service

A workshop entitled "Thermal Imaging Research Needs for First Responders" was hosted by Amon et al. to gain input from the first responder community as well as TIC manufacturers and other stakeholders on how TIC are being used in the field. The knowledge gained from this workshop and other TIC manufacturing literature on TIC applications is listed in Table 1- 1 [Amon 2005].

Table 1- 1 TIC Applications

First Responder Applications for Thermal Imaging Cameras	
Application	**Description**
Search and Rescue	Locate heat sources, such as victims or fallen fire fighters.
Hazard Assessment	Locate and assess the severity of a fire. A TIC can be used to find hot spots and a potential threat to adjoining structures.
Building Assessment	Analyze the integrity of a structure by identifying hazards such as holes in the floor, hanging wires, and the failure of load bearing structural elements.
Navigation	Doors, windows, and other escape points can be located for quick egress. TIC can distinguish furniture and other objects that could block a path.
Fire Attack Directing hose streams	Identify potential flashover or back draft conditions. Find ventilation locations, direct hose streams, analyze the effectiveness of the hose stream and access the severity of the upper layer temperature.
Over-haul	Quickly scan for remaining hot spots and embers that lead to rekindling. Over-haul can be carried out more rapidly and with minimal damage to the structure.
Wild land Fires	TIC can be used on the ground or in the air to locate hot spots in vegetation and root systems. Useful for determining fire fighting strategies and identifying animals, people, and nearby buildings that may be in danger.
Incident Control/Command	Fire fighter activity can be monitored by sending images from TIC back to the incident commander. The images can be used to account for fire fighters, as well as make decisions as to the tactics used to extinguish the fire. This application can be particularly helpful in high-rise building fires where fire fighter coordination is more difficult.
Hazardous Materials	Help identify the level of liquid in hazardous material

	containers and track the movement of hazardous material after spillages. Fire fighters can make more accurate decisions as to where barriers may need to be positioned, how much hazardous material has been spilled, and the potential risks to the nearby area.
Post-incident Investigation	Identify the source of a fire and how the fire spreads. A TIC can capture images of a scene while a fire is occurring. The images can later be used as evidence for understanding and verifying the progress of the fire situation.

The applications listed in Table 1- 1 demonstrate the exposure of TIC to a variety of thermal targets and operating temperatures. As more fire departments are equipped with TIC and the technologies become more advance, additional ways to utilize a TIC will be discovered. The knowledge gained from the BFRL workshop was incorporated into the design of the images used in this study to represent a typical TIC operating environment.

1.3 Development of NFPA 1801

1.3.1 NIST Involvement

The National Fire Protection Association (NFPA) Technical Committee of Electronic Safety Equipment is developing a standard to govern the design, performance, testing, and certification requirements for TIC used by first responders. The standard is currently being created by NIST in collaboration with committees formed by users, manufacturers, technical experts, and the public. NIST provides unbiased science-based research and experience in fire testing including the evaluation of fire fighter personal protective equipment. The suggestions made about the content of the standard provided by NIST will be taken into consideration by the NFPA for use in NFPA 1801, *Standard on Thermal Imagers for the Fire Service*.

The research at NIST, headed by Dr. Francine Amon in the Fire Fighting Technology Group in BFRL, is focused on TIC overall system performance requirements, specifically the output of the display screens. The requirements specified in NFPA 1801, Section 7.1, *Thermal Imager Performance Requirements*, include a range of performance testing on ingress protection, electromagnetic emissions and immunity, resistance to vibration, impact-acceleration resistance, corrosion resistance, viewing surface abrasion resistance, resistance to heat and flame, product label durability, cable pullout test, and most importantly, display image quality.

The performance test methods designed by NIST treat the TIC as a "black box" to focus on the entire system as the TIC would be used by the fire service and not the various components separately. The display quality is of upmost importance because it is the primary mechanism for relaying information to the user. The display image of a TIC is influenced by a large number of factors due to the number of components involved in converting IR radiation into a formidable image on the display screen. There are numerous component packages available on commercial TIC which includes a variety of detector technologies, signal processing algorithms, gain settings, optics, electronics, and displays. However, there are very few manual adjustments to the display image that can be performed by the user. Typically, there is only an on/off switch and maybe one more specialty button depending on the brand of TIC. All adjustments to focus, gain, sensitivity and other image enhancements are all automatically done by the interior functions of the TIC. Each manufacturer has complex (and secret) algorithms to post process the signal output of the detector array to the image formed on the display screen.

Every manufacturer has different techniques to improve the quality of the image and testing each subsystem of every camera would be cumbersome and unnecessary.

Section 7.2, *Imaging Performance Requirements*, of NFPA 1801 applies specifically to the quality of the display image. The test methods designed by NIST measure various aspects of the display image quality including contrast, overall brightness, spatial resolution, and image nonuniformity (noise). For a more detailed description of display measurement techniques refer to the Video Electronics Standards Association (VESA) Flat Panel Display Measurements Standard [VESA 2001]

1.3.2 Bench-Scale Test Methods Developed by NIST

The methods described in NFPA 1801, Section 8.1.6, *Spatial Resolution Procedure*, incorporate measurements of image contrast, overall brightness, and spatial resolution. The procedures require the TIC under testing to be centered one meter (the minimum focusing distance of a TIC) from a spatial resolution target, shown in Figure 1- 2. The TIC is required to have a line of sight perpendicular to the target.
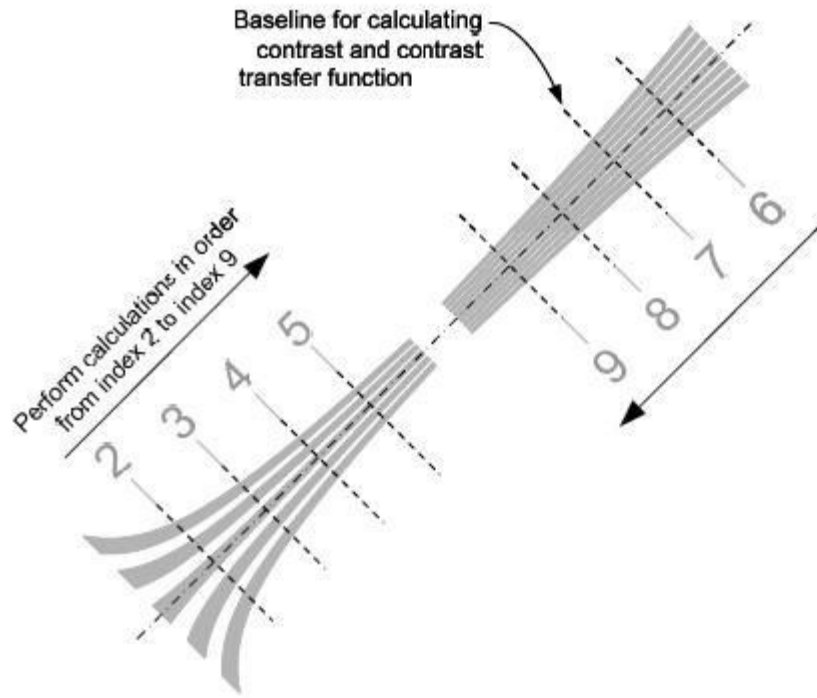
Figure 1- 2 Spatial Resolution Source Target, NFPA 1801-F09-ROP

The target design was an adaptation from a portion of the ISO 12233 test chart (ISO

12233). The target and a black backdrop are required to fill the TIC field of view (FOV).

The spatial resolution target is set to 28 C $\pm$ 0.5 C. A black shroud is placed over the

view path of the camera to block out any glare incident on display.

A calibrated luminance meter is positioned as close as possible to the TIC to capture the

FOV of the display screen. A minimum of 100 uncompressed images at a minimum 16-

bit depth are captured with the luminance meter.

Using the captured images, contrast, brightness, and spatial resolution calculations are performed at each baseline index (shown in Figure 1- 2) which corresponds to a specific spatial frequency. The contrast is calculated according to NFPA 1801 Section 8.1.6.11 at each indexed baseline using the standard deviation of an equal amount of pixel intensities from the heated target and backdrop. Brightness is calculated in NFPA 1801 according to section 8.1.5.13a as the mean pixel intensity over the same region. The spatial resolution is measured using the Modulation Transfer Function (MTF) which is calculated using a Contrast Threshold Function (CTF) as described in the NFPA 1801 Section 8.1.6.10. The spatial resolution target utilizes essentially a square bar target to represent spatial frequencies instead of a sinusoidal target because it is easier to manufacturer. The CTF is defined in Equation 1-4 as

$$CTF = \frac{I_{max} - I_{min}}{I_{max} + I_{min}} \qquad \text{1-4}$$

where I is the pixel intensity at a point of interest. The CTF is defined by the ratio of the difference between the maximum and minimum pixel intensities. The MTF and CTF can be related mathematically through the square and sine wave relationship.

$$MTF = \frac{\pi}{4} CTF \qquad \text{1-5}$$

A more detailed description of the MTF is described in Chapter 2 of this work.

The nonuniformity is calculated using the procedure described in Section 8.1.5 of NFPA 1801. The TIC is positioned near the nonuniformity target to fill the entire FOV of the TIC. The nonuniformity target is a blackbody required to stabilize at a temperature within $\pm$ 0.02 C at temperatures below 160 C and 0.05 at temperature up to 260 C. The luminance meter is positioned again so that the TIC display fills the FOV and placed

13

under a black shroud to eliminate glare from surrounding light sources. A minimum of 100 uncompressed images are taken with the nonuniformity target at set point temperatures of 1 C, 30 C, 100 C, 160 C, and 260 C. The standard deviation and mean pixel intensity are calculating according NFPA 1801 Equation 8.1.5.13a and 8.1.5.13b. The nonuniformity is defined as the ratio of the standard deviation of the pixel intensities over the mean.

$$Nonuniformity = \frac{\sigma}{\mu} \qquad \text{1-6}$$

The maximum nonuniformity at any of the set point temperatures is deemed the nonuniformity of the imaging system as a conservative estimate.

The calculations for contrast, brightness, spatial resolution, at each baseline index and the maximum nonuniformity are then used as the image quality input parameters for the logistic regression model created by the work done in this study to predict if the TIC meets standard requirements for image quality. A complete detailed description of the model is outlined in Chapter 4 of this work.

1. 4 Project Goals

The goal of this study was to determine the effect TIC display image quality has a fire fighter's ability to perform a task typically accomplished using a TIC and complement the image quality performance test methods established at NIST by creating a model to predict the probability of identifying a fire hazard based on the following image quality parameters: contrast, brightness, spatial resolution, and nonuniformity (noise).

To accomplish the goals of this study, a perception experiment was conducted where test subjects, who were a representative group of fire fighters that regularly use TIC, were given a task to identify a fire hazard by observing IR images. Although there are a wide range of tasks a fire fighter could potentially encounter and the type of images that are displayed on the TIC could vary dramatically, hazard recognition is among the most important TIC application and therefore was the focus of this study.

Chapter 2: Image Processing

2. 1 Introduction to Image Processing

Image processing includes a collection of techniques used to manipulate the visual appearance of an image. The fundamentals needed to execute these tools to enhance or degrade the quality of images are the focus of this chapter. Image processing can be accomplished in both the spatial and frequency domains. Although many of the processes are equivalent, processing in both domains will be discussed because there is sometimes value for choosing one over the other. Color will not be included because most TIC display images are composed of only grayscale values. In addition, color is not accounted for in the TIC performance test methods at NIST.

2.2 Histograms

Image histograms are valuable for image processing because they display the distribution of graylevels within an image. Histograms are essentially bar charts that show the number of pixels of an image that have a particular pixel intensity or brightness value. For an 8-bit image, there are 256 different possible pixel values that are usually displayed on the x-axis of a histogram. Each pixel of an image is then placed in one of the 256 categories also known as bins. Peaks in a histogram indicate common pixel intensities within the image while valleys show less common values. Histograms are useful for enhancing the brightness and contrast of an image through a technique called histogram equalization as discussed in Section 2.4.1.2 Histogram Equalization.

2. 3 Image Quality Characteristics

Contrast and brightness are closely related concepts because by definition they are
associated directly to the graylevel intensity value of the pixels of an image and have
common image processing techniques. It is easiest to explain these concepts visually
with images and their corresponding histograms as well as quantitatively in their
definition. For this discussion, consider an 8-bit infrared image of an office work station
shown in Figure 2- 1.

Figure 2- 1 IR image of an office work station
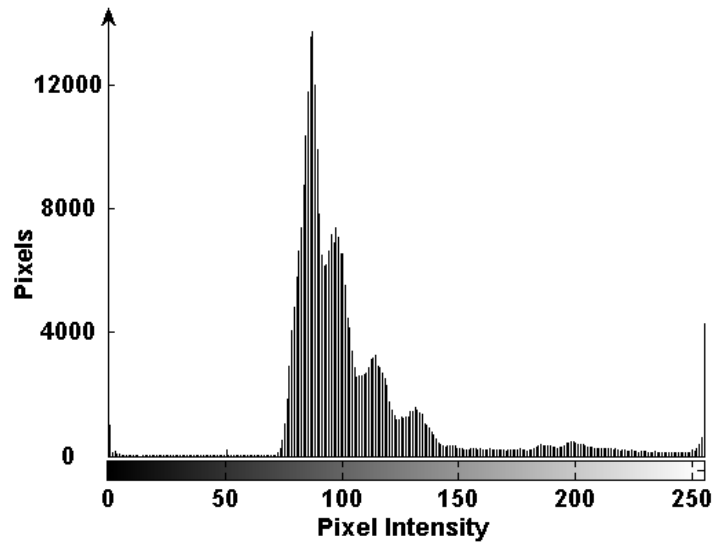
Figure 2- 2 Image histogram of Figure 2- 1

The histogram shown in Figure 2- 2 illustrates the image utilizes the full range of

graylevels of an 8-bit image from 0 to 255.

2.3.1 Contrast

The contrast of an image is the range of graylevels used to represent the scene. There are

a possible 256 shades of gray for an 8-bit imaging system. Typically, the more

graylevels an imaging system uses the higher the contrast. For a TIC, insufficient

contrast within a display image reduces the details of objects that have very similar

emitted or reflected IR radiation. In a low contrast image, more pixels in the display

image are using the same graylevel to depict different levels of radiation in a

corresponding object. Consider Figure 2- 3 and the corresponding graylevel histogram in

Figure 2- 4.

18

Figure 2- 3 Image with low contrast
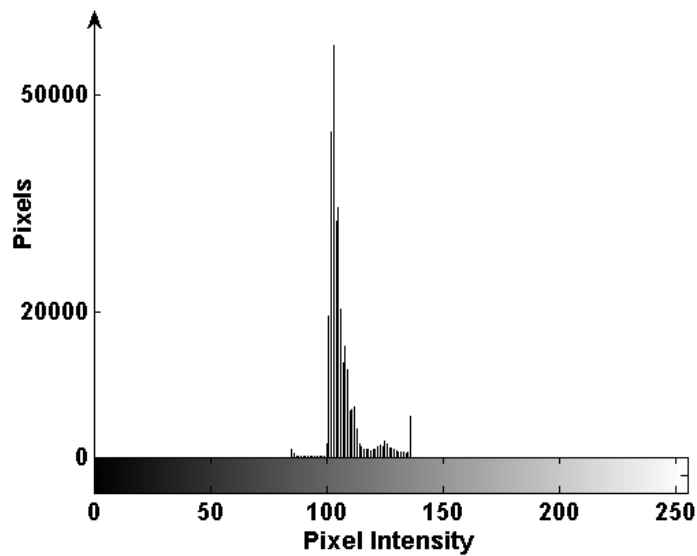
Figure 2- 4 Image histogram of Figure 2- 3.

Figure 2- 3 has a lower contrast than Figure 2- 1 because fewer graylevels are being

utilized. The total number of pixels has been spread over a smaller range of graylevels.

As a result, some of the details such as the power cords and other small items on the desk

that are visible in Figure 2- 1, are indistinguishable in Figure 2- 3.

An image with perfect contrast is subjective and dependent on the scene the imaging system is representing. There is no one value used to define the perfect contrast for an image but there are several methods of quantifying the overall contrast of an image. One method is to measure the average variation in graylevels otherwise known as the standard deviation of graylevels [Weeks 1996]. For an N x M image, the contrast is

$$contrast = \sqrt{\frac{1}{NM}\sum_{y=0}^{M-1}\sum_{x=0}^{N-1}[I(x,y)-B]^2}$$ 2-1

where B is the average pixel intensity. The highest possible contrast for an 8-bit image for example, is half the number of total graylevels or 128.

Another common method of defining contrast is

$$contrast = \frac{I_{max}-I_{min}}{I_{max}+I_{min}}$$ 2-2

where the overall maximum and minimum pixel intensity of the entire image are used. This definition of contrast is normalized from 0 to 1.

Equation 2-1 is a better definition for the contrast of an entire image than Equation 2-2. Using Equation 2-2, two images by definition could have the same contrast but appear very different. An 8-bit image with one pixel at a graylevel intensity of 255 and one pixel at 0 would yield a perfect contrast of 1 even if every other pixel within the image was 128. A second image with many pixels at 0 and 255 would also yield a contrast of 1 but a different perceived look. Equation 2-2 is a well know definition for the CTF calculation at a specific frequency and is typically used as a measure of spatial resolution as described in Section 1.3.2 Bench-Scale Test Methods Developed by NIST

2.3.2 Brightness

Brightness is the overall perceived darkness or lightness of an image. For an 8-bit image, 0 and 255 correspond to black and white and every other pixel intensity corresponds to some shade of gray. For an N x M image I(x,y), brightness is simply defined as the average pixel intensity within the image [Weeks 1996].

$$brightness = B = \frac{1}{NM} \sum_{y=0}^{M-1} \sum_{x=0}^{N-1} I(x, y) \qquad 2\text{-}3$$

Compare Figure 2- 5 with an overall brightness value of 198 to the original image in Figure 2- 1 with a brightness of 107. As the brightness increases or decreases the pixels saturate at a 0 or 255 intensity as evident by the loss of details of the computer shown in the lower left corner of Figure 2- 5.
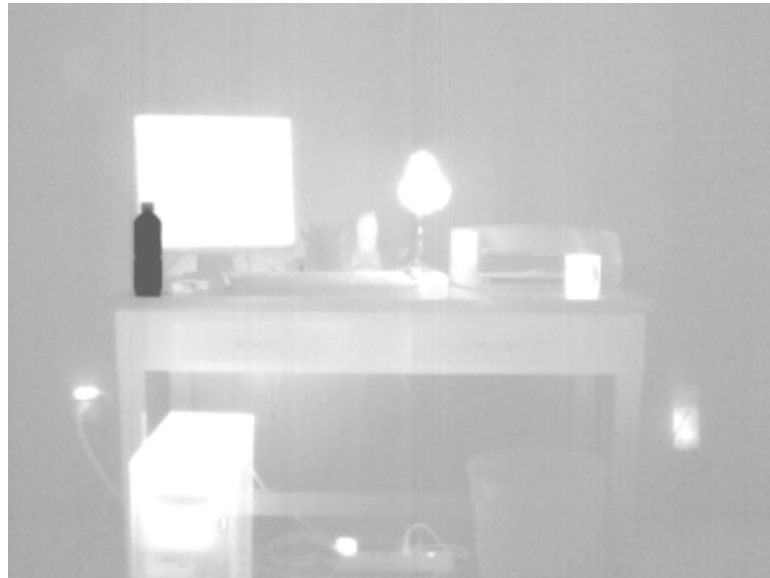
Figure 2- 5 Image of office with high brightness
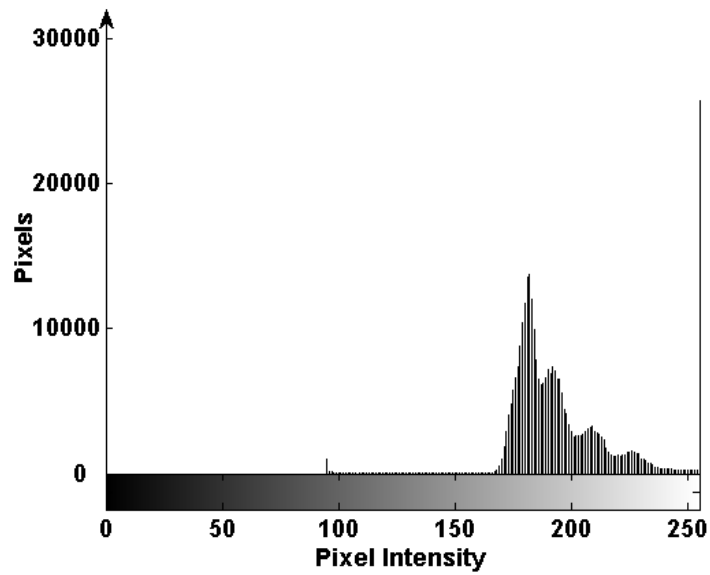
Figure 2- 6 Histogram of Figure 2- 5

Figure 2- 7 has a brightness value of 22. The image is saturated at 0 as shown in the histogram in Figure 2- 8.
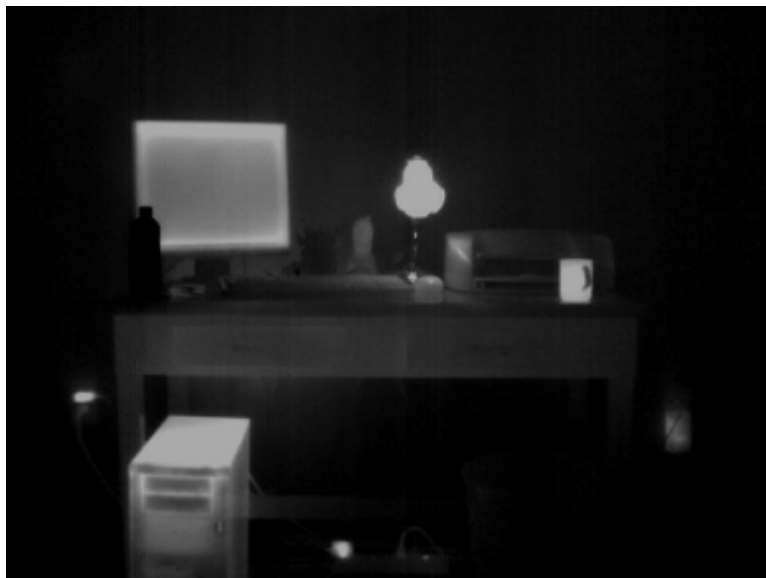
Figure 2- 7 Image with low brightness
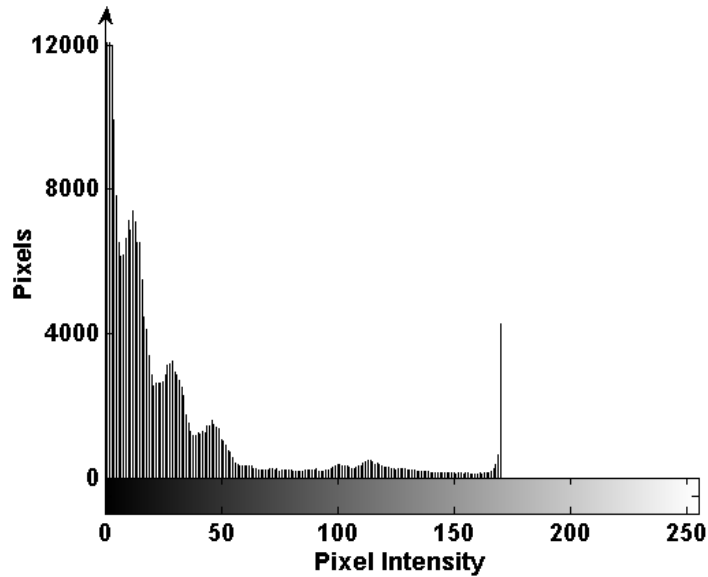
Figure 2- 8 Histogram of Figure 2- 7

2.3.3 Spatial Resolution

The resolution of an imaging system is defined as the separation of two discrete targets necessary to discern these targets on a display image. A classical method of quantifying the spatial resolution of an imaging system is the Modulation Transfer Function (MTF). The MTF is a measure of the ability of an imaging system to recreate the modulation of a target to an image for a range of spatial frequencies. The overall system MTF is the result of many subsystems such as the optics, scanners, detectors, electronics, signal processors, and displays. MTF also applies to any one of these subsystems individual such as display luminance value or the voltage signal of the detector array from an infrared camera [Boreman 2001]. The NIST test methods treat the TIC as a "black box" and focus on the evaluation of the display screen, the final product of the entire system. Modulation is defined in Equation 2-4 as the amplitude of the pixel intensity variations normalized by the bias level at a given frequency [Boreman 2001].

23

$$Modulation = M = \frac{I_{max} - I_{min}}{I_{max} + I_{min}}$$ 2-4

The MTF is the ratio of modulation in the image to the object as a function of spatial frequency described in Equation 2-5.

$$MTF(\gamma) = \frac{M_{image}(\gamma)}{M_{object}(\gamma)}$$ 2-5

Due to the inherent limitation in TIC system components such as the resolution of the display and the detector cell spacing and fill factor, the reduction in the modulation of a signal is frequency dependent. As the spatial frequency of an object increases, the modulation depth of the image decreases and therefore the MTF decreases. Figure 2- 9 illustrates the concept of MTF for a generic imaging system.
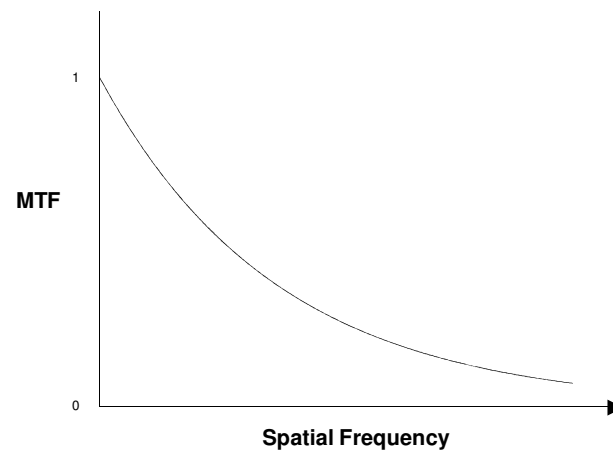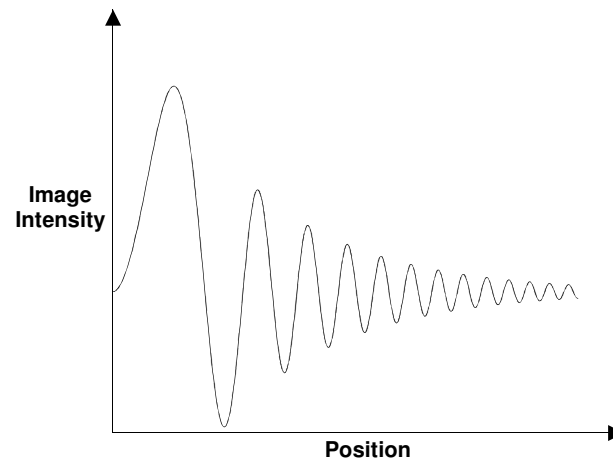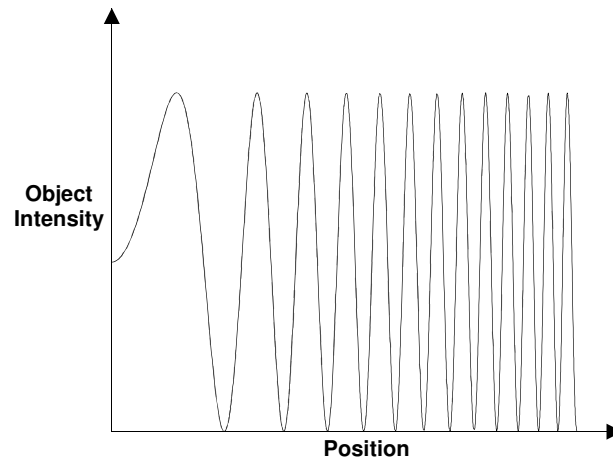
Figure 2- 9 MTF for a generic imaging system

At high spatial frequencies as the MTF approaches zero, the modulation is typically no longer due to the imaging of the target but the random modulation of random in pixel output, known as a type of noise. The noise-equivalent modulation (NEM) characterizes the noise in a TIC in terms of the MTF and is defined as the amount of image modulation necessary to yield a signal to noise ratio (SNR) of unity [Boreman 2001]. This value is also measured using the Nonuniformity calculation shown in Section 8.1.5 of NFPA 1801 [NFPA 1801 2008].

The limiting resolution of an imaging system is the location where the NEM dominates the MTF. Any point on the MTF curve greater than the intersection of these two points is a corrupted signal and not a testament to the resolution of the imaging system.

While the MTF provides a more complete description of image quality at all spatial frequencies it is common to specify a single value for spatial resolution. A common definition of the overall spatial resolution of an imaging system is integration of the MTF curve between 0 and the spatial frequency at the intersection between the NEM and MTF known as the MTF area (MTFA). A larger MTFA indicate better spatial resolution. Figure 2- 10 illustrates the definition of spatial resolution.
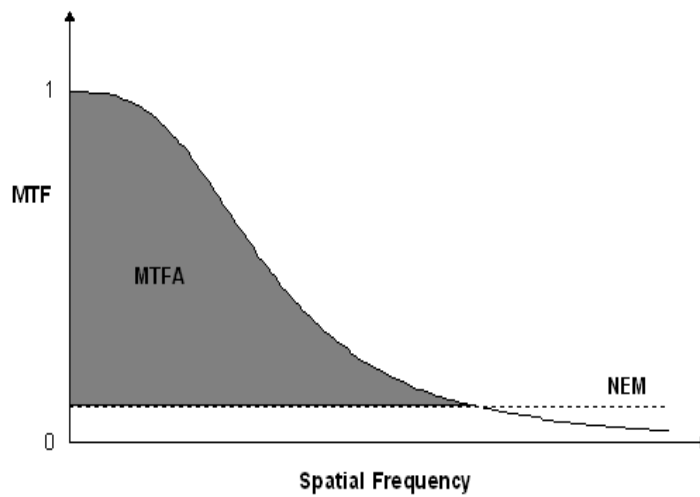
Figure 2- 10 Generic MTFA

The fundamental difficulty in defining spatial resolution using the MTFA is that two imaging systems with the same MTFA but different NEM could have a very different performance in a particular range of spatial frequencies. Consider the two imaging systems MTF curves in Figure 2- 11. Both imagers have the same MTFA but different responses to spatial frequencies.

27
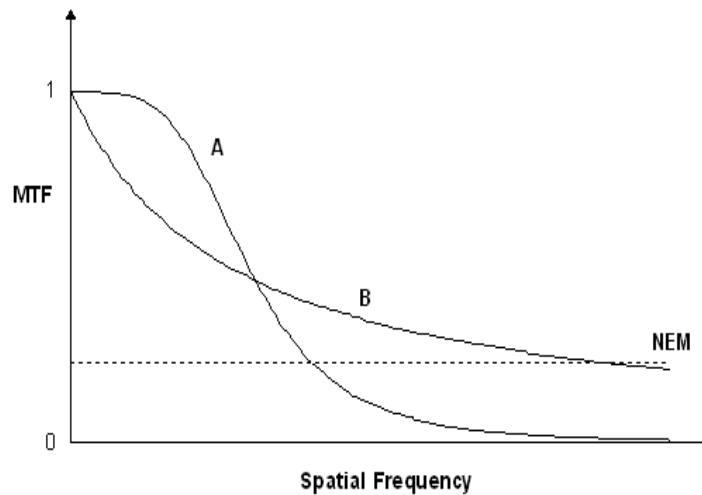
Figure 2- 11 Generic Comparison of MTF curves

TIC A has a higher MTF in the lower frequencies than Imager B. In the mid-range spatial frequencies TIC B is better than TIC A

2.3.4 Nonuniformity and Noise

An undesired deviation from an ideal signal is defined as noise. Noise is typically either a constant amplitude over all signal levels or increases with signal level resulting in more noise in brighter areas than darker areas of an image [Smith 2007]. Noise is inherent in all electro-optical imaging systems in all processes from the optics used to capture the scene to the production of the display image. Detector sensors, amplifiers and cabling are a few of the system processes sources of noise. A wide range of external factors also influence noise, including environmental conditions, radiation, and the instability of a light source. The most common noise that occurs in all imaging systems is detector noise from the counting statistics of the incident photons on a detector pixel due to the discrete nature of radiation [Russ 2002].

28

Noise is generally thought of in two main categories: uncorrelated (independent) noise and correlated (dependent) noise. Uncorrelated noise is defined as the random graylevel variations within an image that have no dependency on the graylevels of neighboring pixels [Weeks 1997]. Noise is generated in images as both additive and multiplicative noise. Our discussion is limited to uncorrelated additive noise where a recorded image $R(i, j)$ can be defined as

$$R(i, j) = T(i, j) + n(i, j) \qquad\qquad 2\text{-}6$$

where $T(i, j)$ is the pixel intensities of the noise free image and $n(i, j)$ is the intensity of the noise.

Noise is generally classified by the probability distribution or the discrete histogram for digitalized images in terms of the mean, M, and the variance σ^2. The mean is defined as

$$mean = M = \sum_{i=0}^{G_{max}} i \bullet n_i \qquad\qquad 2\text{-}7$$

where n_i is the probability of the noise at each graylevel i from 0 to G_{max}. The variance is defined as

$$\sigma^2 = \sum_{i=0}^{G_{max}} i^2 * n_i - M^2 \qquad\qquad 2\text{-}8$$

The standard deviation can be obtained from the variance as

$$\sigma = \left(\sum_{i=0}^{G_{max}} i^2 * n_i - M^2 \right)^{1/2} \qquad\qquad 2\text{-}9$$

A uniform distribution of noise produces random noise values with equal probability in a range of pixel intensities.

$$n(i) = \begin{cases} \dfrac{1}{J-K}, & for \quad K \leq i \leq J \\[2ex] 0, & otherwise \end{cases} \qquad\qquad 2\text{-}10$$

Figure 2- 12 displays a uniform noise histogram.
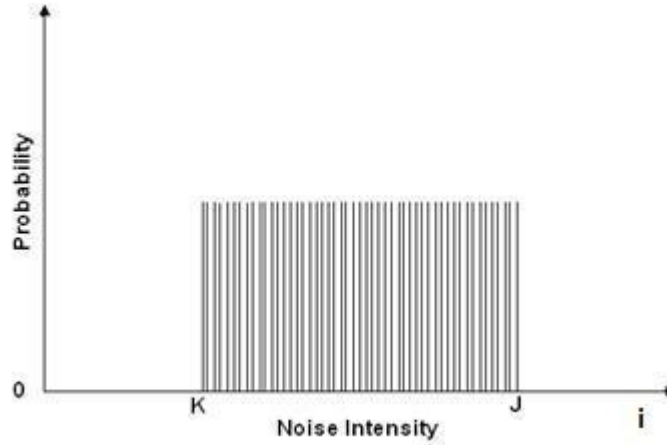
Figure 2- 12 Probability Distribution Histogram of Uniform Noise

Additive uniform noise is then the summation of the random noise value with the original pixel value only for pixel values from $J \rightarrow K$.

Noise is often modeled by an additive Gaussian distributed noise because by the central limit theorem, a large number of additive independent noise sources approaches a Gaussian distribution [Smith 2007]. The Gaussian distribution also describes detector noise which is one of the largest sources of noise in electro-optical imaging systems due to the nature of radiation and the limited time and space for the detector arrays to count the incident photons [Russ 2002].

Gaussian noise is expressed as

$$n(i) = \frac{e^{\frac{-(i-M)^2}{2\sigma^2}}}{\sigma\sqrt{2\pi}}$$

2-11

and by the probability distribution histogram as
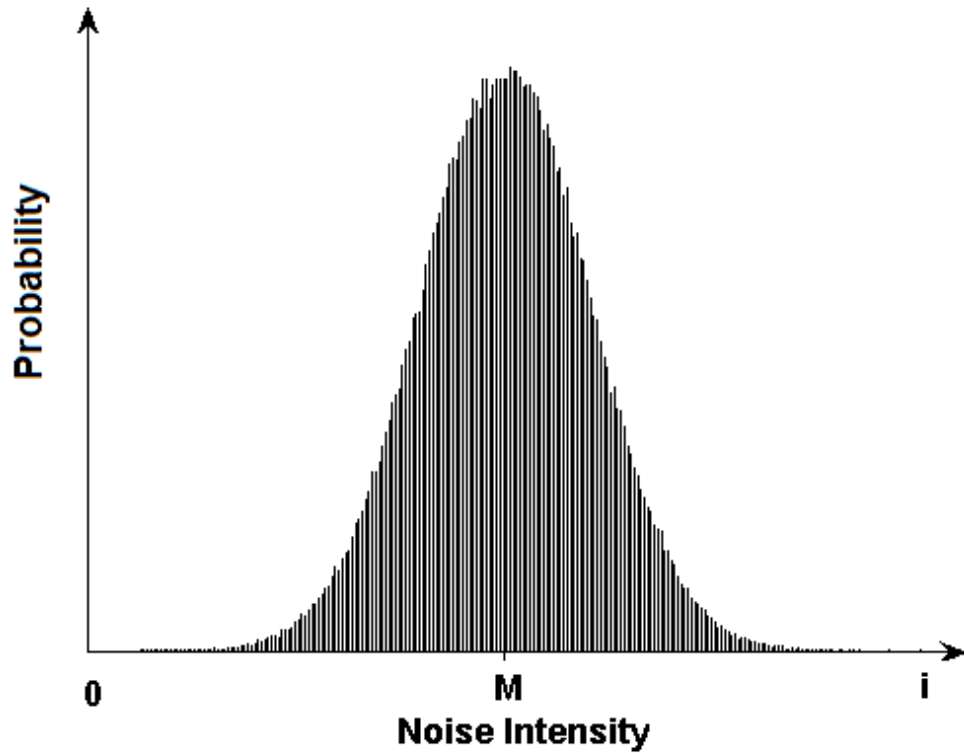
Figure 2- 13 Probability Distribution Histogram of Gaussian Distributed Noise

which has a peak at the mean. Most Gaussian distributed noise is applied to images with

a mean of 0. In other words, the highest probability of an occurrence of Gaussian noise

has a noise value of zero. The probability of the Gaussian noise decreases as the intensity

of the noise increases the farther the graylevels are from the mean. As with any statistical

Gaussian or normal distribution, 68% of the noise values lie within one standard

deviation, 95% within two, and 99.7% within three standard deviations. The variance specifies the thickness of the bell shaped curve. A higher variance would create a greater magnitude in noise intensity for more pixels.

Another common form of noise in electro-optical systems is salt-and-pepper noise where the noise values are generally outliers that deviate far from the expected pixel intensity. In electronic cameras, errors in data transmission generally produce saturated pixels or white and black graylevel intensities. Salt-and-pepper noise can also occur from dust or lint on the optics of the camera during data acquisition. Generally, salt-and-pepper noise takes on two discrete values and occurs at a percentage of the total pixels within the image as defined in Equation 2-12.

$$n(i) = \begin{cases} p \ (pepper) & i = J \\ p \ (salt) & i = K \\ 0 & otherwise \end{cases} \qquad 2\text{-}12$$

The histogram of salt-and-pepper noise is
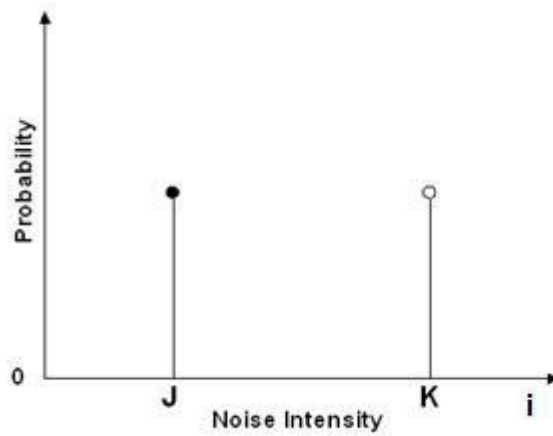
Figure 2- 14 Probability Distribution Histogram of Salt and Pepper Noise

where the probably is equal of having two discrete noise intensity value J and K. Salt-and-pepper noise is quantified by the percentage of pixels that are corrupted.

Figure 2- 15 and Figure 2- 17 display examples of images corrupt by additive Gaussian and salt-and-pepper noise, respectively. The Gaussian noise was added with a mean of 0 and a variance of 290.

Figure 2- 15 Image degraded by Gaussian distributed noise
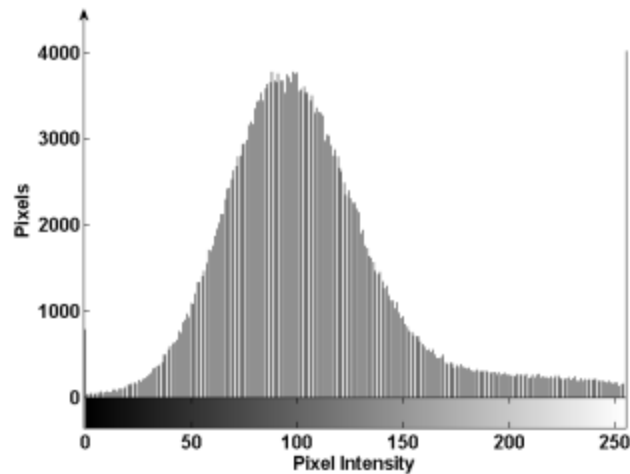
Figure 2- 16 Image histogram

Notice the histogram for the image corrupted with Gaussian noise in Figure 2- 16. The first and last bins of the histogram are higher than would be predicted by the Gaussian distribution because digitized images have only a finite range of pixel intensities and the Gaussian distribution extends to infinity. The summation of the noise and original image pixel values exceed the graylevel range of the image and therefore saturation occurs at the highest or lowest possible pixel value.

The salt-and-pepper noise had a 10% corruption rate. In other words, 5% of the original pixel values were converted to white and 5% were converted to black.

Figure 2- 17 Image degraded by salt and pepper noise
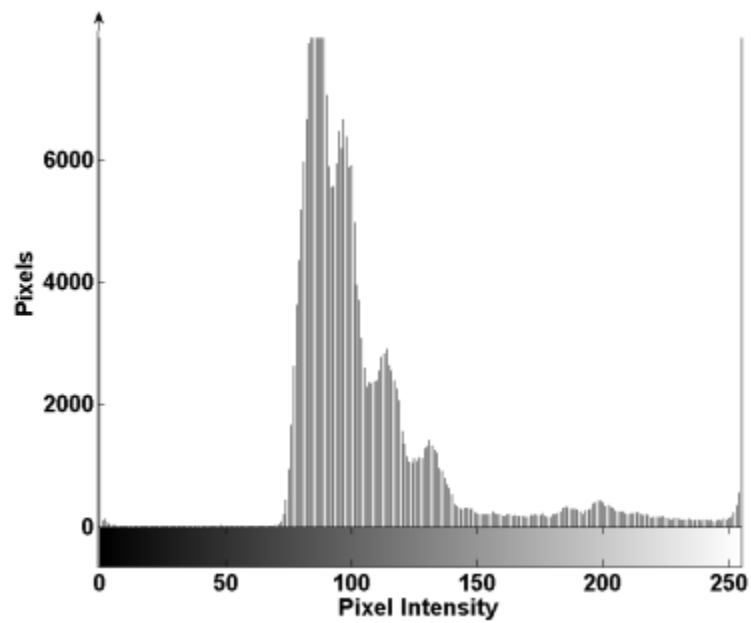
Figure 2- 18 Image histogram

The histogram for the salt-and-pepper noise corrupted image is as expected. The first and last bins are higher than the original image histogram because 10% of the pixels were converted to black and white.

The impact of noise within an image is often defined by the signal to noise ratio. For most applications of SNR, the signal is a distinct or known value, like a DC voltage, with respect to time. The noise is the random unwanted fluctuations in that signal. For this discussion, the SNR is the ratio of the noise free image pixel intensities over the intensity due to noise as function of pixel location within the image. The SNR is quantified as the ratio of the standard deviation over all the pixels in an image such that

$$SNR = \frac{\sigma_T}{\sigma_N}$$ 2-13

where σ_T is the standard deviation of the pixel intensities of the noise-free image and σ_N is the standard deviation of the noise [Fisher 2003]. A high SNR would indicate that the pixel intensities of the noise free image dominate the noise intensities causing very little degradation to the corrupted image. In the same way, a low SNR would indicate the noise values of the corrupted image dominate those of the original image. As the SNR decreases the noise begins to dominate over the signal and the original image is lost.

2.4 Image Processing Techniques

2.4.1. Processing in the Spatial Domain

Processing images in the spatial domain implies modifications or operations are performed directly to the pixel intensity values of each pixel location of the original image. These modifications are made to each pixel value independently, known as local

or point processing, or these adjustments can depend on the combination or comparison of a pixel location with its surrounding pixels, known as neighborhood processing. Image processing in the spatial domain is less computationally demanding than processing in the frequency domain because the images are not transformed into frequency space and therefore advanced mathematics or processing programs are not required. Modifications are applied directly to the image by scanning each pixel value and performing some operation.

2.4.1.1 Point Processing

Contrast and brightness are two images characteristics that are processed in the spatial domain by the manipulation of an image's graylevels. Some transfer function, linear or non-linear, is applied to the original pixel graylevel values to map these values to a new set of graylevels.

Linear transfer functions include addition (subtraction) and multiplication (division). Each original pixel within an image is multiplied and/or added to a constant value to create a new pixel value. Generally, these two functions can be combined as described in Equation 2-14.

$$P_k = m * O_k + d \hspace{3cm} \text{2-14}$$

In Equation 2-14, m describes the slope and d describes the offset. Each original pixel, O_k is then modified by this transfer function to create a new pixel value, P_k for all image pixels, k. Figure 2- 19 illustrates the concept of linear mapping.
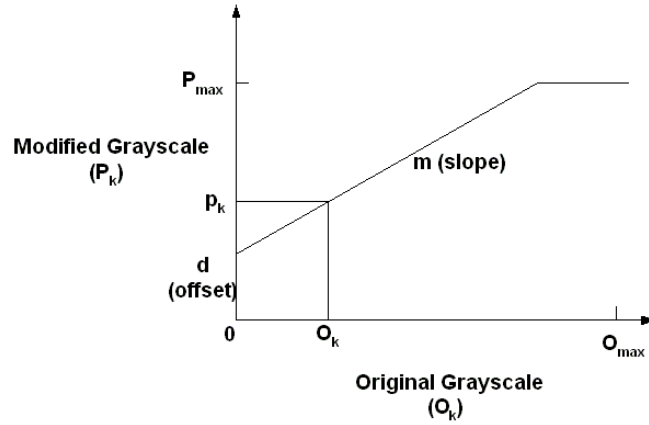
Figure 2- 19 Linear Mapping

The linear mapping of graylevels to new values is only valid within the range of the graylevel scale which is based on the bit depth of the image. An output value exceeding the range of the grayscale is set to the limits of that scale. For an 8-bit image, an output value of greater than 255 would be mapped to 255 and an output value less than 0 would be mapped to 0.   The linear transfer function in Figure 2- 19 created a saturation line at the maximum possible graylevel.

The slope of the linear transfer function in Equation 2-14 changes both the contrast and the brightness of an image and the offset alters only the brightness. To separate the adjustments for contrast and brightness, Equation 2-14 is rewritten as

$$P_k = m*(O_k B) + (B + d)$$ 2-15

where B is the average brightness of the image as defined in Equation 2-3. The variable m changes only the contrast and the offset d changes only the brightness [Weeks 1996].

38

A slope of one and an offset of 0 in the transfer function would take each original pixel

value and map it to the same value in the modified image. If the transfer function had a

slope value greater than one than a smaller range of graylevels in the original image is

linearly spread over a larger range of graylevels in the modified image known as contrast

expansion. This is used for image enhancement to expand an image that does not utilize

the full range of graylevels available for a particular bit depth to the full range of

graylevels. This greatly improves the contrast of an image and enhances detail.

Similarly, a slope value of less than one can be used to degrade the contrast of an image.

A slope of less than one linearly decreases the amount of graylevels in the output image

that are utilized in the original image. A positive offset value would increase the overall

brightness of an image and a negative value would produce a darker image. Figure 2- 20

illustrates the use of Equation 2-15 to modify the brightness and contrast of an image

using point processing. A slope, m, value of 0.3 and an offset, d, value of 80 was used.
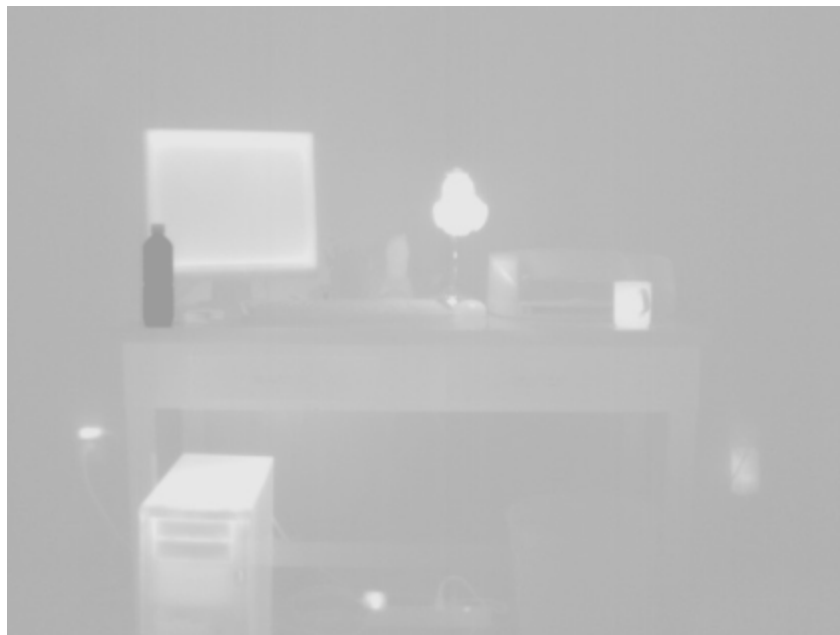
Figure 2- 20 Image degraded using point processing
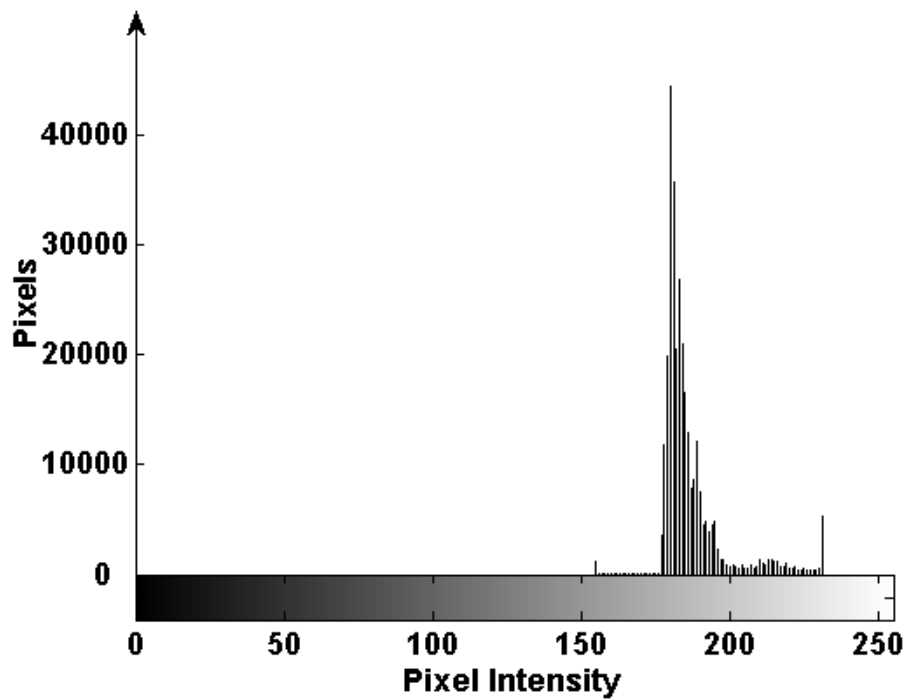
Figure 2- 21 Image Histogram

Figure 2- 20 essentially has a contrast of 30% of the original image shown in Figure 2- 1 and an average overall brightness 80 graylevels higher than the original image.

Non-linear transfer functions operate in a similar fashion to linear functions with the exception that the output pixel value will be dependent on the value of the input pixel. Non-linear functions are typically used to enhance dark or light regions of an image that are of interest to an observer. A non-linear transfer function can expand some portions of grayscale range while compressing others depending on an observer's needs. Several of the most common types of non-linear transfer functions are the exponential and logarithmic among others presented in Figure 2- 22.
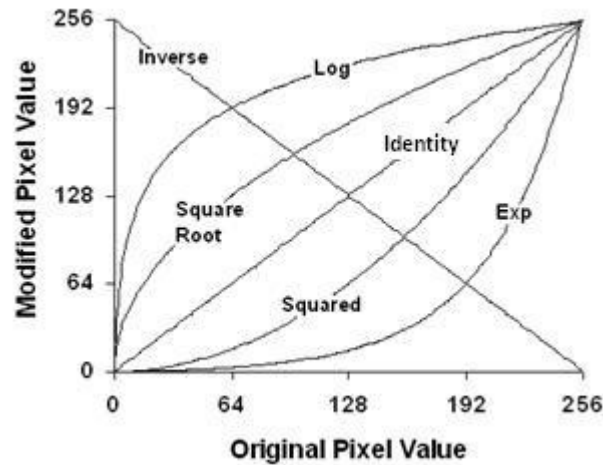
Figure 2- 22 Point processing using nonlinear transfer functions

Figure 2- 22 displays the original image pixel value on the x-axis and the modified pixel value on the y-axis after the application of a transfer function. The exponential or squared transfer function increases the contrast of the light areas of an image while reducing the contrast of dark areas. The logarithmic and square root transfer function have the opposite effect. The inverse function reverses the pixel values and the identity function leaves the image unchanged.

Transfer functions, either linear or non-linear, are an important part of image processing because a reproducible quantitative modification can be applied to a series of images and to create the same effect.

2.4.1.2 Histogram Equalization

Histogram equalization is used to modify the contrast and brightness of an image by modifying the image histogram. The goal is to redistribute the graylevels of an image so

41

each graylevel has an equal probability of occurring while retaining the brightness order of the pixels (See Figure 2- 26). In other words, the new histogram has uniformly distributed pixel intensities but relative intensities remain in the same order as the original image. Peaks in the histogram are spread out over a larger range of graylevels while the valleys are compressed into fewer graylevels creating visibility in minor pixel variations for a greater number of pixels.

For a discrete image, the process of histogram equalization can be described as

$$k = \sum_{i=0}^{j} \frac{N_i}{T} \qquad\qquad \text{2-16}$$

where the sum counts the total number of pixels within an image with original brightness equal to or less than, j, and T is the total number of pixels [Russ 2002]. For each original brightness level, j, the new assigned value is k.

Figure 2- 23 show an original image with its histogram as well as an image using histogram equalization. After histogram equalization, some features in the new image became more apparent and other details were lost.

Figure 2- 23 Original Image
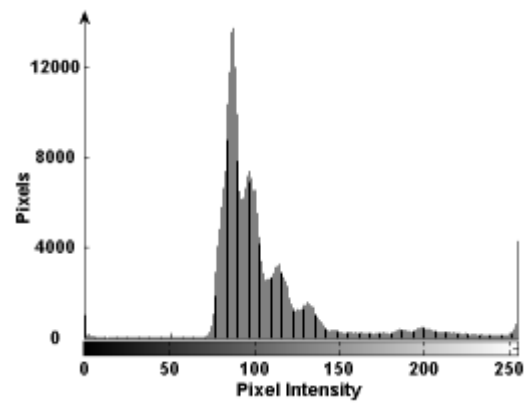
Figure 2- 24 Image histogram of Figure 2- 23
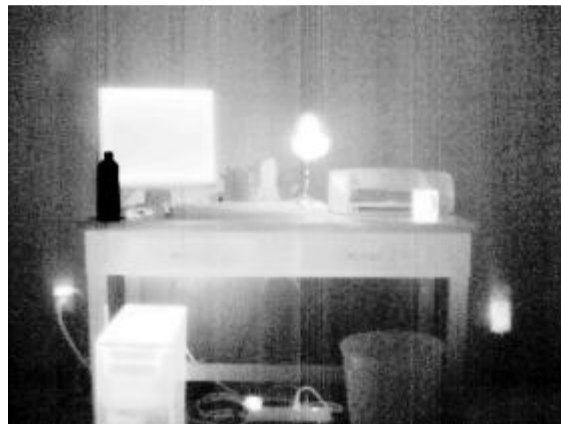
Figure 2- 25 Image after histogram equalization
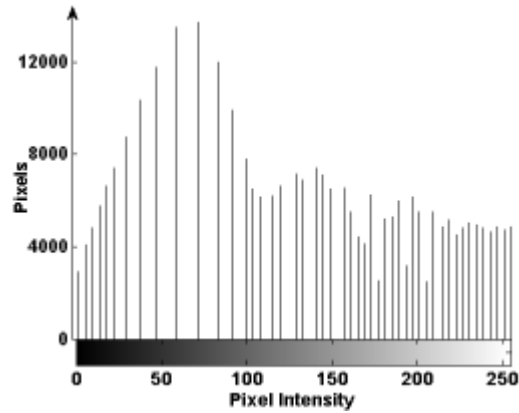
Figure 2- 26 Image histogram after equalization

The surge protector located in the center of the floor, the rim of the trash can, and the table legs had pixel intensity values at a peak in the spectrum in Figure 2- 24. As a result of histogram equalization, the details in these objects are more noticeable. On the other hand, other details were lost such as the variation in color of the computer monitor. The monitor pixel intensities were located in a valley in Figure 2- 24 and therefore the graylevels in this region were compressed.

In practice, after applying histogram equalization, the new histogram does not produce an image with an equal distribution of graylevels. The reason is because histogram equalization assumes the graylevels continuously vary between the minimum and maximum graylevels. Since digitalized images have only a discrete number of graylevels the solution is only an approximation [Weeks 1996].

2.4.1.3 Convolution in the Spatial Domain

Convolution is a common image processing technique used in the spatial domain to filter noise and adjust the spatial resolution of an image by the manipulation of the image

graylevels. Convolution is the replacement of a pixel value with a weighted average of

itself and the neighboring pixels using an array of integer weights known as a kernel. A

kernel is essentially a filter with an impulse response given by the kernel weights that is

applied pixel by pixel to an entire image. Each location in the kernel array corresponds

to a pixel location relative to the pixel being processed. The integer weights in the kernel

are multiplied by their corresponding pixel value and the average of these values is used

to replace the original pixel value. A kernel is typically square with odd dimensions

(3x3, 5x5, 7x7, etc.) so it can be symmetrical about a central pixel. To illustrate, consider

an original image with a pixel location $f(x, y)$ and a 3 x 3 filter kernel $h(x, y)$ with

weights w_k .
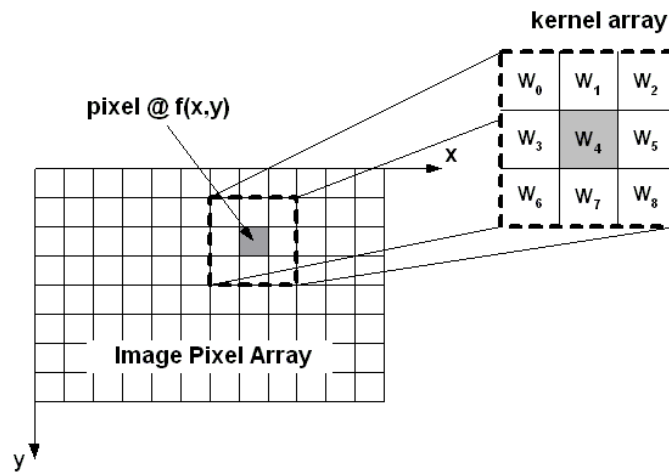
Figure 2- 27 Schematic of kernel operations

The center of the kernel is defined by the coordinate (0, 0) and exists over the range

$x, y \in -1,0,1$. The new pixel value $g(x, y)$ after convolution by $h(x, y)$ with weights W_k

can be described as

45

$$g(x, y) = \frac{\sum\limits_{i=0}^{2}\sum\limits_{j=0}^{2} f(x-1+j, y-1+i) \cdot h_{W(j+3i)}}{\sum\limits_{i=0}^{2}\sum\limits_{j=0}^{2} h_{W(j+3i)}} \qquad\qquad 2\text{-}17$$

The summation of the central and neighborhood pixels multiplied by the kernel weight and then normalized by the sum of the weights produces the new pixel value.

Applying a kernel around a central pixel creates a problem at the border of an image. At pixel location $f(0,0)$ in Figure 2- 27, five of the nine kernel weights do not apply to any neighboring pixel. There are several approaches to deal with this problem. The first approach is to simply not process the edges of the images where some kernel weights would not exist. This is not a major limitation for small kernel sizes because typically edges do not contain the most important details of an image. A second approach is to mirror the edge pixels as if they extended beyond the image. Finally, the kernel could wrap around the image and take the pixel values from the opposite size of the image as if they image was continuous. When using small kernels this problem is not a major limitation. However, when dealing with larger kernel sizes the problem could be significant. The convolution process would not be uniform throughout the image. The impulse response (the values of the kernel weights) and the size of the kernel dictate the effect of convolution on the image. The most common convolution process is a simple neighborhood averaging kernel where the weight of each location within the kernel is equal. This type of filter is beneficial for reducing noise by removing high

frequencies from an image. Figure 2- 28 illustrates a 3 x 3 kernel array for simple

neighborhood averaging.

Figure 2- 28 Neighborhood averaging kernel

The random noise pixel values are reduced because of the contribution of true image

pixel values from neighborhood pixels. In general, the larger the kernel size, the more

noise is filtered out of an image. Convolution also reduces the spatial resolution by

blurring edges and boundaries of objects in the image. In fact, convolution in the spatial

domain can be a useful tool not only for reducing noise but also for image degradation to

reduce the spatial resolution of an image.

To reduce the amount of blurring for a desired amount of noise reduction, the weight

values of the kernel can be adjusted to add a greater emphasis on the original pixel value

and the contribution of neighborhood pixels diminishes the farther away from the central

pixel. The weight values could be chosen somewhat arbitrarily depending on an

observer's opinion when the convolution process has created a desired result. However,

it is useful to use standardized numbers for weight values so the same kernel can be

applied to multiple images for comparison.

The most common weighted kernel is the Gaussian kernel. This type of kernel is an approximation of the Gaussian function along every row, column, and diagonal through the center of the kernel [Russ 2002]. The actual numbers used in the kernel vary particularly in the smaller kernels because discrete values are used to approximate a smooth continuous function. The Gaussian kernel is typically described by the standard deviation which is defined as the radius (in pixels) from the center of the filter containing 68% of the integrated magnitude of the coefficients [Russ 2002]. Consider Figure 2- 29 of an image corrupted with noise.

Figure 2- 29 Image corrupt with noise

Figure 2- 30 shows the convolution of Figure 2- 29 using several size Gaussian kernels. Kernel size increases with standard deviation.

Figure 2- 30 Image processed using associated kernel shown in Figure 2- 31

1	4	1
4	12	4
1	4	1

Figure 2- 31 Gaussian kernel (3x3)
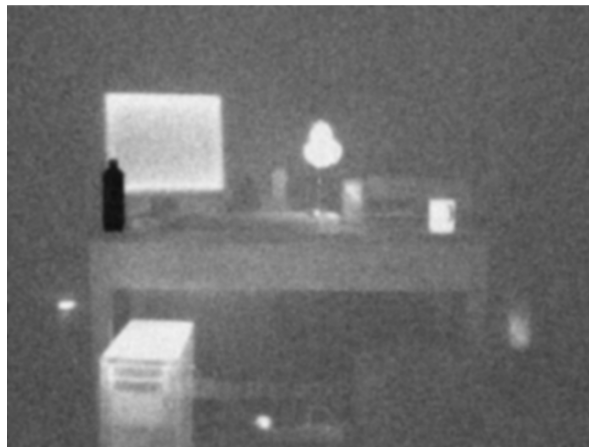
Figure 2- 32 Image processing used associated kernel shown in Figure 2- 33

0	0	1	1	1	1	1	0	0
0	1	2	3	3	3	2	1	0
1	2	3	6	7	6	3	2	1
1	3	6	9	11	9	6	3	1
1	3	7	11	12	11	7	3	1
1	3	6	9	11	9	6	3	1
1	2	3	6	7	6	3	2	1
0	1	2	3	3	3	2	1	0
0	0	1	1	1	1	1	0	0

Figure 2- 33 Gaussian Kernel (9 x 9)

Figure 2- 34 Image processing used Gaussian kernel shown in Figure 2- 35

2	2	3	4	5	5	6	6	6	5	5	4	3	2	2
2	3	4	5	7	7	8	8	8	7	7	5	4	3	2
3	4	6	7	9	10	10	11	10	10	9	7	6	4	3
4	5	7	9	10	12	13	13	13	12	10	9	7	5	4
5	7	9	11	13	14	15	16	15	14	13	11	9	7	5
5	7	10	12	14	16	17	18	17	16	14	12	10	7	5
6	8	10	13	15	17	19	19	19	17	15	13	10	8	6
6	8	11	13	16	18	19	20	19	18	16	13	11	8	6
6	8	10	13	15	17	19	19	19	17	15	13	10	8	6
5	7	10	12	14	16	17	18	17	16	14	12	10	7	5
5	7	9	11	13	14	15	16	15	14	13	11	9	7	5
4	5	7	9	10	12	13	13	13	12	10	9	7	5	4
3	4	6	7	9	10	10	11	10	10	9	7	6	4	3
2	3	4	5	7	7	8	8	8	7	7	5	4	3	2
2	2	3	4	5	5	6	6	6	5	5	4	3	2	2

Figure 2- 35 Gaussian Kernel (15 x 15)

As the Gaussian kernel size increases, the visibility of the noise present in the image decreases but the sharpness of the image also decreases.

The use of neighborhood averaging kernels such as the Gaussian kernel in a convolution process reduces the blurring effect for a given amount of noise reduction but does not completely eliminate the reduction in spatial resolution. Neighborhood averaging kernels operate based on the assumption that every pixel within the kernel size belongs to the same feature in the image. Because this is not true at edges and boundaries there will always be some reduction in the spatial resolution of an image.

To sharpen a blurry image, negative weight values can be given to a kernel for the neighborhood pixels and a positive weight to the central pixels. The intensity of the central pixel is magnified, sharpening edges and creating greater contrast. The process is limited to images with small amounts of noise; otherwise, noise pixels would be magnified and defeat the purpose of sharpening edges.

2.4.2 Image Processing in Frequency Domain

2.4.2.1 Fourier Transforms

The Fourier transform is the most common transform used for image processing in the frequency domain because of the availability of an efficient algorithm for computing it, known as the fast Fourier Transform [Cooley and Tukey, 1965; Bracewell, 1989]. Performing image measurements and processing operations in the frequency domain offers some advantage over the kernel operations in the spatial domain. In many cases, it is desired to filter out a particular spatial frequency of an image such as the removal of a

periodic noise that modulates at a known frequency. It is difficult to know the kernel weights to create an impulse response that would produce the desired effect on a particular frequency. Additionally, the computational cost of performing operations such as convolution using extremely large kernel sizes in the spatial domain can be significantly greater than the calculation of the Fourier transforms needed for the same operations in the frequency domain.

Other transforms such as the Hadamard, Walsh, and discrete cosine transform are typically used for image compression [Weeks 1997]. Most image characteristics are defined in the lower spatial frequencies and therefore eliminating high frequency components reduces the necessary storage for an image with minimal impact on image quality. The conversion of an image in the spatial domain to the frequency domain using the Fourier transform will provide the framework for filtering operations used to adjust noise and spatial resolution discussed in the following sections.

4.2.4.1.1 The 1-D Fourier Transform

Consider a continuous function f(x) such as spatially-varying image brightness where x is the distance in one direction across an image. Fourier's theorem states that a one-dimensional continuous function f(x) can be decomposed into a summation of a series of sine and cosine terms of increasing frequency known as the forward Fourier transform, denoted F[f(x)] and written as:

$$F(u) = \int_{-\infty}^{\infty} f(x)e^{-2\pi iux}dx \qquad \text{2-18}$$

where $i = \sqrt{-1}$. Using Euler's formula to expand Equation 2-18, the Fourier transform,

F(u), can be separated into real and imaginary components.

$$F(u) = R(u) + iI(u)$$
<div align="right">2-19</div>

where $R(u)$ is the real part of $F(u)$ and is defined as

$$R(u) = \int_{-\infty}^{\infty} f(x)\cos(2\pi ux)dx$$
<div align="right">2-20</div>

and $I(u)$ is the imaginary part of $F(u)$

$$I(u) = -\int_{-\infty}^{\infty} f(x)\sin(2\pi ux)dx$$
<div align="right">2-21</div>

Each sinusoidal term in the Fourier series corresponds to a spatial frequency or

specifically for this demonstration, a frequency where the brightness of the image

modulates. The Fourier frequency components can be written in terms of magnitude

otherwise known as the magnitude spectrum,

$$|F(u)| = \sqrt{R(u)^2 + I(u)^2}$$
<div align="right">2-22</div>

and phase also known as the phase spectrum,

$$\phi(u) = \tan^{-1}\left(\frac{I(u)}{R(u)}\right)$$
<div align="right">2-23</div>

The magnitude is essentially the amplitude of the brightness modulation and the phase

represents the shift in the sinusoid relative to the origin [Weeks 1996].

The Fourier Transform encodes a series of sinusoids for a range of spatial frequencies

from zero or no modulation (the average brightness of the image) to the highest spatial

frequency. Up until now we have considered a continuous function and the highest

spatial frequency would be dependent on the function f(x). However, digital images have

discrete brightness values at each pixel location. The integrals shown in Equations 2-20

and 2-21 are evaluated from minus to plus infinity. The discrete forward Fourier

transform for a digital image would be limited by the finite spacing of the pixels and can

be written as

$$F(u) = \frac{1}{N} \sum_{x=0}^{N-1} f(x) \cdot e^{i2\pi ux/N} \qquad\qquad 2\text{-}24$$

where N depends on the number of pixels in the X-direction. The summation is

performed over terms up to one-half the dimension of the image in pixels. The final

frequency term is known as the nyquist frequency and is defined as the highest spatial

frequency that can be encoded in a digital image. The nyquist frequency is one half the

total pixels in a dimension because it requires a minimum of two pixel brightness values

to define a frequency. Because each frequency component has a real and imaginary part,

the total number of values produced by the Fourier Transform is the same as the total

number of pixels in the x-direction [Russ 2002].

One of the most important aspects of the Fourier Transform is that given $F(u)$, the

original spatial domain function f(x) can be recovered using the same technique.

$$f(x) = \int_{-\infty}^{\infty} F(u)e^{-2\pi iux} du \qquad\qquad 2\text{-}25$$

or in the discrete case

$$f(x) = \sum_{u=0}^{N-1} F(u) \cdot e^{i2\pi ux/N} \qquad\qquad 2\text{-}26$$

This property of Fourier transform is extremely important when using linear filtering techniques to modification the spatial frequencies present within an image.

4.2.4.1.2 The 2-D Fourier Transform

Expanding the properties of the one-dimensional Fourier transform into two-dimensions, entire images can be decomposed into frequency space where each pixel corresponds to a complex value representing a magnitude and phase component. The 2-dimensional Fourier Transform is

$$F(v,w) = \frac{1}{NM} \int\int_{-\infty}^{\infty} f(x,y) e^{-i2\pi(vx+wy)} dxdy \qquad \text{2-27}$$

and its inverse as

$$f(x,y) = \frac{1}{NM} \int\int_{-\infty}^{\infty} F(v,w) e^{-i2\pi(vx+wy)} dvdw \qquad \text{2-28}$$

where v and w are the frequencies in the x and y directions. For an N x M finite size image the discrete 2-dimensional Fourier transform is

$$F(n,m) = \frac{1}{NM} \sum_{y=0}^{M-1}\sum_{x=0}^{N-1} f(x,y) \cdot e^{-j2\pi(nx/N+my/M)} \qquad \text{2-29}$$

and its inverse as

$$f(x,y) = \sum_{m=0}^{M-1}\sum_{n=0}^{N-1} F(n,m) \cdot e^{j2\pi(nx/N+my/M)} \qquad \text{2-30}$$

The terms in the Fourier series are independent of each other. Most of the image characteristics are described in the first few terms of the series. Adding higher and higher frequency terms improves the quality of the image, sharpening edges and providing the

fine details. Performing the transform at higher and higher frequencies does not alter the previous terms.

Images in frequency space are commonly represented based on only the magnitude values of the sinusoids called the magnitude spectrum. Sometimes the square of the magnitude or the power is used. An image is created from the magnitude spectrum by simply scaling the values to coincide with the graylevel range based on the bit depth of the image (0 to 255 for an 8-bit image). The distance from the origin of the magnitude spectrum corresponds to an increase in spatial frequency. The origin is the zero frequency component otherwise known as the DC level (no modulation or the average pixel intensity). The magnitude spectrum is commonly represented with the origin in the center and increasing frequency with the radius. The orientation depends on the angle. Figure 2- 36 and Figure 2- 38 are real images of two shapes. Figure 2- 37 and Figure 2- 39 are the representations of the corresponding magnitude spectrum.
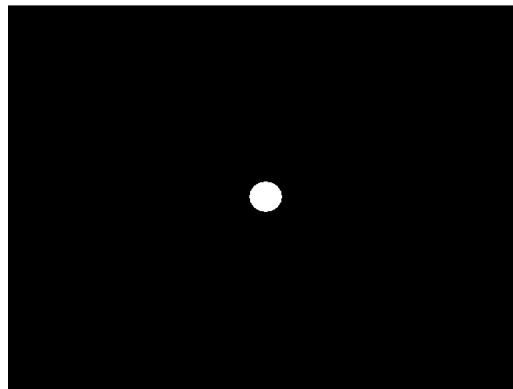
Figure 2- 36 Image of a circle
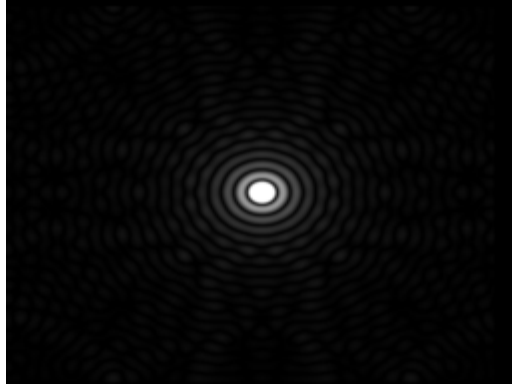
Figure 2- 37 Frequency Magnitude Spectrum of Figure 2- 36
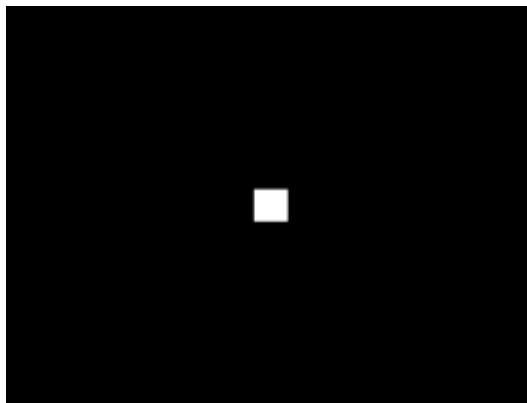
Figure 2- 38 Image of square
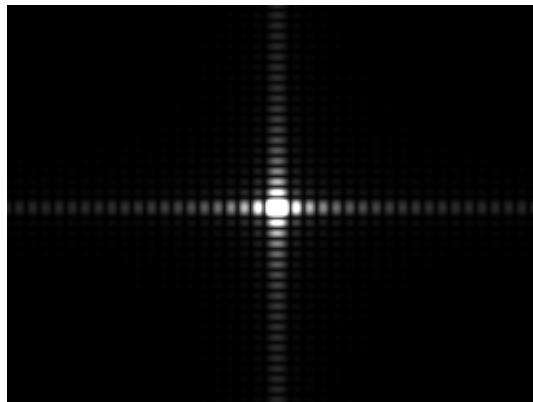
Figure 2- 39 Frequency Magnitude Spectrum of Figure 2- 38

Notice most of the image in frequency space is located near the origin or at the lowest

spatial frequencies. The magnitudes of the lowest frequencies are high creating bright

pixels in the magnitude spectrum. At higher frequencies, the magnitudes become smaller representing gray to black values in the magnitude spectrum.

2.4.2.2 Spatial Frequency Filtering

The decomposition of an image into a series of frequency terms using the Fourier transform is the basis for filtering images in the frequency domain. The modification of a particular spatial frequency term has no effect on any other spatial frequencies because each term in the series is independent. The effect of filtering in the frequency domain is exactly the same as convolution in the spatial domain. In the spatial domain, a filter with a given impulse response determined by the weights of the kernel, was applied to each image pixel. Filtering in the frequency domain is accomplished by multiplying the Fourier transform of both the image and the filter's impulse response as shown in 2-31.

$$G(n,m) = F(n,m) * H(n,m) \qquad\qquad 2\text{-}31$$

where n and m are the spatial frequencies in the x and y direction and $H(n,m)$, $F(n,m)$, and $G(n,m)$ are the Fourier components of the impulse response $h(x,y)$, the original image $f(x,y)$, and the filtered image $g(x,y)$. The reverse Fourier transform is then used to convert the frequency components back into the image as outlined in Figure 2-40.
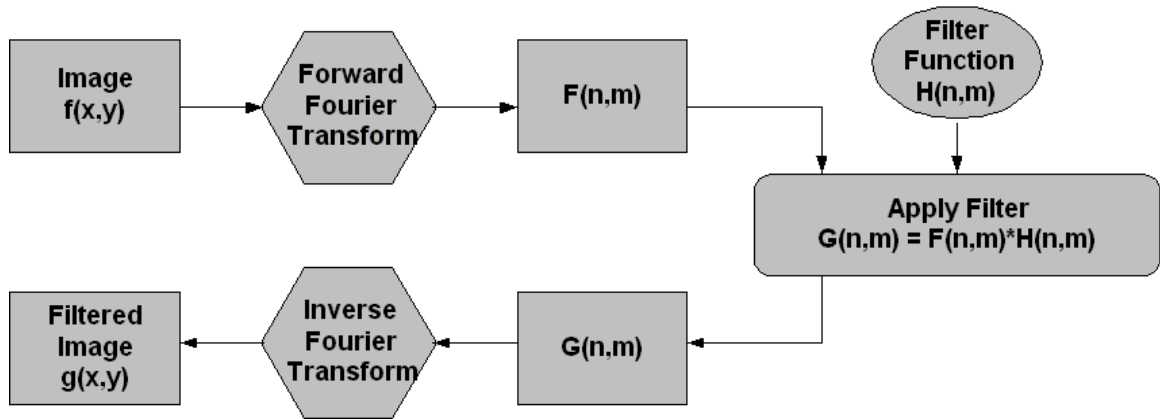
Figure 2- 40 Flow chart of frequency filtering of images

The Fourier transform of the impulse response of a filter is a function $H(n,m)$ used to modify an image's frequency components. However, it is not necessary to know the impulse response directly (although it can be found by taking the inverse Fourier transform of the frequency response of the filter). Instead an arbitrary function can be used to modify the spatial frequencies directly without knowing the impulse response. This is advantageous because typically the effect the impulse response of a filter has on the spatial frequencies is unknown and it is the spatial frequencies that are important to manipulate.

A common way to make a filter is to create a function in one dimension with respect to spatial frequency from the center of the magnitude spectrum of the Fourier transform of an image and then expand the function into two dimensions. Each spatial frequency has a designated location or radius from the origin (DC component) located at the center of the magnitude spectrum. The one-dimensional filter $H(n,m)$ is rotated 360 degrees based on the radius from the center shown in Equation 2-32 and Equation 2-33 .

59

$$H(n,m) = H(\rho)$$
<div align="right">2-32</div>

where

$$\rho^2 = n^2 + m^2$$
<div align="right">2-33</div>

to create a circular filter. The phase components of the frequency terms must be preserved in order to ensure an inverse Fourier transform can transform the image in the frequency domain back to the spatial domain. The only requirement to be a phase preserving filter is that the values of $H(n,m)$ must be real. The filter values are multiplied by both the real and imaginary parts of the Fourier Transform corresponding to spatial frequency component. The circular property of the filter ensures that the same filter value is applied to all phase components at a given spatial frequency.

The filter function typically ranges from 0 to 1 over the range of spatial frequencies present in the image (DC component or zero frequency to the Nyquist frequency). If the filter function has a value of zero, this essentially changes the magnitude at the corresponding spatial frequency to zero or no modulation. If the filter function has a value of 1, the modified magnitude at the corresponding frequency is equal to the original magnitude.

2.4.2.2.1 Filtering Techniques

The most common filters are low-pass, high-pass, and band-pass. A low-pass filter attenuates high frequencies while passing low frequencies. The effect of low-pass filters is the same as convolution in the spatial domain with simple averaging kernel weights. The image loses sharp edges and fine details and essentially blurs the image because the higher frequency information is subtracted from the image. The most common filter is

the ideal low-pass filter where frequencies below a cutoff frequency f_c are allowed to pass and the frequencies above f_c are blocked. The ideal low-pass filter has no transition period from passing to attenuation of frequencies and can be described for the one and two dimensional cases in Equation 2-34.

$$H(f) = \begin{cases} 1 & for \quad f \le f_c \\ 0 & for \quad f > f_c \end{cases} \rightarrow H(n,m) = \begin{cases} 1 & for \quad n^2 + m^2 \le f_c \\ 0 & for \quad n^2 + m^2 > f_c \end{cases} \qquad 2\text{-}34$$

Figure 2- 41 shows the magnitude spectrum of a one dimensional ideal low-pass filter and Figure 2- 42 shows the one dimensional filter rotated 360 degrees about n and m in the x and y directions to create a two dimensional filter for an image size of 640 x 480.
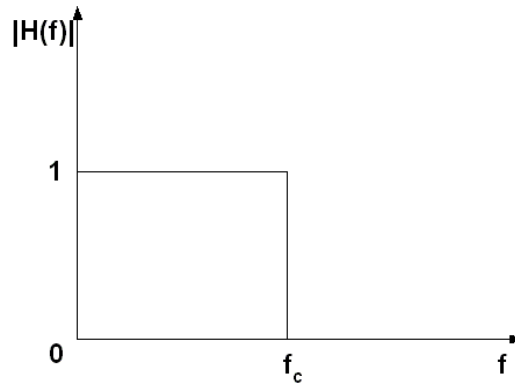
Figure 2- 41 One-dimensional low pass filter
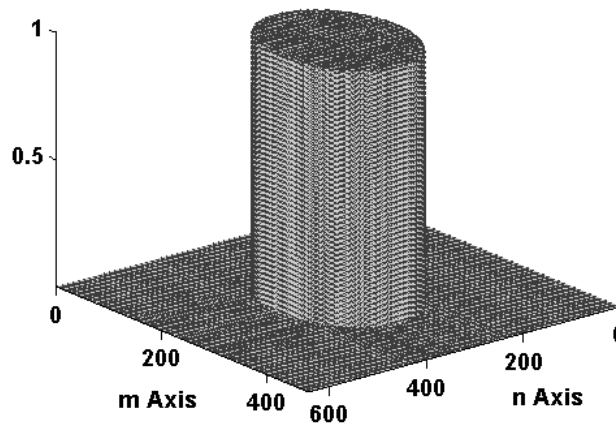
Figure 2- 42 Two-dimensional low pass filter

The magnitude spectrum of the two dimensional filter is designed to coincide with the magnitude spectrum of Fourier transform of the image which is commonly displayed with the DC component in the center and distance from the center corresponding to an increase in spatial frequency. The ideal low-pass filter starts at 1 at the lowest frequency and drops to 0 at a desired frequency f_c.

Ideal low-pass filters create a finite discontinuity in the magnitude spectrum and therefore create a finite discontinuity in the Fourier transformed image. The truncation of the Fourier spectral components at the cutoff frequency introduce artifacts commonly called ringing when the filtered image is transformed back into the spatial domain [Weeks 1997]. To illustrate the concept of ringing an ideal low pass filter was applied to Figure 2- 1 to create Figure 2- 43.
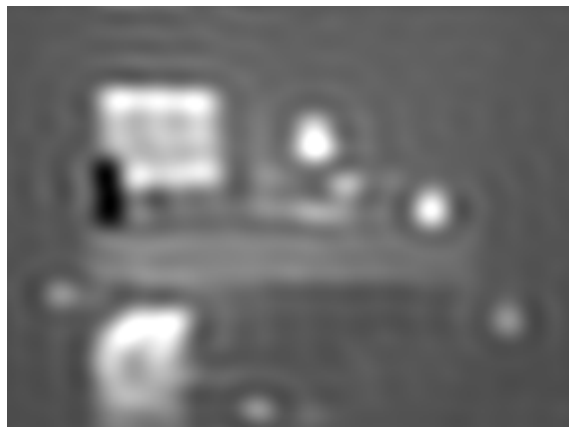
Figure 2- 43 Example of ringing artifacts

An ideal low pass filter was applied to Figure 2- 1 to produce the artifacts that appear in Figure 2- 43.

To circumvent the effect of ringing at sharp discontinuities a smooth edge can be applied

at the transition point of the low-pass filter. There are several common filter functions

used in digital image processing such as a parabolic or cosine function. The most

appropriate function is the Gaussian shape because the filter never drops to zero but

leaves a long tail beyond the cutoff frequency. The inverse Fourier transform of the

Gaussian filter is another Gaussian filter which would eliminate the effect of ringing. It

is also common to use the discrete approximation to the Gaussian filter known as the

Butterworth filter to produce the same effect. It is important to note that only the

magnitude spectrums of these filters can be used in image processing due to the phase

preserving requirements.

The magnitude of the Butterworth filter is described by Equation 2-35:

$$H(D) = \left[1 + C \left(\frac{D}{D_c} \right)^{2n} \right]^{-1} \qquad\qquad 2\text{-}35$$

where D is the distance from the center of the filter or the zero frequency to a particular

frequency and D_c is the distance to the nominal filter cutoff value f_c. Again, ultimately

this distance corresponds to a specific spatial frequency. The constant C is commonly set

to 1 or 0.414 to set the magnitude of the filter at the nominal filter cutoff value to 50% or

$1/\sqrt{2}$ respectively. The integer n is the order of the filter commonly 1 or 2. The higher

the function order, the steeper the filter profile. Figure 2- 44 displays three Butterworth

filter curves with common cutoff distances (frequencies) and Figure 2- 45 displays

different function orders.
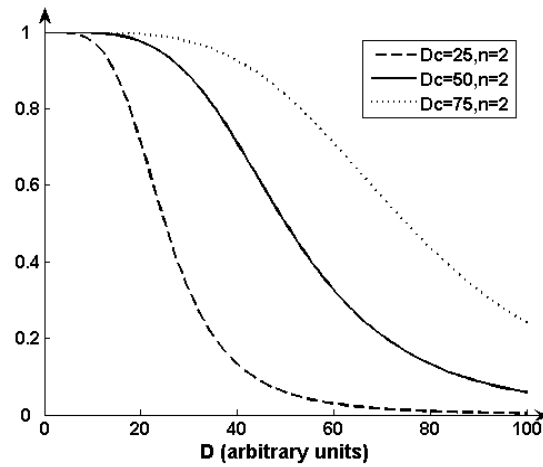
Figure 2- 44 Butterworth filter curves with varying cutoff frequencies
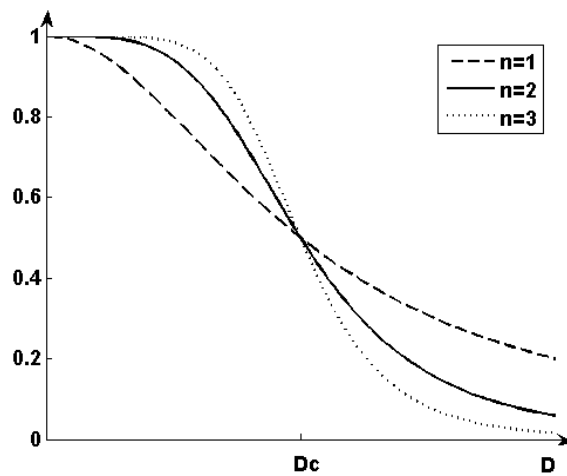
Figure 2- 45 Butterworth filter curves with varying function orders

Figure 2- 45 shows three Butterworth filters with different cutoff distances but the same function order. The best function to use would depend on the image and the desired effect on the image. At the least, the order should be chosen to eliminate the ringing effect at sharp edges. The two dimensional representation of the Butterworth filter is displayed in the magnitude spectrum shown in Figure 2- 46. Figure 2- 47 and Figure 2- 48 show the original and filtered image respectively. Notice the ringing effect evident in Figure 2- 43 using the ideal low-pass filter is eliminated.

64
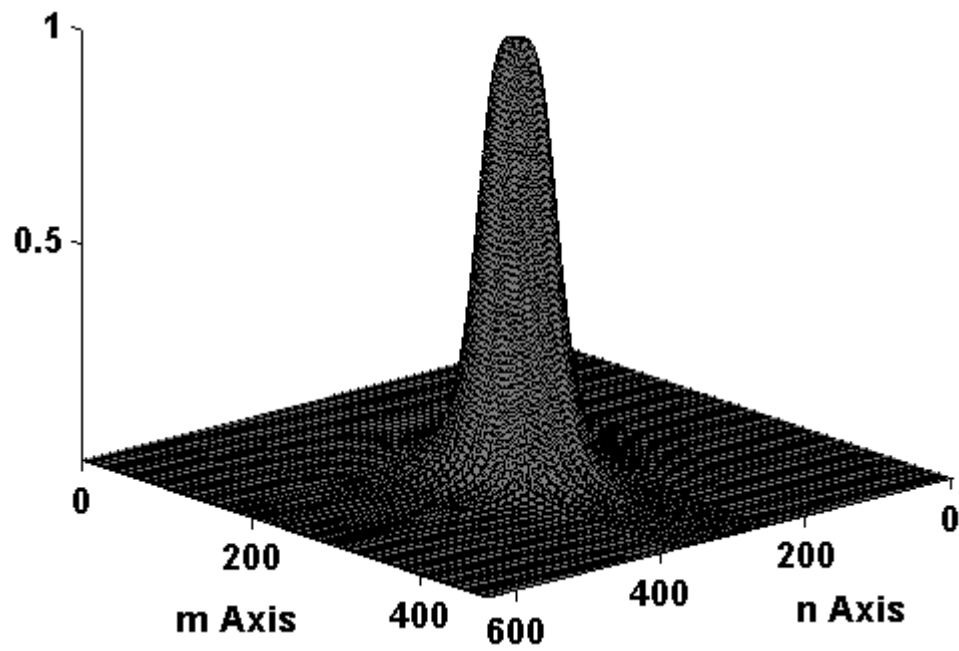
Figure 2- 46 Magnitude spectrum of 2-D Butterworth filter

Figure 2- 47 Original Image

Figure 2- 48 Image modified using Butterworth filter

High-pass filters pass high frequency information and attenuate low frequency information. The filters previously discussed for low-pass can be modified to create high pass filters. When applying a high-pass filter, the edges of image features are retained but the overall detail of the image is lost. To illustrate the effect of a high-pass filter, consider a high-pass Butterworth filter described by Equation 2-36.

$$H(D) = \left[1 + C \left(\frac{D_c}{D} \right)^{2n} \right]^{-1} \qquad \qquad 2\text{-}36$$

and represented in two dimensions in Figure 2- 49.
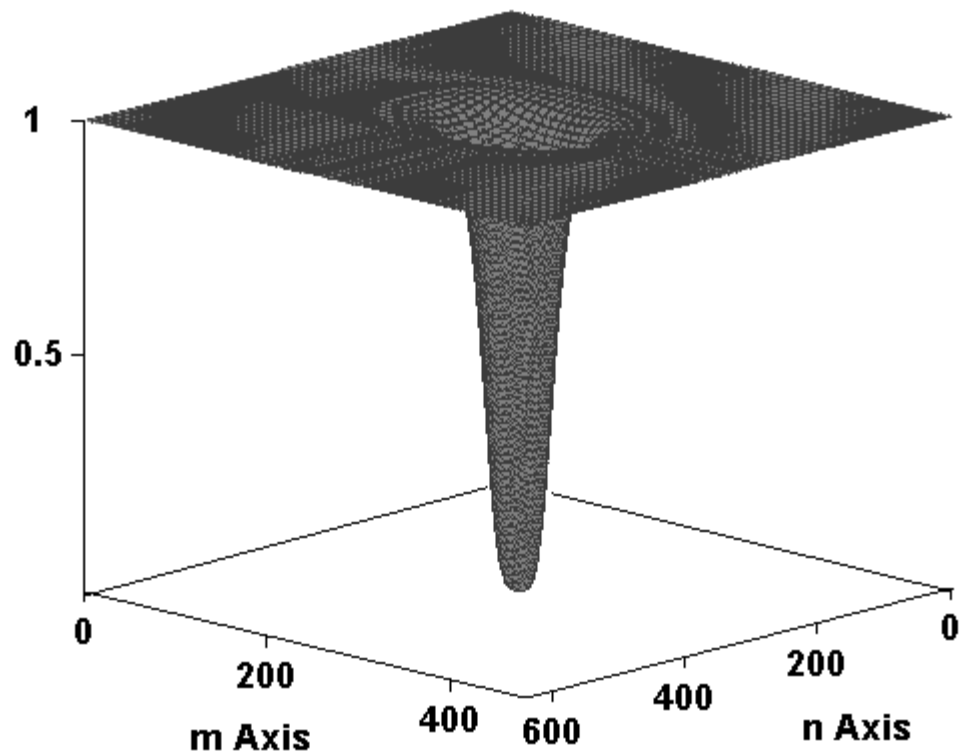
Figure 2- 49 High Pass 2-D Butterworth filter

The result of applying this filter to Figure 2- 47 is shown in Figure 2- 50.

Figure 2- 50 Image processed with high pass Butterworth filter

Notice the edges at sharp brightness differences are retained in the filtered images shown

by the outline in components such as the computer screen, PCU, and the lamp. It is

important to note that when using high pass filters the average overall brightness of an image is usually kept the same. Therefore the filter magnitude at the DC level is left unchanged.

Finally, band-pass filters are used to attenuate or pass a particular band of spatial frequencies of interest. A common procedure for noise removal is to analyze the magnitude spectrum for peaks at frequencies where there is periodic or unwanted noise. These frequencies can simply be subtracted from an image by applying a filter function that equals zero at these frequencies. The filter functions used for band-pass filters are equivalent to those used for low and high pass filters. The edges of the bands can be sharp like the ideal filter or smooth like Gaussian or Butterworth filter.

Chapter 3: Human Perception Experimental Design

3.1 Approach

To understand the effect TIC display quality has on human perception, fire fighters were given a typical TIC task: identifying a fire hazard by observing an IR image. A series of images were presented to the test subjects, which were a representative sample of fire fighters that regularly use TIC, on well-characterized computer screens in an ergonomically designed perception laboratory. The images were adjusted to quantitatively degrade image contrast, brightness, noise level, and spatial resolution. These image quality parameters were labeled the primary factors. Robustness factors, such as the amount of thermal clutter, the type of thermal scene, the shape and relative location of the fire hazards within the image were added to the image test matrix to control for variables that could potentially affect the results. The matrix of images presented to the test subjects was statistically constructed using a Taguichi experimental design so that it was possible to deconvolve the results to understand the interactions of the primary factors and their weighted effect on perception. Using the results of this study, a model was developed to predict a fire fighter's probability of successfully completing the recognition task given the key primary factors. A pilot study, using NIST personnel, was conducted as a proof of concept and to aid in the design of the full scale test.

The project was investigated through the collaboration between the National Institute of Standards and Technology (NIST), the Fire Protection Engineering Program at the University of Maryland, and the Army's Night Vision Laboratory (NVL).

3.2 Night Vision Laboratory (NVL)

NVL is a military laboratory at Fort Belvoir in Virginia that is dedicated to the research and development of night vision technology for military applications. As part of NVL's mission, a perception lab is devoted to testing soldiers' ability to identify and recognize targets based on the information gained from a thermal image. NVL evaluates military tasks such as recognizing and identifying ships, weapons, explosives and video clips of threatening human movements based on thermal imaging of the scenario.

Because of NVL's experience in human testing and data collection methods, NVL's ergonomically designed perception lab was an ideal environment to conduct the testing on fire fighter task performance. The lab included ten test stations with 12-bit cathode ray tube (CRT) monitors that differentiate 4096 levels of gray, far greater than a standard monitor that distinguish only 256 gray levels. The CRT grid was also more fine then the grid of the TIC system. Therefore the CRT grid adequately sampled the image and therefore any impact of resolution was not due to the screens at NVL but the resolution of the imaging system. Sampling is critical to avoid aliasing artifacts. For a more detailed discussion of the sampling of system resolution refer to work done by Boreman [Boreman 2001].

Each station was equipped with sufficient lighting, comfortable chairs and temperature control to create an ideal comfortable atmosphere and windowless to avoid glare issues.

3.3 Image Production

3.3.1 Hazards

The study was designed to investigate the ability to identify fire hazards in office and living room scenes that fire fighters are trained to understand and accustomed to viewing with a TIC. Hazards such as hotspots in walls, overheated electrical equipment, hot wires, and buried hot spots in furniture were used to simulate a smoldering or flaming fire in early stages where there would be no visual evidence of a flame or the origin of smoke. According to fire fighters trained in TIC, one of the most common reasons fire department are called to a scene is because building occupants smell smoke but cannot determine the origin. Fire fighters use TIC to scan the room.

One hazard type that was used for this study was a faulty connection in an electrical system that caused a low-resistance connection such as a wire, to carry a large amount of current to a source not equipped to handle the voltage. Figure 3- 1 displays infrared images of overheated electrical outlets.
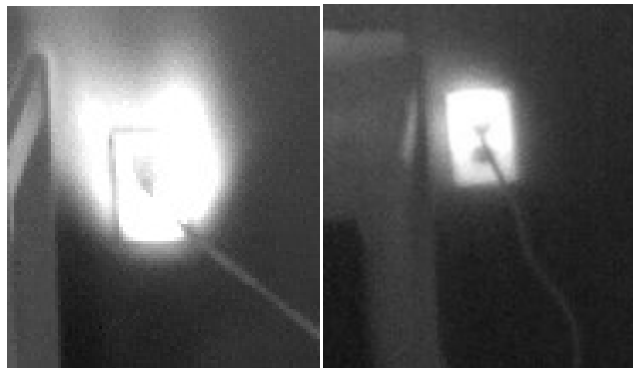
Figure 3- 1 Overheated electrical outlets

Overheated wiring or devices could occur for various reasons such as lightning strikes

sending current through an electrical system, poor connections, or uninsulated wiring.

Another common occurrence of overheated wires occurs when a table or desk leg crushes

a wire and causes a considerable amount of resistance heating as shown Figure 3- 2.
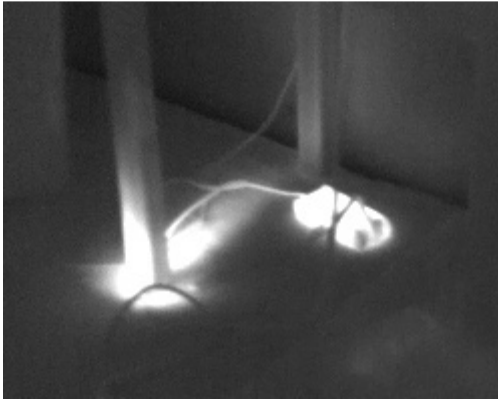
Figure 3- 2 Crushed wire under table leg

Other hazards used for this study included buried hot spots in trash cans and furniture as

shown in Figure 3- 3.

Figure 3- 3 Buried hotspot in chair

Buried hazards were used to represent a cigarette or match that was thrown away or dropped which has the potential to be slow developing and could elude a building occupant of the origin of the burning.

Although this experiment focused on one of the most common applications of TIC, it is important to note that TIC are used in a dynamic range of environments and applications. Due to a number of limiting factors, other scenarios and uses of TIC were beyond the scope of this work.

As an alternative to physically creating wall fires, buried hazards and short circuiting electrical devices, external heat sources were used to simulate the effect the radiation from the actual hazards would have on the TIC detectors. Heat rope and heat tape, which are essentially high resistance wires, were used to reproduce over heated wires and receptacles. To reproduce a generic hot spot, a high intensity halogen lamp and heat guns were used. The intent of this work was only to replicate the radiation emitted from a real hazard on a TIC display screen and not to reproduce the hazards.

A balance between the realism of the hazards and a controlled experiment was necessary. Fire fighters must be able to positively identify realistic fire hazards and at the same time create controlled images to focus the experiment on image quality parameters and conditions that could influence detection probability. To ensure the validity of the thermal images and the type of hazards, the images were sent to fire fighters who train others on the applications and techniques used for TIC in the field. In addition, the

feedback from the pilot study images was used to tweak the types of images used for the

real perception experiment.

3.3.2 Scene

A small one compartment structure was constructed to be a representative room or office

a fire fighter could encounter. A 12' by 12' room was built from gypsum wallboard

backed by 2 x 4 constructional lumber at 16" on center spacing. Electrical outlets,

overhead lights, wall lamps, and carpet were installed in the room.

The room was furnished with living room furniture on two walls and office equipment on

the other two walls to capture two scenes with one room to reduce construction costs.

Figure 3- 4 and Figure 3- 5 displays the living room scene assembled on two walls and

Figure 3- 6 and Figure 3- 7 displays the office work station.

Figure 3- 4 Living room scene

Figure 3- 5 Living room scene

Figure 3- 6 Office scene

Figure 3- 7 Office scene

Common living furniture such as tables, chairs, and standing lamps were added to the living room scene. Other items such as candles, lamps, plants, coffee cups, etc were also added as thermal clutter. The office work station included desks and computer chairs as well as computers, monitors, coffee makers, surge protectors, battery chargers among other electronic equipment.

3.3.3 Image Capturing

The images were captured using a FLIR Systems ThermaCam P640 commercial infrared camera. The display image quality of the FLIR P640 was chosen because it had far better display image quality than any fire fighting TIC available on the market. Most commercial fire fighting TIC have detectors with 320 x 240 or 160 x 120 pixel arrays.

The ThermaCam P640 has a detector pixel array of 640 x 480, four times the resolution of fire fighting TIC. Each detector pixel can distinguish 16-bit of information. In other words, the image produced on the display considers 65536 different intensity values or graylevels to create the image. A fire fighting TIC typically uses an 8-bit or 256 graylevel scale.

3.4 Defining the Scenario Criteria

3.4.1 Robustness Factors

Robustness factors were included in the test design to ensure the conclusions of the study would apply to a broad range of scenarios. There were a total of four robustness factors that included, hazard position, hazard type, thermal clutter, and scene type which were considered the most important factors that may influence the results according to pilot study results. The number of levels associated with each hazard and the definition of these levels are shown in Table 3- 1 .

Table 3- 1 Robustness Definitions

	Robustness Factor	Number of Levels	Level Definition
1	Target Position	6	Center
			Upper Left
			Upper Right
			Lower Left
			Lower Right
			No Target
2	Hazard Type	5	1 Overheated receptacle
			2 Overheated wire
			3 Buried hotspot in furniture/ trash can
			4 Small hotspot in wall
			5 Large hotspot in wall
3	Amount of Clutter	2	Small: 2-5 thermal objects
			Large: 8-10 thermal objects
4	Scene	2	Office work station
			Living room

One hazard type was used in each image (except for images with no hazard) in one of five locations as shown in Figure 3- 8.
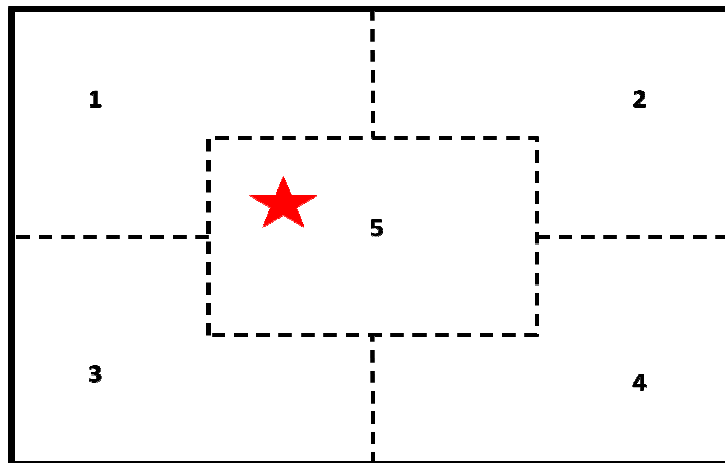
Figure 3- 8 Hazard location divisions

In addition to the hazard, thermal clutter was added to the image. Clutter was defined as an object that emits or reflects enough radiation operating in normal operating conditions to create a hot spot on a TIC. Clutter was used to make the images challenging and force the test subject to distinguish hazards from other objects. Figure 3- 9 displays several objects that were used as thermal clutter.
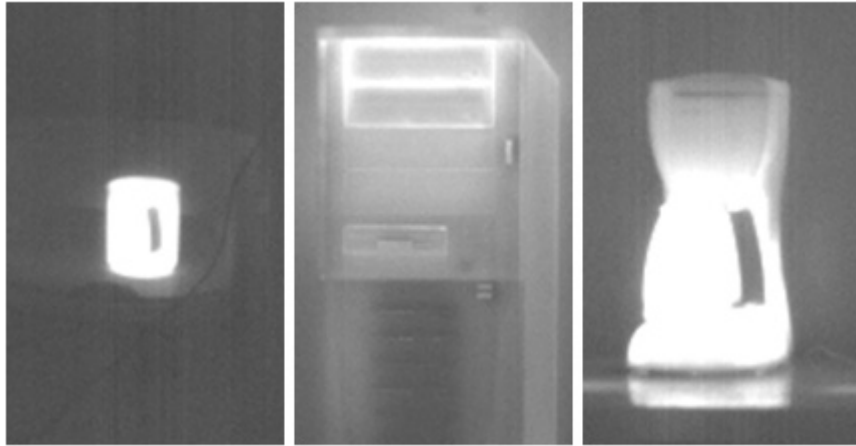
Figure 3- 9 Thermal clutter

The robustness factors were also used to ensure test subjects would not become too familiarized with images. A preconceived notion of the location and type of objects in the scene would simplify the task of identifying the location of the hazard on the image.

3.4.2 Primary Factors

The main focus of the study was to investigate display image quality in terms of four characteristic or primary factors; contrast, brightness, spatial resolution, and noise. The primary factors and definitions were chosen to understand their impact on a user's probability of successfully completing a hazard recognition task. The primary factors, definitions, and ranges are shown in Table 3- 2.

Table 3- 2 Primary Factor Definitions

Image Characteristic	Definition	Range	
		Min	Max
Contrast	$Contrast = \sigma_{lu\,min\,ance}$	0	∞
Brightness	$Brightness = \mu_{lu\,min\,ance}$	0	∞
Spatial Resolution	$SR = \int_0^A (MTF_{curve} - NEM)$ where A= intersection of MTF and NEM	0	$f_{nyquist} = 0.5 \, cycles \big/ pixel$
Noise	$Nonuniformity = \dfrac{\sigma_{noise}}{\mu}$	0	∞

The results of this study must have a connection to the NIST test methods to establish the minimum requirements for the image quality parameters in NFPA 1801, *Standard for Thermal Imagers for the Fire Service*. Conceptually, the perception experiment was designed to find the minimum image quality for a user to perform a task and the NIST test methods evaluate a TIC ability to reproduce an equivalent image quality. The definitions used to quantify image quality in terms of contrast, brightness, spatial resolution, and noise are equivalent in both cases but these parameters are evaluated on dissimilar images. However, conceptually we are still evaluating the same principal; the ability of a TIC to distinguish relatively hot and cold objects and the ability of a user to distinguish relatively light and dark objects.

As discussed in Section 1.3.2 Bench-Scale Test Methods Developed by NIST, contrast, brightness, and spatial resolution are evaluated using a controlled thermal image of a heated bar target over an ambient background. In the perception experiment, the parameters are evaluated over images of heated realistic objects in an ambient scene. In a similar fashion, nonuniformity is evaluated in the NIST test method as the random

fluxuations of pixel intensities from a uniform blackbody. In the perception experiment, random fluxuations were simply added to the images to produce similar false variations in pixel intensity. The perception experiment makes the connection between the user and the image while the NIST test methods make the connection from the image to the TIC resulting in a relationship between the user and the TIC.

3.5 Defining the Image Set

3.5.1 Restrictions

An image matrix was methodically constructed to ensure that each image contained a combination of the primary and robustness factors and so that statistically it was possible to extract the interactions between the factors and determine the weighted effect of each factor on detection probability. The number of observations that could be completed in one day was deemed to be 1250 according to recommendations made by the staff at NVL that have experience conducting similar experiments that took a period of days. 1250 observations per day minimized the fatigue and boredom, human factors that could influence test results. The total number of images or "observations" was restricted to 5,000 so that the test could be completed in four day window (1250 observations per day * 4 days) to maximum the number of fire fighters and thus increasing the sample size for more valid statistical data.

3.5.2 Pristine Image Set

All combinations of the robustness factors were considered in a full factorial matrix to create a "pristine" image set that did not include image degradation from the primary

factors. From Table 3- 1, multiplying the number of levels for each robustness factor

leads to 6 x 5 x 2 x 2 or 120 settings. In addition to a full factorial, one half of the images

were "replicated", for a total of 180 images. Replication for this experiment did not

mean identical images but rather the replicated images had the same robustness settings.

The 180 pristine images were created from the FLIR ThermaCam. The detailed image

set is shown in Appendix A.

3.5.3 Primary Factor Design Points

A subset of an m^k Factorial Grid was driven by a Taguchi L25 Orthogonal Design to

create the combinations (design points) of primary factors. A total of approximately 27

design points were possibly to satisfy the 5,000 image constraint (5000 total images / 180

pristine images~ 27 design points). A 5^4 grid design or five levels at each of the four

primary factors consists of 625 design points. The Taguichi L25 Orthogonal subset of

the grid consists of only 25 design points, meeting the 27 point restriction while retaining

orthogonality. Orthogonality is important to ensure no correlation between any two

factors and therefore each design point is independent providing different information

improving the efficiency of the results (Sanchez 2007).

The 25 design points are shown in Table 3- 3.

Table 3- 3 Design Points

Design Point	Factor Settings			
	Contrast	Brightness	Spatial Resolution	Noise
1	0.4000	0.5015	0.0284	0.3333
2	0.4000	3.6339	0.0522	0.2000
3	0.4000	6.7696	0.0760	0.1429
4	0.4000	9.9021	0.0998	0.1111
5	0.4000	13.0346	0.1234	0.0909
6	0.9330	0.5015	0.0522	0.1429
7	0.9330	3.6339	0.0760	0.1111
8	0.9330	6.7696	0.0998	0.0909
9	0.9330	9.9021	0.1234	0.3333
10	0.9330	13.0346	0.0284	0.2000
11	1.4669	0.5015	0.0760	0.0909
12	1.4669	3.6339	0.0998	0.3333
13	1.4669	6.7696	0.1234	0.2000
14	1.4669	9.9021	0.0284	0.1429
15	1.4669	13.0346	0.0522	0.1111
16	1.9993	0.5015	0.0998	0.2000
17	1.9993	3.6339	0.1234	0.1429
18	1.9993	6.7696	0.0284	0.1111
19	1.9993	9.9021	0.0522	0.0909
20	1.9993	13.0346	0.0760	0.3333
21	2.5317	0.5015	0.1234	0.1111
22	2.5317	3.6339	0.0284	0.0909
23	2.5317	6.7696	0.0522	0.3333
24	2.5317	9.9021	0.0760	0.2000
25	2.5317	13.0346	0.0998	0.1429

A pilot study was conducted using NIST personnel to get an idea of the amount of image

degradation in terms of the four primary factors was necessary to impact the hazard

detection probability. The TIC display quality test methods in NFPA 1801 require the

TIC to produce an image that would yield a detection probability of 95% [NFPA 1801].

Using the results of the pilot study, the 25 design points were chosen to fine tune the

settings of the images to capture a high probability of hazard detection ranging between

50-95%. Using a focused range of image settings, more data could be collected within the range of interest.

3.5.4 Calculations

3.5.4.1 Contrast and Brightness

Contrast is the standard deviation of the 640 x 480 2-D luminance array of the image captured with the FLIR Thermacam corresponding to the image as it would be seen on the monitors at NVL.

$$contrast = c = \sqrt{\frac{1}{NM} \sum_{y=0}^{M-1} \sum_{x=0}^{N-1} [f(x,y) - B]^2} \qquad \text{3-1}$$

where B is the brightness or mean luminance as

$$brightness = B = \frac{1}{NM} \sum_{y=0}^{M-1} \sum_{x=0}^{N-1} f(x,y) \qquad \text{3-2}$$

and N and M are 640 and 480 respectively.

3.5.4.2 Spatial Resolution

The spatial resolution of an imaging system over all spatial frequencies from 0 (DC or zero modulation) to the nyquist frequency (the highest spatial frequency that can encoded in a digital image) is defined by the MTF as described in Chapter 2 Section 2.3.3 Spatial Resolution. The MTFA, a single number value to describe the spatial resolution of an imaging system is found by integrating the area under the MTF curve between the MTF and the NEM of the imaging system.

To generate an MTF or a known frequency response for the images used in this study, a low-pass Butterworth filter (a discrete approximation to the Gaussian filter) was applied to the 2-D Fourier Transforms of the pristine images. The Butterworth filter was chosen because it offered the ability to control the attenuation rate of the filter for increasing frequency components. In addition, the filter changes from the pass band to the attenuation band without producing ringing artifacts in the filter image as common in other filters such as the ideal lowpass filter.

The Butterworth filter reduces the modulation depth at increasing spatial frequencies of each pristine image according to specified slope properties as described in Section2.4.2.2.1 Filtering Techniques. The design points for spatial resolution used for this study were dependent on the nominal cutoff frequency (D_c) of the low-pass Butterworth filter. For design points 1, 10, 14, 18 and 22 the nominal cutoff frequency was set to $0.02 \; {}^{cycles}\!/_{pixel}$. The constant C was set to 1 to adjust the magnitude of the filter at the nominal filter cutoff value to 50%. The integer n was set to 2. The magnitude of the Butterworth filter H(D) which when multiplied by the pristine image to create the MTF of the degraded image is shown in Equation 3-3.

$$H(D) = \left[1 + C\left(\frac{D}{D_c} \right)^{2n} \right]^{-1} \rightarrow MTF(f) = \left[1 + \left(\frac{f}{0.02} \right)^{4} \right]^{-1} \qquad \text{3-3}$$

To calculate the MTFA, the NEM is also required. The NEM was calculated using the methods described in NFPA 1801 section 8.1.5 specifically for the FLIR camera used to capture the IR images in this study. The dimensionless value is 0.02861. The final step

is to define the bounds of the integration for the MTFA by calculating the intersection of the MTF and the line created by the NEM as described in Section 2.3.3 Spatial Resolution. To find the intersection, both equations were set to be equal to each other and solved for the frequency.

$$\left[1+\left(\frac{f}{0.02}\right)^4\right]^{-1} = 0.02861 \rightarrow f = 0.048278\ cycles\Big/pixel \qquad 3\text{-}4$$

The MTFA is then

$$MTFA(f) = \int_0^{0.048278} \left[1+\left(\frac{f}{0.02}\right)^4\right]^{-1} - 0.02861 =$$

$$\int_0^{0.048278} \left[1+\left(\frac{f}{0.02}\right)^4\right]^{-1} - \int_0^{0.048278} 0.02861 = 0.0203\ cycles\Big/pixel \qquad 3\text{-}5$$

The MTFA must then be converted from cycles/pixel to a universal unit of frequency, cycles/mrad because cycles/pixel is dependent on the imaging system's detector array. The detector array typically does not fill the enter cell or pixel area. The ratio of the active detector element to the actual cell is known as the fill factor. A finite fill factor affects the resolution of the imaging system [Lloyd 1979]. If the frequency of target is high enough to fit between the active detector elements there will be no output from the imaging system.

Although cycles/mrad is a universal frequency unit, the conversion factor from cycles/pixel to cycles/mrad is unique to a specific camera at a specific distance away from the target. To calculate the conversion factor for the FLIR camera used for this

study, a path length of one meter was used to position a blackbody of known dimensions

from the lens of the TIC to yield a conversion factor of

$$1\,pixel = 0.7147\,mrad \qquad\qquad 3\text{-}6$$

One meter was chosen as the pathlength because it is the distance specified for the

performance test methods in the NFPA 1801.

The final value for the MTFA is

$$0.0203\,cycles\!\!\bigg/\!\!_{pixel} * 1\,pixel\!\!\bigg/\!\!_{0.7147\,mrad} = 0.0284\,cycles\!\!\bigg/\!\!_{mrad} \qquad 3\text{-}7$$

3.5.4.3 Noise and Nonuniformity

To quantify the amount of noise added to the images used in this study the inverse of a

signal to noise ratio otherwise called Nonuniformity was used. Nonuniformity is a

classical measurement in optical systems and is defined in section 8.1.5.13 of NFPA 1801

as

$$Nonuniformity = \frac{\sigma_{noise}}{\mu} \qquad\qquad 3\text{-}8$$

The amount of noise added to each image was dependent on the mean pixel intensity to

obtain a constant nonuniformity for each design point.

TIC nonuniformity patterns can vary dramatically and no one type of nonuniformity is

evident in all TIC. For a more complete discussion of nonuniformity measurements in

TIC refer to work done by Amon et al [Amon 2008]. Due to limitation in the number of

images and factors that could be included in this study, all types of nonuniformity where not investigated. A Gaussian distributed noise was added to the pristine image to act as a general nonuniformity.

A Gaussian distribution was chosen because it was the most common type of electronic noise present in cameras and sensors (Weeks 1996). It is often also used to model unknown additive noise sources from different parts of the image system. By the central limit theorem, the sum of a large number of independent noise sources approaches Gaussian distributed noise [Smith 2007].

3.6 Image Processing

Due to the interactions of the image degradation techniques used to manipulate each of the primary factors to create an image with specific values for contrast, brightness, spatial resolution and noise, the order of image processing was critical. Image processing is typically used to improve not degrade the quality of images. Techniques such as frequency filtering effect many image characteristics, specifically contrast and noise. While a low-pass filter such as the Butterworth was used in this study to reduce and remove the higher frequency components to blur the images and generate a frequency response (MTF) of the image, the filter also decreased the contrast and adjusted the noise of an image.

Low pass filtering limits the span of graylevels used to create the image. Blurring reduces sharp edges and therefore the contrast [Russ 2002]. Sharp distinctions in graylevels between objects in an image correspond to a high contrast. As the image

becomes blurry due to a low pass filter, the span of graylevels used to create the objects in the images shrink, reducing contrast.

To circumvent the interactions of contrast and filtering for this study an iterative approach was use to find a balance that would create an image that met the design points for both the contrast and spatial resolution as shown in Figure 3- 10. The contrast and brightness of the images were adjusted first to meet their design points. The low pass Butterworth filter was then applied to the image to adjust the MTF of the image. The contrast and brightness were then readjusted so that at the end of the process each primary factor met the desired design point. Up until this point in the image processing program, noise was not introduced into the image.

The quantity of noise in the final images was assumed to only be a result of the additive Gaussian noise. Although all images have noise, the amount of noise present in the images before the application of noise was assumed to be negligible to the amount of desired Gaussian noise added. Noise is hard to quantify unless there are obvious spikes in the magnitude spectrum of the Fourier transform of the image that do not contribute to the quality of the image but random fluxuations in the image signal.

To further justify this assumption, the application of the low-pass Butterworth filter removed the high frequency signal components. At higher spatial frequencies the magnitude of the frequency response is not due to the quality of the camera but the random pixel to pixel variations associated with noise [Russ 2002]. The Butterworth

filter eliminated the high frequencies in particular the frequencies above the intersection of the MTF and the NEM. Any frequency response of the image above the NEM is due to noise and not the quality of the image. For these reasons, noise was the last component added to the image set. A flow chart of the image processing is shown in Figure 3- 10.
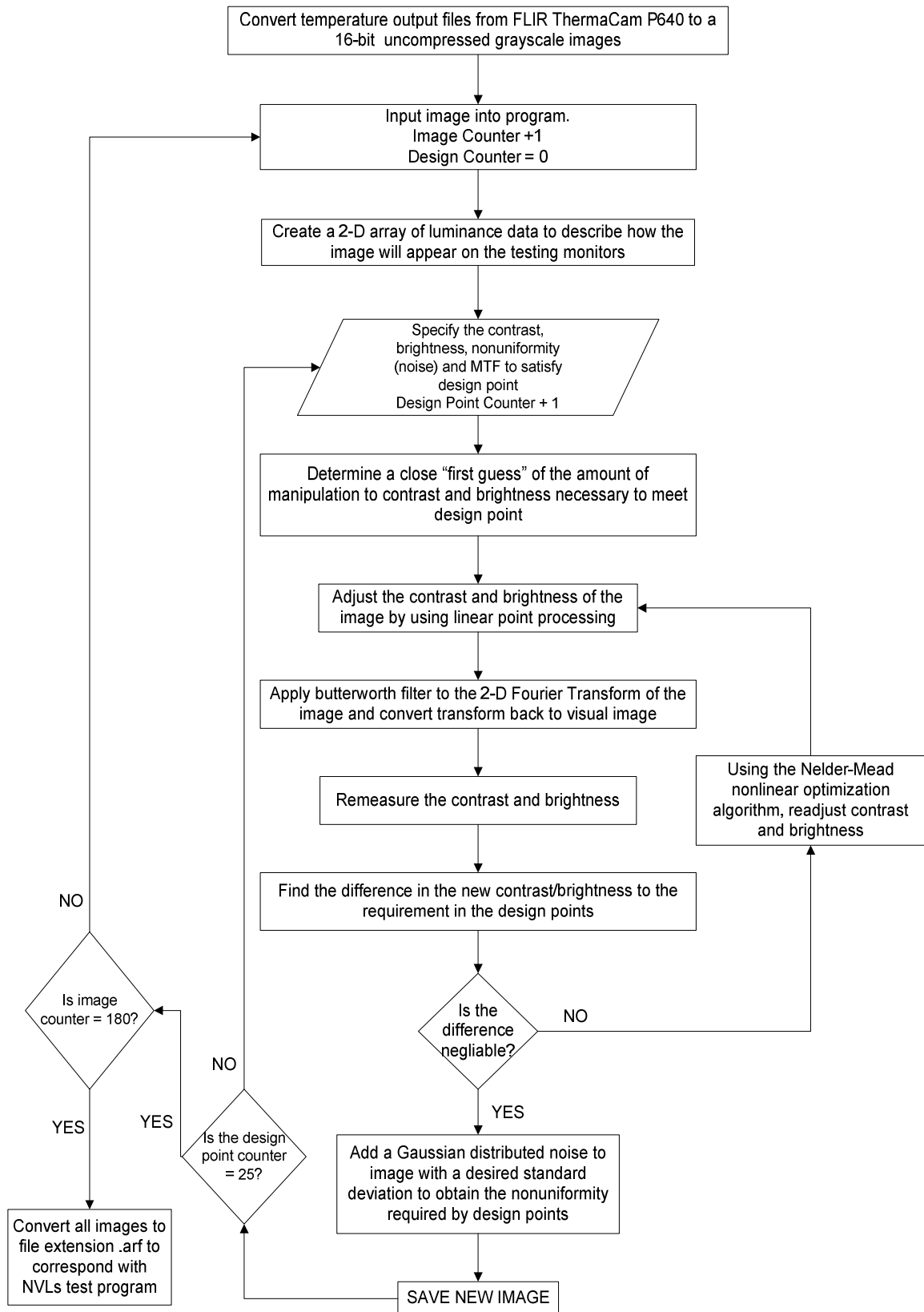
Figure 3- 10 Flowchart of image processing

92

To implement the degradation process outlined in Figure 3- 10, Matlab R2006b Version

7.3.0 was used to write a program to manipulate the pristine images to meet each of the

25 design points. The complete custom made program can be found in Appendix B

Image Processing Program. An example of how this program manipulated one of the

images from the pristine image set to meet each of the 25 design points can be found in

Appendix D.

Chapter 4: Modeling Human Perception

4.1 Objective

Create a model to predict the probability of a fire fighter successfully completing a hazard recognition task with the aid of only an IR image.

4.2 Test Subjects

A group of sixteen TIC users of varying age, fire fighting experience, TIC experience and skill level were used to capture data from a representative portion of the fire fighting community to help identify any bias in the test results that could link test subject performance with experience. A list of fire fighter backgrounds can be seen in Appendix C Test Subject Background.

The test subjects were required to attend an informative session which included a Power Point presentation followed by a hazard training exercise on the NVL testing program. The Power Point presentation described the project goals as well as the types of scenes, thermal clutter, and hazards that would be seen in the images. Because of the diversity of the fire fighter's training backgrounds, to avoid possible confusion, test subjects were given a training exercise that included pristine images similar to the types of scenes that would be seen in the actual study. The test subjects were required to select the hazard in each of the training images. Only test subjects who scored a 100% on the training exercise were allowed to proceed to the real study to ensure any wrong answers could be attributed to the image quality and not the definition of a hazard. The training program

also familiarized the test subjects on how to navigate through the images and select the hazards using NVL's testing program.

4.3 Experiment

The test was conducted in NVL's ergonomically designed perception laboratory using their testing system as well their procedures to avoid any impact on a test subject's performance that could not be attributed to the image quality. The experiment included 4500 images split up into 25 sessions containing 180 images each. The images were presented in a strategic order by progressively improving the quality of the images to minimize the effect of learning during the tests. The ranking of design point order was chosen based on pilot study results.

Time limitation was not a variable. Each image was presented on the screen for an unlimited amount of time until a selection was made. A five minute break was required between each of the sessions to avoid fatigue and boredom which could potentially influence their alertness and performance on the study.

The test subjects were asked to view each of the images and located the hazard via a mouse click on the screen. A "No Hazard" selection box was also incorporated on the test screen for images without a hazard. The user's mouse click location was compared to the actual hazard location. If the mouse click was within the coordinates of the hazard a correct answer was registered by NVL's program. A '1' indicated a correct answer and a '0' represented incorrect. The program automatically consolidated each test subject's test results in a comma delimited text file that included the test subject ID, the mouse

click coordinates on the screen, the result of the selection, and the time to make the decision.

4. 4 Data

Several of the 16 user's were unable to complete the entire test, therefore, rather than 4,500 x 16 = 72,000 data points, only 54,540 points were recorded. These data points were binary; either a 1 for correct response or 0 for incorrect response. Each data point corresponded to a design point (1-25) for contrast, brightness, spatial resolution, and nonuniformity. The average probability of successfully identifying a fire hazard for each design points is summarized in Figure 4- 1.
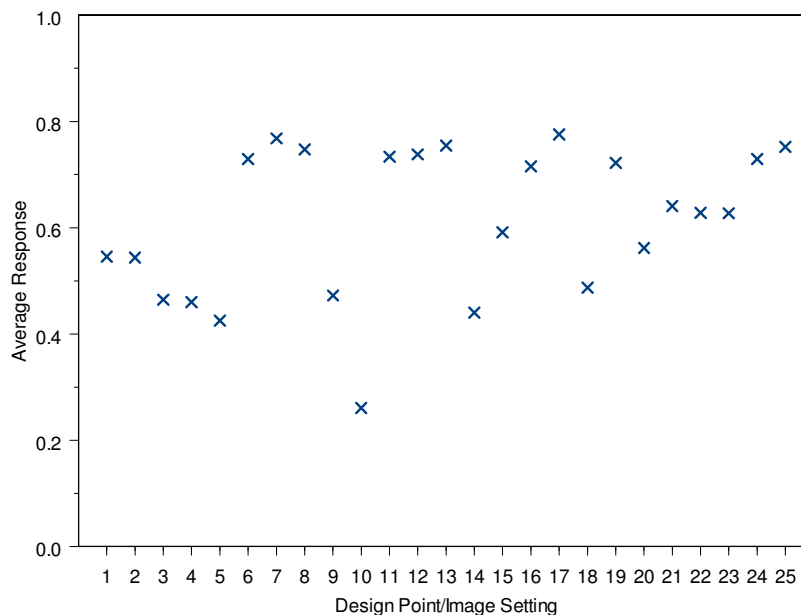
Figure 4- 1 Average response for design points

It is important to note that the design points were not ranked based on difficulty.

4. 5 Logistic Regression Model

When the response variable is binary, the response function often follows the shape of a logistic regression function. This model is typically sigmoidal and monotonic having a stretched "S" (increasing) or reverse "S" (decreasing) shaped response with asymptotes at 0 and 1 and takes on the following form (Agresti, 1990).

$$\hat{p} = \frac{\exp(\beta'X)}{1+\exp(\beta'X)} \qquad \qquad 4\text{-}1$$

The probability of success is predicted based on X which can be any number of input parameters. X in this study corresponded to the primary factors to define image quality: contrast, brightness, spatial resolution, and nonuniformity. Several versions of the model were considered including the primary factors only, the primary factors plus two terms interactions, and primary factors plus all interactions. The primary factors are shown in Table 4- 1.

Table 4- 1Primary Factors

Variable	Description
X_1	Contrast
X_2	Brightness
X_3	Spatial Resolution
X_4	Nonuniformity (noise)

Based on the diagnostics discussed later in this section, a modification to the primary factors plus two term interaction multiple logistic regression model was chosen. The coefficients of each parameter, β, are regression coefficients typically calculated using computer-intensive numerical search procedures. For a more detailed description of how

the coefficient values are produced refer to work done by Neter et al (Neter, Kutner,

Nachtsheim, &Wasserman, 1996). The calculated regression coefficients are shown in

Table 4- 2.

Table 4- 2 Multiple logistic regression coefficients

Coefficient	Description	Value	Std. Error	t-value
β_0	Intercept	-1.030	0.140	-7.346
β_1	Contrast	0.076	0.040	1.929
β_2	Brightness	-0.172	0.008	-20.220
β_3	Spatial Resolution	0.991	0.343	2.893
β_4	Noise	44.510	2.238	19.885
β_5	Contrast-Brightness Interaction	0.169	0.005	36.195
β_6	Contrast-Noise Interaction	-12.350	0.708	-17.449
β_7	Brightness-Spatial Resolution Interaction	-0.216	0.027	-7.975
β_8	Brightness-Noise Interaction	-1.597	0.108	-14.753
β_9	Spatial Resolution-Noise Interaction	-16.935	3.947	-4.291

Expanding Equation 4-1 to account for two term interactions

$$\hat{p} = \frac{\begin{aligned}&\exp(-1.030+0.076X_1-0.172X_2+0.991X_3+44.510X_4\\&+0.169X_1X_2-12.350X_1X_4-0.216X_2X_3-1.597X_2X_4-16.935X_3X_4)\end{aligned}}{\begin{aligned}&1+\exp(-1.030+0.076X_1-0.172X_2+0.991X_3+44.510X_4\\&+0.169X_1X_2-12.350X_1X_4-0.216X_2X_3-1.597X_2X_4-16.935X_3X_4)\end{aligned}} \quad 4\text{-}2$$

Given constant values for the primary factors X_1, X_2, X_3, and X_4, the probability of

successfully identifying the target in the images is predicted by $\hat{p}$.

4.6 Cross Validation

A cross validation study was used to compare the performance of various versions of the

logistic regression model. From the original dataset of 54,540 points, two thirds of the

records from each image set was randomly selected to create the modeling dataset, and

the remaining one third of the records from each design point was used as a validation dataset. The process is displayed in Figure 4- 2.
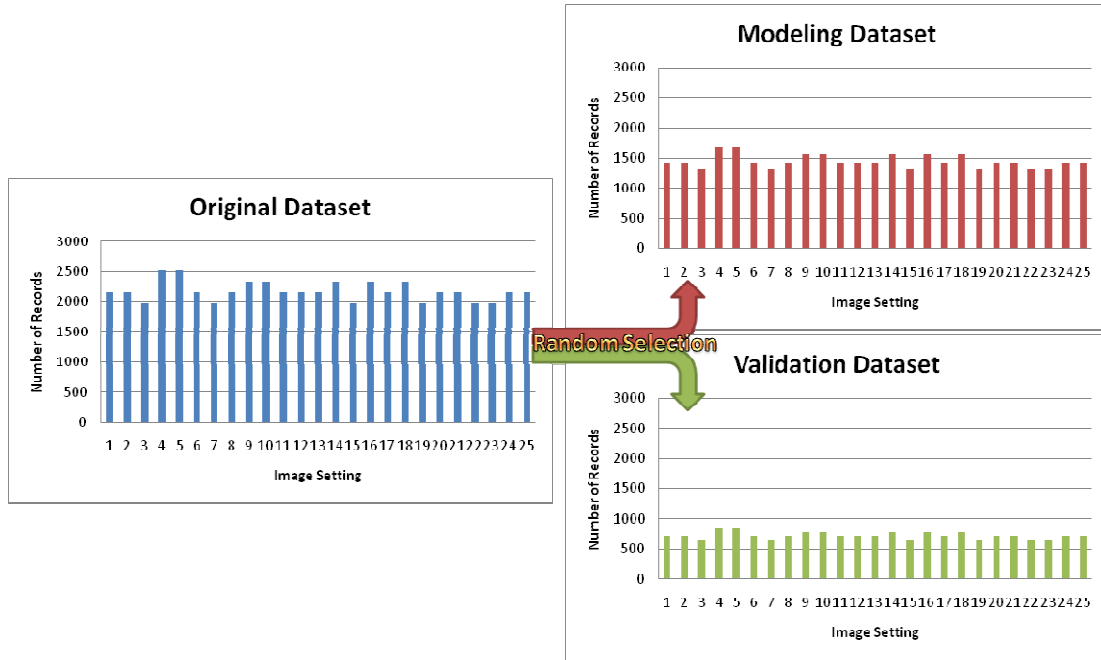
Figure 4- 2 Formation of modeling and validating datasets

Using the modeling dataset, several model structures were considered including primary factors only, primary factors with two term interactions minus the contrast-spatial resolution, primary factors with all two term interactions, and primary factors with all interactions. Each model was used to get an estimate of the probability of successfully completing the recognition task of the validating dataset. The difference between the empirical value and the predicted values are calculated at each image setting. The process was repeated 100 times and the results are shown in Figure 4- 3 through Figure 4-6 and summarized in Figure 4- 7.
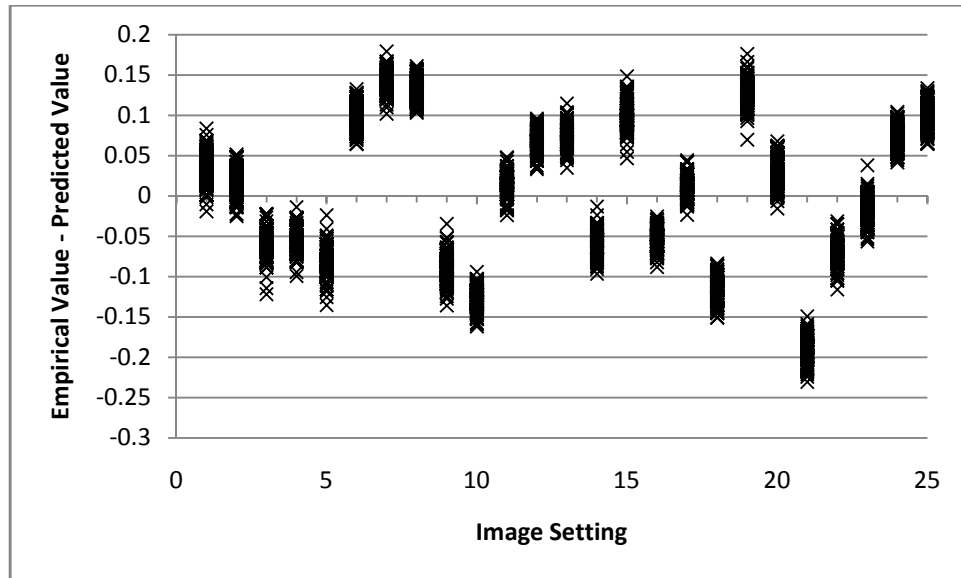
Figure 4- 3 Main effects only
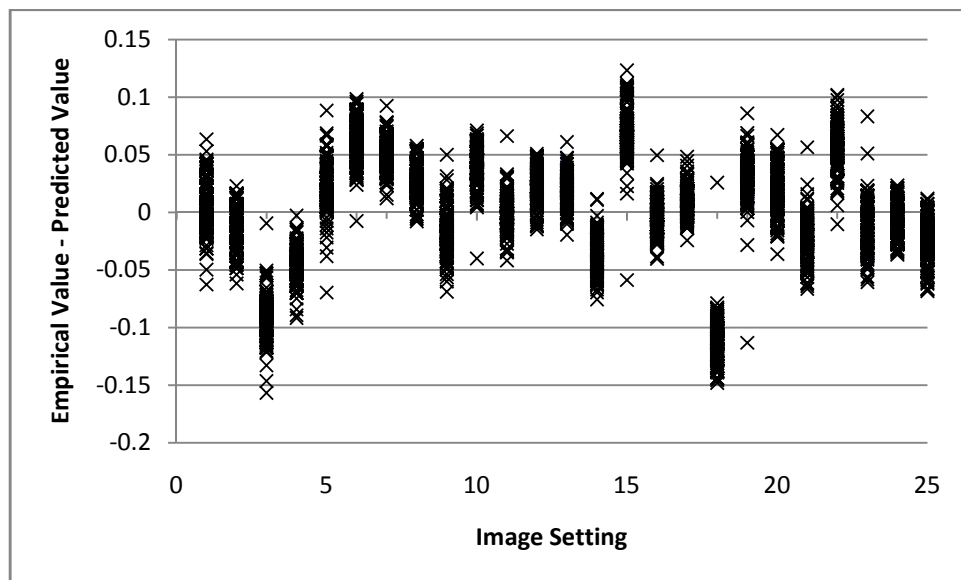
Figure 4- 4 Main effects + all two term interactions

100
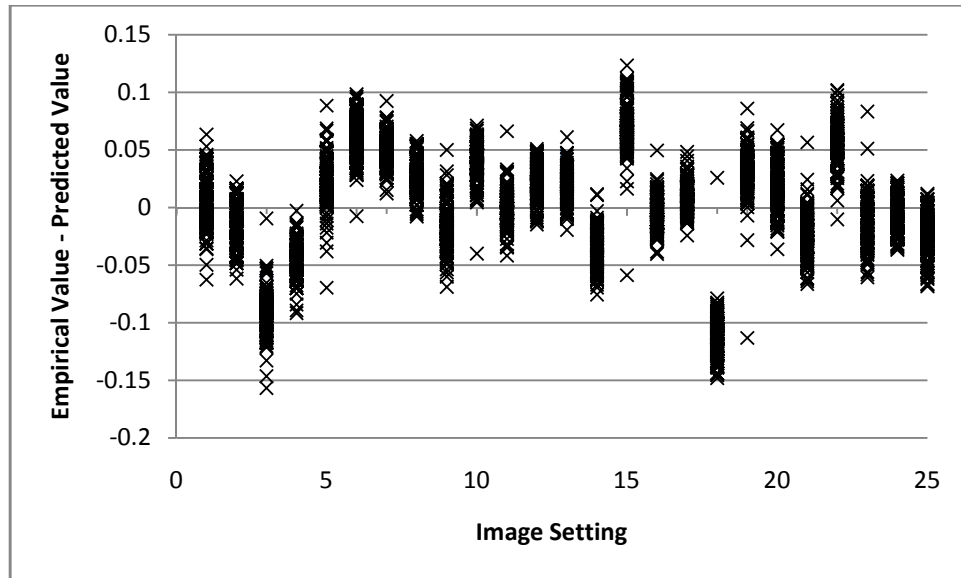
Figure 4- 5 Main effects + all two term interactions - contrast/spatial resolution interaction
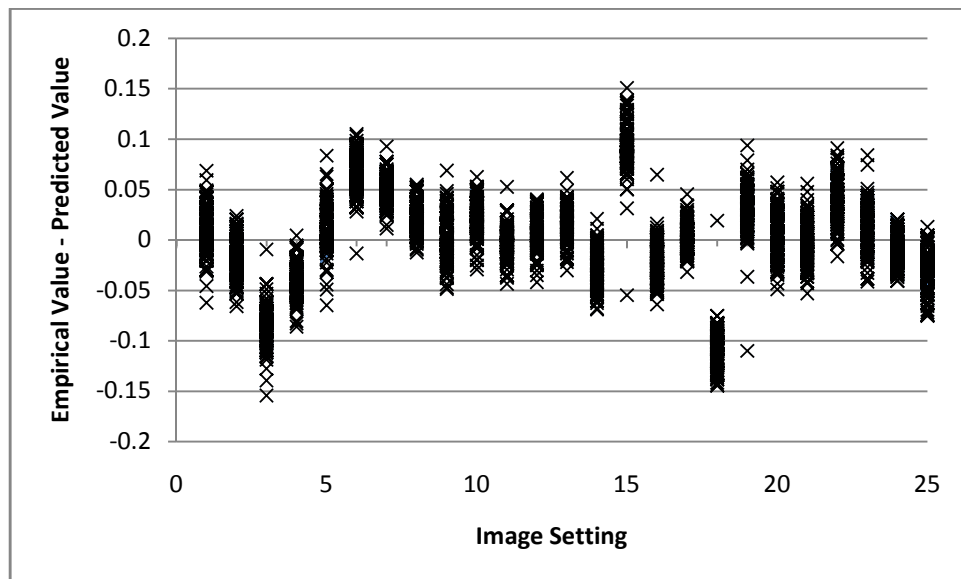
Figure 4- 6 Main effects +all two term interactions
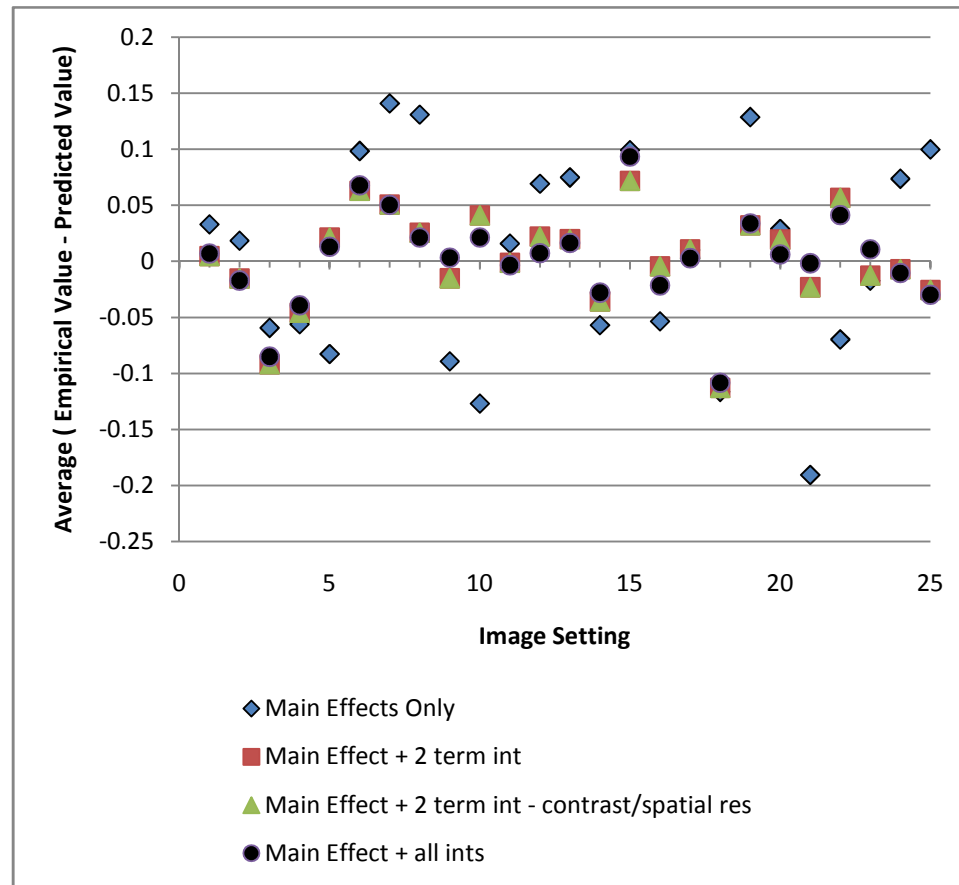
Figure 4- 7 Average deviation from observed values

The main effect plus 2 term interactions as well as subsequent models with additional parameters show significant improvement upon the main effect only model. The average greatest deviation over 100 trials from the observed data and the model incorporating main effects plus two term interactions was 11.3%. The data also shows that the main effect plus all interaction model had an average greatest deviation of 10.8%. Since the model with additional terms did not offer a substantial gain over models with less parameters, it was discarded.

4.7 Model Deviance and Partial Deviance

When creating a logistical regression model, the model deviance and partial deviance can be informative tests in determining the number factors contributing to the model fit. The deviance of a fitted model determines the relationship of the fitted model to the model that fits all n observations perfectly, otherwise known as the saturated model (Neter, Kutner, Nachtsheim, & Wasserman, 1996). The partial deviance is the difference between the model deviances for two fitted models and is used to determine if a reduced fitted model is comparable to a larger model. When the partial deviance is small, the reduced parameter model provides a similar fit to that of the larger model (Neter, Kutner, Nachtsheim, & Wasserman, 1996). When the number of data points, n, is reasonably large, as in our case, the partial deviance follows approximately a chi-squared distribution with p-q degrees of freedom; where p is the number of parameters in the larger model, and q the number of parameters in the subset model.

The first test is to determine if the any of the primary factors X_i, do not contribute to the model fit; or in other words, do $\beta_q = \beta_{q+1} = \ldots = \beta_{p-1} = 0$? A partial deviance test was conducted between the null model, a model that simply relies on a constant, to the expanded modeling incorporating the primary factors.

The selected model, shown in Equation 4-2, incorporated all the primary factors plus two term interactions less contrast- spatial resolution interactions.

$$DEV(X_0, X_1, \ldots, X_9) = 68{,}979.70$$

Comparing this model deviance, in a partial deviance test, to that of the null model where $DEV(X_0) = 73,057.14$, we can see a significant improvement to the model fit.

$$DEV(X_1, \ldots, X_9 | X_0) = 73,057.14 - 68,979.70 = 4,077.44$$

With a chi-square critical value of $\chi^2_{.95;9} = 16.92$, we can strongly reject the null hypothesis that $\beta_1 = \beta_2 = \ldots = \beta_9 = 0$.

A further look at the partial deviance between the model with primary factors plus all two term interactions versus the subset model used in this study shows the additional contrast-spatial resolution interaction term, corresponding to the coefficient β_{10}, does not provide additional improvement on the model fit.

$$DEV(X_{10} | X_0, X_1, \ldots, X_9) = 68,979.70 - 68,979.70 = 0$$

With a chi-square critical value of $\chi^2_{.95;1} = 3.84$, we can accept the null hypothesis that $\beta_{10} = 0$.

4.8 Informal Goodness of Fit Test

For a fitted multiple logistic regression model to be appropriate, the shape of the estimated response function must be monotonic and sigmoidal; key properties of a logistic response function. To perform an Informal Goodness of Fit Examination records with similar fitted values, $\hat{\pi}$, are grouped into a number of classes (typically between 5 and 10) with approximately the same number of n observations. Within each class, the estimated proportion of 1s, denoted by p_j, is calculated for all n. These values are then plotted against the midpoint of the fitted values for each class. Table 4- 3 and Figure 4- 8

display the Informal Goodness of Fit data, using five classes, for the selected human

perception model.

Table 4- 3 Informal Goodness of Fit Test with 5 Classes

Class j	$\hat{\pi}$ Interval		Midpoint	n_j	p_j
1	0.222 ,	0.507	0.364	10912	0.409
2	0.507 ,	0.562	0.534	10904	0.532
3	0.562 ,	0.671	0.617	10908	0.612
4	0.671 ,	0.724	0.698	10916	0.736
5	0.724 ,	0.779	0.751	10900	0.749
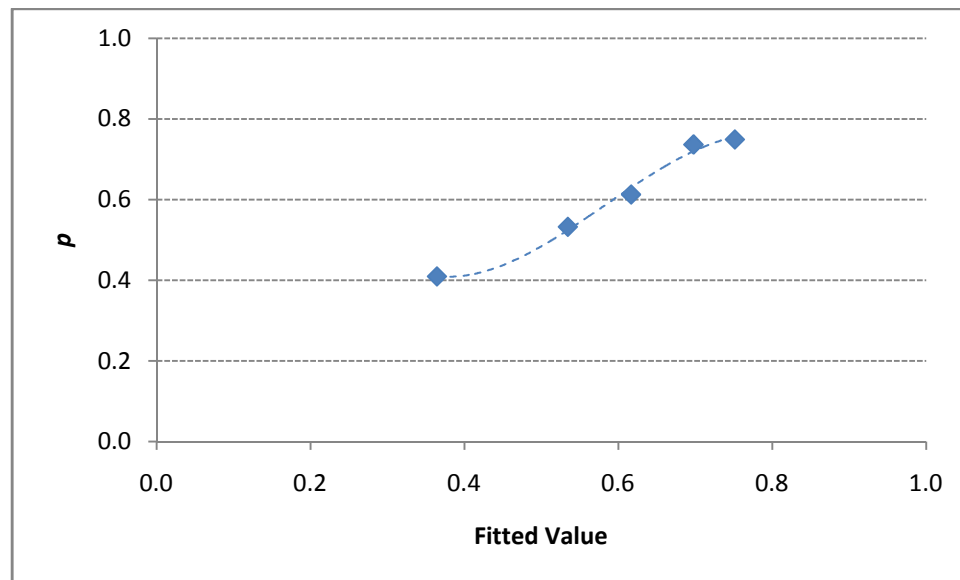
Figure 4- 8 Diagnostic plot of estimated proportions with 5 classes

Figure 4- 8 clearly indicates the model is monotonic, and sigmoidal in nature. Expanding

the Informal Goodness of Fit Test to seven classes yields the following result shown in

Table 4- 4 and Figure 4- 9.

Table 4- 4 Informal Goodness of Fit Test using 7 Classes

Class j	$\hat{\pi}$ Interval		Midpoint	n_j	p_j
1	0.222 ,	0.486	0.354	7798	0.380
2	0.486 ,	0.546	0.516	7790	0.522
3	0.546 ,	0.570	0.558	7792	0.536
4	0.570 ,	0.671	0.621	7796	0.593
5	0.671 ,	0.719	0.695	7784	0.735
6	0.719 ,	0.736	0.727	7792	0.738
7	0.736 ,	0.779	0.757	7788	0.750
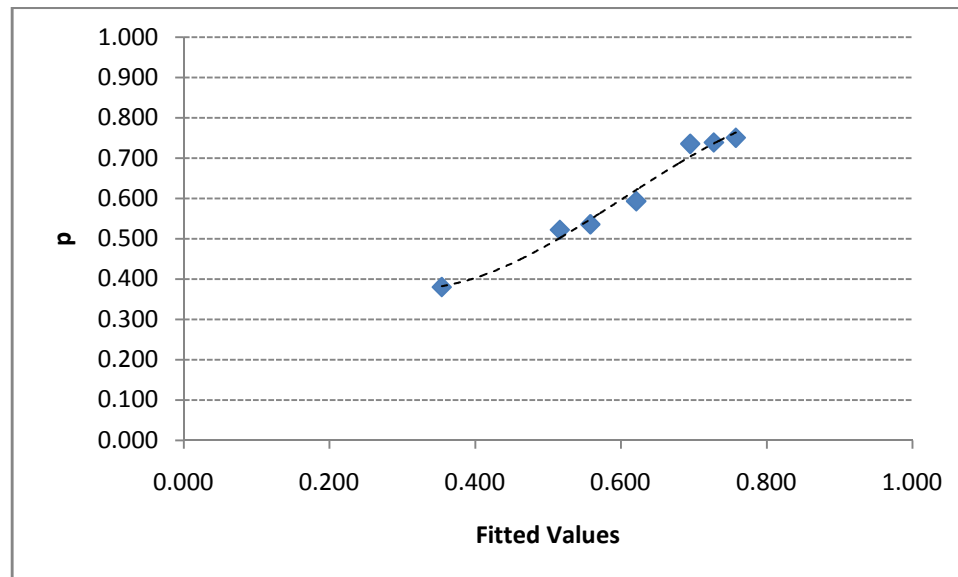
Figure 4- 9 Diagnostic plot of estimated proportions using 7 classes

Again, Figure 4- 9 suggests that a monotonic, sigmoidal relationship is tenable.

4.9 Chi-Square Goodness of Fit Test

The Informal Goodness of Fit Test can be extended into a formal Chi-Square Goodness

of Fit Test provided the observations are independent and the sample size is large. This

test provides the ability to detect large departures from the logistic response function.

Similarly, to the Informal Goodness of Fit Test, the records are again divided into classes

of approximately equal size with similar fitted values, $\hat{\pi}$. The number of observed

successes (1's) and failures (0's) are denoted by O_{j1} and $O_{j0,}$ respectively. If the logistic

response function is appropriate, the expected number of successes within a class will be

equal to the sum of the fitted values for that class; likewise, the number of failures will be

equal to the sum of $1 - \hat{\pi}$. This leads to the Chi-Square Goodness of Fit Test statistic:

$$\chi^2 = \sum_{i=1}^{c} \sum_{k=0}^{1} \frac{\left(O_{jk} - E_{jk}\right)^2}{E_{jk}} \qquad \qquad 4\text{-}3$$

with decision rules:

If $X^2 \leq \chi^2(1 - \alpha; c - 2)$, conclude H_0, logistic response appropriate
If $X^2 > \chi^2(1 - \alpha; c - 2)$, conclude H_a, logistic response not appropriate

The classes, observed and expected number of successes and failures for the calculation

of the test statistic are displayed in Table 4- 5.

Table 4- 5 Goodness of Fit Test

Class j	$\hat{\pi}$ Interval	n_j	Number of Failures		Number of Successes	
			Observed O_{j0}	Expected $\sum 1 - \hat{\pi}$	Observed O_{j1}	Expected $\sum \hat{\pi}$
1	0.222 , 0.507	10912	6447	6426.54	4465	4485.46
2	0.507 , 0.562	10904	5101	5004.68	5803	5899.32
3	0.562 , 0.671	10908	4230	4098.98	6678	6809.02
4	0.671 , 0.724	10916	2878	3139.85	8038	7776.16
5	0.724 , 0.779	10900	2739	2724.96	8161	8175.04

The test statistic for the selected human perception model is calculated as:

$$X^2 = \frac{(6447 - 6426.54)^2}{6426.54} + \frac{(4465 - 4485.46)^2}{4485.46} + \cdots + \frac{(2739 - 2724.96)^2}{2724.96}$$

$$+ \frac{(8161 - 8175.04)^2}{8175.04} = 41.04$$

The critical value is found to be $\chi^2_{.95;3} = 7.81$, thus the null hypothesis of the logistic

response function being appropriate is rejected. The associated p-value with this test is

6.40 x 10^{-9}.

4.10 Deviance Goodness of Fit Test

Given a large sample size, n, the model deviance, $DEV(X_0, X_1, \ldots, X_{p-1})$, will follow

approximately a chi-square distribution with $n - p$ degrees of freedom if the logistic

response function is correct. The decision rules for the deviance goodness of fit test are:

If $DEV(X_0, X_1, \ldots, X_{p-1}) \leq \chi^2(1 - \alpha; n - p)$, conclude H_0 , logistic response

appropriate

If $DEV(X_0, X_1, \ldots, X_{p-1}) > \chi^2(1-\alpha; n-p)$, conclude H_a, logistic response not appropriate

The deviance of the selected human perception model is found to be:

$$DEV(X_0, X_1, \ldots, X_9) = 68,979.7$$

With $n = 54540$ and $p = 10$, the critical value is found to be $\chi^2_{.95;54530} = 55,074.33$, and thus the null hypothesis of the logistic response function being appropriate is rejected.

4.11 Fitted Values and Confidence Intervals

Given the estimated parameters for the selected model, the estimated logistic response function can be expressed as:

Using the logistic regression model found in Equation 4-2, $\hat{p}$ is the estimate of the probability a user will successfully complete a recognition task given an image's values of contrast (x_1), brightness (x_2), spatial resolution (x_3), and nonuniformity (x_4). As an example, consider an image with a contrast $x_1 = 0.40$, brightness $x_2 = 0.50$, spatial resolution $x_3 = 0.33$, and nonuniformity $x_4 = 0.03$. $\hat{p}$ is calculated as:

$$\hat{p} = \frac{\exp(-1.03 + 0.076*0.4 - 0.172*0.5 + 0.991*0.33 + 44.51*0.03 + 0.169*0.4*0.5 - 12.35*0.4*0.3 - 0.216*0.5*0.33 - 1.597*0.5*0.03 - 16.935*0.3*0.03)}{1 + \exp(-1.03 + 0.076*0.4 - 0.1720.5 + 0.991*0.33 + 44.51*0.03 + 0.169*0.4*0.5 - 12.35*0.4*0.3 - 0.216*0.5*0.33 - 1.597*0.5*0.03 - 16.935*0.3*0.03)}$$

$$= 0.545$$

With an estimated regression function there is uncertainty in the parameters. This uncertainty leads to uncertainty in the fitted value, $\hat{p}$. One way to capture this uncertainty is in the form of a confidence interval about the fitted value. The lower, L, and upper, U, $(1-\alpha)\%$ confidence interval values for $\hat{p}$ are found by:

$$L = \frac{\exp(b'X - z_{(1-\alpha/2)}\sqrt{X's^2\{b\}X})}{1+\exp(b'X - z_{(1-\alpha/2)}\sqrt{X's^2\{b\}X})} \qquad \text{4-4}$$

$$U = \frac{\exp(b'X + z_{(1-\alpha/2)}\sqrt{X's^2\{b\}X})}{1+\exp(b'X + z_{(1-\alpha/2)}\sqrt{X's^2\{b\}X})} \qquad \text{4-5}$$

where b is the vector of regression coefficients provided in Table 4- 2;

X is the vector of predictor variable terms, to include interactions terms:

$\{1, x_1, x_2, x_3, x_4, x_1x_2, x_1x_4, x_2x_3, x_2x_4, x_3x_4, \}$;

$z_{(1-\alpha/2)}$ is the inverse of the standard normal cumulative distribution at $(1-\alpha/2)\%$;

and $s^2\{b\}$ is the variance-covariance matrix for the regression parameters found to be:

$$s^2\{b\} =$$

0.020	-0.004	-0.001	-0.041	-0.280	0.000	0.082	0.001	0.011	0.370
-0.004	0.002	0.000	0.008	0.051	0.000	-0.020	0.000	-0.001	-0.068
-0.001	0.000	0.000	0.001	0.002	0.000	0.000	0.000	0.000	0.003
-0.041	0.008	0.001	0.117	0.521	0.000	-0.135	-0.003	-0.018	-1.038
-0.280	0.051	0.002	0.521	5.010	0.008	-1.472	0.000	-0.207	-6.288
0.000	0.000	0.000	0.000	0.008	0.000	-0.002	0.000	0.000	-0.006
0.082	-0.020	0.000	-0.135	-1.472	-0.002	0.501	0.001	0.058	1.510
0.001	0.000	0.000	-0.003	0.000	0.000	0.001	0.001	0.000	-0.030
0.011	-0.001	0.000	-0.018	-0.207	0.000	0.058	0.000	0.012	0.173
0.370	-0.068	0.003	-1.038	-6.288	-0.006	1.510	-0.030	0.173	15.577

The variance-covariance matrix is calculated using statistical computer programs and will not be discussed further here. Please refer to work by Neter et al (Neter, Kutner, Nachtsheim, &Wasserman, 1996).

For the considered example of contrast $x_1 = 0.40$, brightness $x_2 = 0.50$, spatial resolution $x_3 = 0.33$, and nonuniformity $x_4 = 0.03$, the lower and upper 95% confidence bounds for $\hat{p} = 0.545$ can be calculated as:

$$\boldsymbol{b'X} = \begin{bmatrix} -1.03 \\ 0.076 \\ -0.172 \\ 0.991 \\ 44.510 \\ 0.169 \\ -12.350 \\ -0.216 \\ -1.597 \\ -16.935 \end{bmatrix}' \begin{bmatrix} 1 \\ 0.40 \\ 0.50 \\ 0.33 \\ 0.03 \\ 0.20 \\ 0.01 \\ 0.17 \\ 0.01 \\ 0.01 \end{bmatrix} = 0.1835; \quad \boldsymbol{X's^2\{b\}X} = \begin{bmatrix} 1 \\ 0.40 \\ 0.50 \\ 0.33 \\ 0.03 \\ 0.20 \\ 0.01 \\ 0.17 \\ 0.01 \\ 0.01 \end{bmatrix}' \boldsymbol{s^2\{b\}} \begin{bmatrix} 1 \\ 0.40 \\ 0.50 \\ 0.33 \\ 0.03 \\ 0.20 \\ 0.01 \\ 0.17 \\ 0.01 \\ 0.01 \end{bmatrix} = 0.0015;$$

$$z_{(1-0.05/2)} = z_{(0.975)} = 1.96;$$

Hence:

$$L = \frac{\exp(0.1835 - 1.96\sqrt{0.0015})}{1 + \exp(0.1835 - 1.96\sqrt{0.0015})} = 0.526 \quad \text{and}$$

$$U = \frac{\exp(0.1835 + 1.96\sqrt{0.0015})}{1 + \exp(0.1835 + 1.96\sqrt{0.0015})} = 0.565$$

Chapter 5: Summary and Conclusions

5.1 Summary of Model Fit

The chosen model function to estimate the probability of successfully identifying the target utilizes the main effects (contrast, brightness, spatial resolution, and noise) plus two term interactions less the spatial resolution/contrast interaction term. Through a cross validation study, this model's prediction never deviated more than approximately 11% from the observed data. A more complex model, utilizing all interaction terms, only improved the model fit by less than 1%.

Of all the models compared in this study, the selected model was chosen because it was the simplest form (least amount of terms) while offering the most accurate results. The selected function showed significant improvement over a constant model as indicated by the partial deviance test. In addition, the Informal Goodness of Fit test suggests that the response function follows a sigmoidal and monotonic shape, key indicators of the validity of using a logistic response function to model binary response data. Although further diagnostic testing, using the Chi-Squared Goodness of Fit Test and the Deviance Goodness of Fit test, debunk the use of a logistic response function to characterize the data, there is no one statistical test that offers concrete evidence. With the use of confidence intervals, the uncertainty in the model can be characterized and therefore the failed goodness of fit tests should not be justification to eliminate the model.

5.2 Recommendation for Model Use in NFPA 1801

One of the most important findings of this study was that the interactions between contrast, spatial resolution, brightness, and noise in an image have a greater effect on

112

human perception than any one variable by itself. When considering test methods to adequately characterize the ability of a TIC to produce a quality image, interactions must be accounted for.

The predictions made by the fitted model will be more conservative when using the lowest primary factors measurements in the NIST test methods. As discussed in 1.3.2 Bench-Scale Test Methods Developed by NIST, contrast, brightness, spatial resolution, and nonuniformity (noise) are calculated from many images captured, from thermal targets over a range of temperatures, and the measurements will vary. Since the test methods are designed to investigate temperatures indicative of actual scenarios, the TIC must be required to provide adequate image quality over the entire range. The method by which the model should be used is outlined below. For additional details on these procedures refer to the draft of NFPA 1801 [NFPA 1801 2008].

1. Perform Image Recognition Test (spatial resolution). Calculate the contrast and CTF at each numbered step (predetermined bar frequency), from lowest to highest step number, on the spatial resolution target shown in Figure 1- 2. Also, calculate the average brightness of the pixels used in the contrast calculation.

    a. The contrast calculated at step 2 is X_1 and is held constant.

    b. The brightness calculated at step 2 is X_2 and is held constant.

    c. Convert the CTF measurement, using the bar frequency at each step, to the MTF as defined by the procedures outlined in this work in Table 3- 2. The result is the spatial resolution, X_3 and will vary in value from step to step.

2. The nonuniformity test is independent. It is calculated over a temperature range from 0 to 260C. The maximum nonuniformity at any of the set point temperatures is deemed the nonuniformity of the imaging system as a conservative estimate for X_4 in the model. This value is held constant.

3. For the above data collected at each numbered step on the Image Recognition Test target, plug in the values for contrast (X_1), brightness (X_2), spatial resolution (X_3), and noise (X_4).

    a. Use the model to calculate $\hat{p}$ at each numbered step.

4. Note that the Nonuniformity Test in step 2 need be conducted only one time. The noise value (X_4), can be used in all further image quality testing.

These procedures, as outlined in the draft form of NFPA 1801, are conducted over a range of temperatures. NIST and the NFPA technical committee will have to make a decision as to what value for $\hat{p}$ indicates acceptable performance by a TIC.

5.3 Future Work

This study was the first attempt at trying to model the relationship between TIC image quality and fire fighter task performance and therefore there is an extensive list of future possibilities to further improve the model. One suggestion would be to create a more diverse set of images expanding further into the TIC applications such as images incorporating flames, water mist, steam, and smoke. Expanding from still images, three dimensional images of a scene could provide a user interactive test offering the ability of the test subjects to scan a 3-D image. Incorporating dynamic motion videos, could further the realism of the imagery set.

The statistical analysis of the dataset could also be expanded. The logistic regression model used to fit the data found in the perception experiment is a class of generalized linear models. This approach transforms the response by use of a link function, which relates the linear combination of the predictor variables to the mean response. One may consider an approach using a generalized additive model. The generalized additive model also considers a link function, but rather than a linear combination of the predictor values, it considers a linear combination of functions of the predictor values.

Although the user and robustness factors were not considered in the creation of this model, as they cannot be controlled in real-world scenarios, their impact and the improvement they may bring to the model could be investigated. Such an investigation may lead to insights and improvements in system use and training.

Appendices

Appendix A

Pristine ID	Robustness Factors - (Levels)			
	Target Position (6)	Hazard Type (5)	Clutter (2)	Scene (2)
1	Center (C)	1	Small	Office
2	Upper Left (UL)	1	Small	Office
3	Upper Right (UR)	1	Small	Office
4	Lower Left (LL)	1	Small	Office
5	Lower Right (LR)	1	Small	Office
6	No Target (N)	1	Small	Office
7	Center (C)	2	Small	Office
8	Upper Left (UL)	2	Small	Office
9	Upper Right (UR)	2	Small	Office
10	Lower Left (LL)	2	Small	Office
11	Lower Right (LR)	2	Small	Office
12	No Target (N)	2	Small	Office
13	Center (C)	3	Small	Office
14	Upper Left (UL)	3	Small	Office
15	Upper Right (UR)	3	Small	Office
16	Lower Left (LL)	3	Small	Office
17	Lower Right (LR)	3	Small	Office
18	No Target (N)	3	Small	Office
19	Center (C)	4	Small	Office
20	Upper Left (UL)	4	Small	Office
21	Upper Right (UR)	4	Small	Office
22	Lower Left (LL)	4	Small	Office
23	Lower Right (LR)	4	Small	Office
24	No Target (N)	4	Small	Office
25	Center (C)	5	Small	Office
26	Upper Left (UL)	5	Small	Office
27	Upper Right (UR)	5	Small	Office
28	Lower Left (LL)	5	Small	Office
29	Lower Right (LR)	5	Small	Office
30	No Target (N)	5	Small	Office
31	Center (C)	1	Large	Office
32	Upper Left (UL)	1	Large	Office
33	Upper Right (UR)	1	Large	Office
34	Lower Left (LL)	1	Large	Office
35	Lower Right (LR)	1	Large	Office
36	No Target (N)	1	Large	Office
37	Center (C)	2	Large	Office

38	Upper Left (UL)	2	Large	Office
39	Upper Right (UR)	2	Large	Office
40	Lower Left (LL)	2	Large	Office
41	Lower Right (LR)	2	Large	Office
42	No Target (N)	2	Large	Office
43	Center (C)	3	Large	Office
44	Upper Left (UL)	3	Large	Office
45	Upper Right (UR)	3	Large	Office
46	Lower Left (LL)	3	Large	Office
47	Lower Right (LR)	3	Large	Office
48	No Target (N)	3	Large	Office
49	Center (C)	4	Large	Office
50	Upper Left (UL)	4	Large	Office
51	Upper Right (UR)	4	Large	Office
52	Lower Left (LL)	4	Large	Office
53	Lower Right (LR)	4	Large	Office
54	No Target (N)	4	Large	Office
55	Center (C)	5	Large	Office
56	Upper Left (UL)	5	Large	Office
57	Upper Right (UR)	5	Large	Office
58	Lower Left (LL)	5	Large	Office
59	Lower Right (LR)	5	Large	Office
60	No Target (N)	5	Large	Office
61	Center (C)	1	Small	Living
62	Upper Left (UL)	1	Small	Living
63	Upper Right (UR)	1	Small	Living
64	Lower Left (LL)	1	Small	Living
65	Lower Right (LR)	1	Small	Living
66	No Target (N)	1	Small	Living
67	Center (C)	2	Small	Living
68	Upper Left (UL)	2	Small	Living
69	Upper Right (UR)	2	Small	Living
70	Lower Left (LL)	2	Small	Living
71	Lower Right (LR)	2	Small	Living
72	No Target (N)	2	Small	Living
73	Center (C)	3	Small	Living
74	Upper Left (UL)	3	Small	Living
75	Upper Right (UR)	3	Small	Living
76	Lower Left (LL)	3	Small	Living
77	Lower Right (LR)	3	Small	Living
78	No Target (N)	3	Small	Living
79	Center (C)	4	Small	Living
80	Upper Left (UL)	4	Small	Living
81	Upper Right (UR)	4	Small	Living
82	Lower Left (LL)	4	Small	Living
83	Lower Right (LR)	4	Small	Living

84	No Target (N)	4	Small	Living
85	Center (C)	5	Small	Living
86	Upper Left (UL)	5	Small	Living
87	Upper Right (UR)	5	Small	Living
88	Lower Left (LL)	5	Small	Living
89	Lower Right (LR)	5	Small	Living
90	No Target (N)	5	Small	Living
91	Center (C)	1	Large	Living
92	Upper Left (UL)	1	Large	Living
93	Upper Right (UR)	1	Large	Living
94	Lower Left (LL)	1	Large	Living
95	Lower Right (LR)	1	Large	Living
96	No Target (N)	1	Large	Living
97	Center (C)	2	Large	Living
98	Upper Left (UL)	2	Large	Living
99	Upper Right (UR)	2	Large	Living
100	Lower Left (LL)	2	Large	Living
101	Lower Right (LR)	2	Large	Living
102	No Target (N)	2	Large	Living
103	Center (C)	3	Large	Living
104	Upper Left (UL)	3	Large	Living
105	Upper Right (UR)	3	Large	Living
106	Lower Left (LL)	3	Large	Living
107	Lower Right (LR)	3	Large	Living
108	No Target (N)	3	Large	Living
109	Center (C)	4	Large	Living
110	Upper Left (UL)	4	Large	Living
111	Upper Right (UR)	4	Large	Living
112	Lower Left (LL)	4	Large	Living
113	Lower Right (LR)	4	Large	Living
114	No Target (N)	4	Large	Living
115	Center (C)	5	Large	Living
116	Upper Left (UL)	5	Large	Living
117	Upper Right (UR)	5	Large	Living
118	Lower Left (LL)	5	Large	Living
119	Lower Right (LR)	5	Large	Living
120	No Target (N)	5	Large	Living
121	Upper Left (UL)	1	Small	Office
122	Upper Right (UR)	1	Small	Office
123	Lower Right (LR)	1	Small	Office
124	Center (C)	2	Small	Office
125	Upper Left (UL)	2	Small	Office
126	Lower Left (LL)	2	Small	Office
127	Center (C)	3	Small	Office
128	Lower Right (LR)	3	Small	Office
129	No Target (N)	3	Small	Office

130	Center (C)	4	Small	Office
131	Lower Left (LL)	4	Small	Office
132	No Target (N)	4	Small	Office
133	Upper Left (UL)	5	Small	Office
134	Upper Right (UR)	5	Small	Office
135	Lower Right (LR)	5	Small	Office
136	Center (C)	1	Large	Office
137	Lower Left (LL)	1	Large	Office
138	No Target (N)	1	Large	Office
139	Upper Right (UR)	2	Large	Office
140	Lower Right (LR)	2	Large	Office
141	No Target (N)	2	Large	Office
142	Upper Left (UL)	3	Large	Office
143	Upper Right (UR)	3	Large	Office
144	Lower Left (LL)	3	Large	Office
145	Upper Left (UL)	4	Large	Office
146	Upper Right (UR)	4	Large	Office
147	Lower Right (LR)	4	Large	Office
148	Center (C)	5	Large	Office
149	Lower Left (LL)	5	Large	Office
150	No Target (N)	5	Large	Office
151	Center (C)	1	Small	Living
152	Lower Left (LL)	1	Small	Living
153	No Target (N)	1	Small	Living
154	Upper Right (UR)	2	Small	Living
155	Lower Right (LR)	2	Small	Living
156	No Target (N)	2	Small	Living
157	Upper Left (UL)	3	Small	Living
158	Upper Right (UR)	3	Small	Living
159	Lower Left (LL)	3	Small	Living
160	Upper Left (UL)	4	Small	Living
161	Upper Right (UR)	4	Small	Living
162	Lower Right (LR)	4	Small	Living
163	Center (C)	5	Small	Living
164	Lower Left (LL)	5	Small	Living
165	No Target (N)	5	Small	Living
166	Upper Left (UL)	1	Large	Living
167	Upper Right (UR)	1	Large	Living
168	Lower Right (LR)	1	Large	Living
169	Center (C)	2	Large	Living
170	Upper Left (UL)	2	Large	Living
171	Lower Left (LL)	2	Large	Living
172	Center (C)	3	Large	Living
173	Lower Right (LR)	3	Large	Living
174	No Target (N)	3	Large	Living
175	Center (C)	4	Large	Living

176	Lower Left (LL)	4	Large	Living
177	No Target (N)	4	Large	Living
178	Upper Left (UL)	5	Large	Living
179	Upper Right (UR)	5	Large	Living
180	Lower Right (LR)	5	Large	Living

Appendix B Image Processing Program

Main Programs

```matlab
%This program converts the temperature output (.mat) file from the
%FLIR ThermaCam P640 to a 16-bit uncompressed image
close all
clear all

%Input a .mat file into Matlab
im=input('What file would you like to load?\n');
im1=strcat(im,'.mat');
load(im1);

im2=input('What image you want to convert?No file extension\n');

%Find image size
[ymax xmax]=size(im2);

%Find minimum and maximum temperature in file
minimum=min(im2);
minval=min(minimum);
maximum=max(im2);
maxval=max(maximum);

%Enter temperature range that produces best quality image
temp1=input('What is the minimum temp\n');
temp2=input('What is the max temp\n');

image1=zeros(ymax, xmax);

%Normalize temperature data
for i=1:xmax
    for j=1:ymax
            image1(j,i)=(im2(j,i)-minval)/(maxval-minval);
    end
end

image2=zeros(ymax,xmax);

%Create a 16-bit grayscale with temperature data
for q=1:i
    for r=1:j
        image2(r,q)=image1(r,q)*65535;
    end
end

%Solve for variables needed to adjust image to correct grayscale
p=((temp1+273.15)-minval)/(maxval-minval);
xkcd=0;
if p<0
    p=0;
    xkcd=(minval-(273.15+temp1))/(temp2-temp1);
end
```

```matlab
z=((temp2+273.15)-minval)/(maxval-minval);

%Create 16 bit image from temperature data
image3=uint16(image2);

%Adjust image to match desired gray-scale
image4=imadjust(image3,[p,z],[xkcd,1]);

%Verify image is appropriate
imshow(image4)

%Create filename
filename = strcat(im,'.png');

%Save image as 16-bit uncompressed .png file
imwrite(image4,filename,'png','BitDepth',16)
%----------------------------------------------------------------
%ImagePro is an image processing program to adjust the contrast,
%brightness, spatial resolution, and noise of an image to meet the
% 25 design points
clear all
close all
fprintf('Beginning LumImageProLoop')

%Image Counter
ii=1;
%Design Point Counter
iii=1;

%Allocate memory
conarray=zeros(4500,1);
brightarray=zeros(4500,1);
spatialarray=zeros(4500,1);
noisearray=zeros(4500,1);

%Start outerloop to loop through 180 pristine images (image filenames
are
%numerical labeled from 1 to 180)

while ii<=180

%Input Image
name=num2str(ii);
name1=strcat('image',name,'.png');
im = imread(name1);

%Convert the image to an array of numbers to manipulate
im2=double(im);

%Find the size of the array
[M N]=size(im2);

%Create an array of luminance data to describe the image as it will
appear
```

```matlab
%on the test monitors at NVL
lumimage=zeros(M,N);
for j=1:M
    for k=1:N
        if im2(j,k)>8192
        lumimage(j,k)=((1*10^-8)*((im2(j,k))^2))-
(0.0002*(im2(j,k)))+1.6159;
        elseif im2(j,k)<=8192
            lumimage(j,k) = (3*(10^(-05)))*im2(j,k)+0.0266;
        else
            fprintf('ERROR\n')
        end
    end
end

%Find the brightness of the original image in pixel intensity
bright = round(mean(mean(im2)));
%Find the corresponding luminance on NVL displays
lumbright=round(mean(mean(lumimage)));

%Find the contrast of the original image in pixel intensity
values=zeros(M,N);
for j=1:M
    for k=1:N
      values(j,k)=((im2(j,k)-bright)^2);
    end
end
contrast=sqrt(mean(mean(values)));
 %Find the corresponding contrast on NVL display
lumvalues=zeros(M,N);
for j=1:M
    for k=1:N
        lumvalues(j,k)=((lumimage(j,k)-lumbright)^2);
    end
end
lumcontrast=sqrt(mean(mean(lumvalues)));

%Loop through all 25 design points
counter=1;
while counter<=25

%Input design point parameters
if counter==1
    stdcon=900;
    lumstdcon=0.4;
    newbright=12800;
    lumnewbright=0.5015;
    Wn=0.02;
    SNR=15.0;
    LumSNR=3.0;

elseif counter==2
    stdcon=900;
    lumstdcon=0.4;
    newbright=27200;
    lumnewbright=3.6339;
```

```
    Wn=0.0366;
    SNR=20.0;
    LumSNR=5.0;

elseif counter==3
    stdcon=900;
    lumstdcon=0.4;
    newbright=33600;
    lumnewbright=6.7696;
    Wn=0.0533;
    SNR=25.0;
    LumSNR=7.0;
elseif counter ==4
    stdcon=900;
    lumstdcon=0.4;
    newbright=40000;
    lumnewbright=9.9021;
    Wn=0.07;
    SNR=30.0;
    LumSNR=9.0;
elseif counter ==5
    stdcon=900;
    lumstdcon=0.4;
    newbright=43200;
    lumnewbright=13.0346;
    Wn=0.0866;
     SNR=35.0;
    LumSNR=11.0;
elseif counter ==6
    stdcon=1500;
    lumstdcon=0.933;
    newbright=12800;
    lumnewbright=0.5015;
    Wn=0.0366;
    SNR=25.0;
    LumSNR=7.0;
elseif counter ==7
    stdcon=1500;
    lumstdcon=0.933;
    newbright=27200;
    lumnewbright=3.6339;
    Wn=0.0533;
    SNR=30.0;
    LumSNR=9.0;
elseif counter ==8
    stdcon=1500;
    lumstdcon=0.933;
    newbright=33600;
    lumnewbright=6.7696;
    Wn=0.07;
    SNR=35.0;
    LumSNR=11.0;
elseif counter ==9
    stdcon=1500;
    lumstdcon=0.933;
    newbright=40000;
    lumnewbright=9.9021;
```

```
        Wn=0.0866;
        SNR=15.0;
        LumSNR=3.0;
    elseif counter ==10
        stdcon=1500;
        lumstdcon=0.933;
        newbright=43200;
        lumnewbright=13.0346;
        Wn=0.02;
        SNR=20.0;
        LumSNR=5.0;
    elseif counter ==11
        stdcon=2000;
        lumstdcon=1.4669;
        newbright=12800;
        lumnewbright=0.5015;
        Wn=0.0533;
        SNR=35.0;
        LumSNR=11.0;
    elseif counter ==12
        stdcon=2000;
        lumstdcon=1.4669;
        newbright=27200;
        lumnewbright=3.6339;
        Wn=0.07;
        SNR=15.0;
        LumSNR=3.0;
    elseif counter ==13
        stdcon=2000;
        lumstdcon=1.4669;
        newbright=33600;
        lumnewbright=6.7696;
        Wn=0.0866;
        SNR=20.0;
        LumSNR=5.0;
    elseif counter ==14
        stdcon=2000;
        lumstdcon=1.4669;
        newbright=40000;
        lumnewbright=9.9021;
        Wn=0.02;
        SNR=25.0;
        LumSNR=7.0;
    elseif counter ==15
        stdcon=2000;
        lumstdcon=1.4669;
        newbright=43200;
        lumnewbright=13.0346;
        Wn=0.0366;
        SNR=30.0;
        LumSNR=9.0;
    elseif counter ==16
        stdcon=2500;
        lumstdcon=1.9993;
        newbright=12800;
        lumnewbright=0.5015;
        Wn=0.07;
```

```matlab
        SNR=20.0;
        LumSNR=5.0;
    elseif counter ==17
        stdcon=2500;
        lumstdcon=1.9993;
        newbright=27200;
        lumnewbright=3.6339;
        Wn=0.0866;
        SNR=25.0;
        LumSNR=7.0;
    elseif counter ==18
        stdcon=2500;
        lumstdcon=1.9993;
        newbright=33600;
        lumnewbright=6.7696;
        Wn=0.02;
        SNR=30.0;
        LumSNR=9.0;
    elseif counter ==19
        stdcon=2500;
        lumstdcon=1.9993;
        newbright=40000;
        lumnewbright=9.9021;
        Wn=0.0366;
        SNR=35.0;
        LumSNR=11.0;
    elseif counter ==20
        stdcon=2500;
        lumstdcon=1.9993;
        newbright=43200;
        lumnewbright=13.0346;
        Wn=0.0533;
        SNR=15.0;
        LumSNR=3.0;
    elseif counter ==21
        stdcon=3000;
        lumstdcon=2.5317;
        newbright=12800;
        lumnewbright=0.5015;
        Wn=0.0866;
        SNR=30.0;
        LumSNR=9.0;
    elseif counter ==22
        stdcon=3000;
        lumstdcon=2.5317;
        newbright=27200;
        lumnewbright=3.6339;
        Wn=0.02;
        SNR=35.0;
        LumSNR=11.0;
    elseif counter ==23
        stdcon=3000;
        lumstdcon=2.5317;
        newbright=33600;
        lumnewbright=6.7696;
        Wn=0.0366;
        SNR=15.0;
```

```matlab
    LumSNR=3.0;
elseif counter ==24
    stdcon=3000;
    lumstdcon=2.5317;
    newbright=40000;
    lumnewbright=9.9021;
    Wn=0.0533;
    SNR=20.0;
    LumSNR=5.0;
elseif counter ==25
    stdcon=3000;
    lumstdcon=2.5317;
    newbright=43200;
    lumnewbright=13.0346;
    Wn=0.07;
    SNR=25.0;
    LumSNR=7.0;
end

%Finding an initial guess for slope of linear point processing for
contrast
slope=stdcon/contrast;


%Finding the y-intercept d as initial guess for the amount of increase
in
%brightness
d=newbright-bright;

%Wn is the nominal cutoff frequency used in a butterworth filter
Wn = Wn*sqrt(M.^2+N.^2);
%n defines the order of the butterworth equation of the slope of the
filter
n=2;

countername=num2str(counter);

%fminsearch varies the values for the slope and d so that after the
spatial
%resolution test all three parameters of the degraded image are as
desired

slopei = slope;
%Initial guess for point processing of contrast and brightness
X0 = [slopei,d];

options=optimset('TolX',1e+00,'Tolfun',1e+00);
X = fminsearch(@Lumsearchfile, X0, options, im2, newbright, Wn, n,
contrast, bright,stdcon,lumbright,lumcontrast,lumstdcon,lumnewbright);

%Final slope and intercept values for contrast and brightness
slope=X(1);
d=X(2);
%...............................................................
...
```

```
%ConBrighta manipulates contrast/brightness
[contrastimage]= LumConbrighta(im2,slope,d,bright);


%Spatialresa adjusts the spatial resolution of the image using a
butterworth
%filter in the frequency domain.
[freqimage,Fplot,Gplot,newbright3,SR,contrastf, lumnewbright3,
lumcontrastf, Dmax]=LumSpatialresa(contrastimage,im2,Wn,n);

 %fprintf('Your adjusted image has the following parameters\n')
 %fprintf('Your new contrast is %g\n',2*lumcontrastf/32.562)
 %fprintf('Your new brightness is %g\n',lumnewbright3/32.562)
 %fprintf('Your spatial resolution is %g\n', SR)


%Getting the desired nonuniformity by adding noise

%Find the amount of noise necessary to create the desired nonuniformity
%Based on brightness
DevVar1=newbright3/SNR;
LumDevVar1=lumnewbright3/LumSNR;

%First guess
Vari = 0.01;
X0 = [Vari];
options=optimset('Tolfun',1e-06,'TolX',1e-06);
X = fminbnd(@LumNoisesearch,0,0.1,options,
freqimage,DevVar1,LumDevVar1);

%Var is the final variance needed to reach the desired nonuniformity
Var=X(1);


[noiseimage,lumDevNoise,lumnoisy]=LumNoise(freqimage,Var);

%Final Nonuniformity
LumSNR1=lumnewbright3/lumDevNoise;

% fprintf('You deviation of noise is %g\n',DevNoise)

%Minor adjustment to get image back to 640x 480
%Add one more col and row
noiseimage1=double(noiseimage);
[q,p]=size(noiseimage1);
toprow = noiseimage1(1,:);
finalimage1 = [toprow;noiseimage1];
[q,p]=size(finalimage1);
lastcol = finalimage1(:,p);
finalimage = [finalimage1, lastcol];


%Put numbers back into 16-bit image
finalimage=uint16(finalimage);
```

```matlab
%Variable Output Names
Wn1=num2str(Wn/sqrt(M.^2+N.^2));
n1=num2str(n);


Lumnewbright31=num2str(lumnewbright3);
SR1=num2str(SR);
LumDevNoise1=num2str(lumDevNoise);


Lumcontrastf1=num2str(lumcontrastf);



finalimage(:,:,2) = finalimage(:,:);
finalimage(:,:,3) = finalimage(:,:,1);



%Write the file as a .tif 16-bit gray scale image with NO Compression
 imwrite(finalimage,finalname,'tif','Compression','none')



 conarray(iii,1)=(2*lumcontrastf)/32.562;
 brightarray(iii,1)=lumnewbright3/32.562;
 spatialarray(iii,1)=SR;
 noisearray(iii,1)=LumSNR1;



 iii=iii+1;
 counter=counter+1;
end

ii=ii+1;
fprintf('Image %g\n',ii)


end
%-------------------------------------------------------------------
%Find slope and intercept values needed to adjust contrast and
brightness
%to desired levels
function Y = Lumsearchfile(X, im2,newbright, Wn, n, contrast, bright,
stdcon, lumbright, lumcontrast, lumstdcon, lumnewbright)

slope = X(1);
d = X(2);

%Manipulates contrast/brightness
[contrastimage]= LumConbrighta(im2,slope,d,bright);

%Adjusts the spatial resolution of the image using a butterworth
filter.
[freqimage,Fplot,Gplot,newbright3,SR,contrastf, lumnewbright3,
lumcontrastf, Dmax]=LumSpatialresa(contrastimage,im2,Wn,n);

%Calculate error and minimize with fminsearch
Y = (lumcontrastf-lumstdcon)^2 + (lumnewbright - lumnewbright3)^2;
```

129

```
end

%-------------------------------------------------------------------
%Use linear point processing to adjust contrast and brightness
function [contrastimage]= LumConbrighta(im2,slope,d,bright)

%Adjust contrast and brightness and output image
[M N]=size(im2);
im3=zeros(M,N);
for j=1:M
    for k=1:N
      im3(j,k)=(slope*(im2(j,k)-bright))+(bright+d);
    end
end

%Convert contrast/brightness adjusted pixels back into an image
contrastimage=uint16(im3);
%-------------------------------------------------------------------
%Butterworth filter is multiplied by the forward Fourier Transform of
image
function [freqimage,Fplot,Gplot,newbright3,SR,contrastf, lumnewbright3,
lumcontrastf, Dmax]=LumSpatialresa(contrastimage,im2,Wn,n)

%Convert image to grayscale numbers
im5 = double(contrastimage);

%Find size of image
[M1,N1] = size(im5);

%Subtrast 1 row and 1 column to create 2-d array with odd dimensions
Mlogic = ceil(M1/2);
Nlogic = ceil(N1/2);
if Mlogic==M1/2
    im5 = im5(1:M1-1,:);
end
if Nlogic==N1/2
    im5 = im5(:,1:N1-1);
end

%Find size of new image
[M,N] = size(im5);

%Take 2-D fourier transform of the image
F = fft2(im5);

% Rearrange the quadrants so zero frequency is located at the center
% Need for plotting magnitude spectrum and applying filter
F1=fftshift(F);

%Plot magnitude spectrum of frequencies
Fplot = uint16(F1);

%Create a array of numbers for mapping 2-d space for applying filter
```

130

```matlab
u = 0:(M-1); % Create a vector u from zero to M-1
v = 0:(N-1); % Create a vector v from zero to N-1

%The fourier transform is symmetrical about the nyquist frequency, or
M/2
%the second half is often considered to be the response of negative
%frequencies, thus the following steps create these negative values

idx=find(u>M/2); % Create a vector that is the index(position) of the
second half of the vector u
u(idx)=u(idx)-(M-1); % Replace the second half of u with negative
values
idy=find(v>N/2); % create a vector that is the index of the second half
of the vector v
v(idy)=v(idy)-(N-1); % Replace the second half of v with negative
values

% Create a 2-D map of all possible combinations of u and v.
%This map of numbers will be used to identify the distance from the
zero
%frequency to apply filter
[V,U]=meshgrid(v,u);

% Solve for D which is essentially the radius of a point in the fourier
% transform
D=sqrt(U.^2+V.^2);
Dmax=max(max(D));


%Create filter
H = 1./(1+(D./Wn).^(2*n));
%Apply filter by multiplying by fourier transform of image
G = H.*F;

%Calculate the MTFA of the butterworth filter
SR = quad(@(x)Lumfiltercurve(x,Wn,n),0,Dmax)./(2*Dmax);

%Find inverse fourier transform of image
image=real(ifft2(double(G)));

%convert the filtered fourier back into an image
freqimage=uint16(image);

%Plot magnitude spectrum of filtered image
G1=fftshift(G);
Gplot=uint16(G1);


newfreq=double(freqimage);

%Create Luminance array to recalculate contrast and brightness
lumnewfreq=zeros(M,N);

for j=1:M
    for k=1:N
```

```matlab
        if newfreq(j,k)>8192
        lumnewfreq(j,k)=((1*10^-8)*((newfreq(j,k))^2))-
(0.0002*(newfreq(j,k)))+1.6159;
        elseif newfreq(j,k)<=8192
            lumnewfreq(j,k) = (3*(10^(-05)))*newfreq(j,k)+0.0266;
        else
            fprintf('ERROR\n')
        end
    end
end

%Repeat contrast and brightness measurements

newbright3=mean(mean(newfreq));
lumnewbright3=mean(mean(lumnewfreq));

values=zeros(M,N);
for j=1:M
    for k=1:N
      values(j,k)=((newfreq(j,k)-newbright3)^2);
    end
end
contrastf=sqrt(mean(mean(values)));

lumvalues=zeros(M,N);

for j=1:M
    for k=1:N
      lumvalues(j,k)=((lumnewfreq(j,k)-lumnewbright3)^2);
    end
end
lumcontrastf=sqrt(mean(mean(lumvalues)));

%----------------------------------------------------------------
%Function finds the amount of noise needed to create desired
nonuniformity
function Y = LumNoisesearch(X, freqimage,DevVar1, LumDevVar1)

Var = X(1);

[noiseimage,LumDevNoise,noisy]=LumNoise(freqimage,Var);

Y = (LumDevNoise-LumDevVar1)^2;

end
%----------------------------------------------------------------
%Adds noise to image
function [noiseimage,LumDevNoise,lumnoisy]=LumNoise(freqimage,Var)
[X,Z] = size(freqimage);

freqimage1=double(freqimage);

lumfreqimage1=zeros(X,Z);
%Calculate luminance array as seen on NVL displays
```

132

```matlab
for j=1:X
    for k=1:Z
        if freqimage1(j,k)>8192
        lumfreqimage1(j,k)=((1*10^-8)*((freqimage1(j,k))^2))-
(0.0002*(freqimage1(j,k)))+1.6159;
        elseif freqimage1(j,k)<=8192
            lumfreqimage1(j,k) = (3*(10^(-05)))*freqimage1(j,k)+0.0266;
        else
            fprintf('ERROR\n')
        end
    end
end

%Add Noise to the contrast/brightness/spatial resolution adjusted image
noiseimage=imnoise(freqimage,'Gaussian',0,Var);
noiseimage1=double(noiseimage);

lumnoiseimage1=zeros(X,Z);

for j=1:X
    for k=1:Z
        if noiseimage1(j,k)>8192
        lumnoiseimage1(j,k)=((1*10^-8)*((noiseimage1(j,k))^2))-
(0.0002*(noiseimage1(j,k)))+1.6159;
        elseif noiseimage1(j,k)<=8192
            lumnoiseimage1(j,k) = (3*(10^(-
05)))*noiseimage1(j,k)+0.0266;
        else
            fprintf('ERROR\n')
        end
    end
end

%Calculating the noise added
lumnoisy=zeros(X,Z);
for j=1:X
    for k=1:Z
lumnoisy(j,k)=(lumfreqimage1(j,k)-lumnoiseimage1(j,k));
    end
end

%Calculating actual standard deviation of noise
fullarray = [];

for i = 1:Z
    fullarray = [fullarray;lumnoisy(:,i)];
end

LumDevNoise = std(fullarray,1);
%-------------------------------------------------------------------
%Integration of butterworth filter
function y = Lumfiltercurve(x,Wn, n)
y =1./(1+(x./Wn).^(2*n));

%-------------------------------------------------------------------
```

133

```matlab
%tif2arf
%This script takes 16-bit tiff images and converts them to 12-bit
ARF's.  It
%reads in all tiff files in a driectory and writes them out to a new
%directory with the same filename but different extension.

tifDir = 'F:\Images\';  %Directory containing the tiff files
newDir = 'F:\Thesis\PerceptionExp_08\TIC_PerceptionTest_08\Images\';
%Directory to write the new images to
tifFiles = dir([tifDir '*.tif']);
index = size(tifFiles,1);
for ii=1:index
    filename = tifFiles(ii).name;
    pathname = [tifDir filename];
    outfile = [newDir filename(1:end-4) '.arf'];

    %Read in the tiff image and shift it so that the mean is at 2048
(4096/2)
    tifImg = imread(pathname,'tif');
    tifImg = tifImg(:,:,1);
    sizeImg = size(tifImg);


imagetif=double(tifImg);
[M,N]=size(imagetif);

for j=1:M
    for k=1:N
        if imagetif(j,k)>65520
        imagetif(j,k)=65520;
        end
    end
end

shiftedImage= round(imagetif/16);

%------------------------------------------------------------------
```
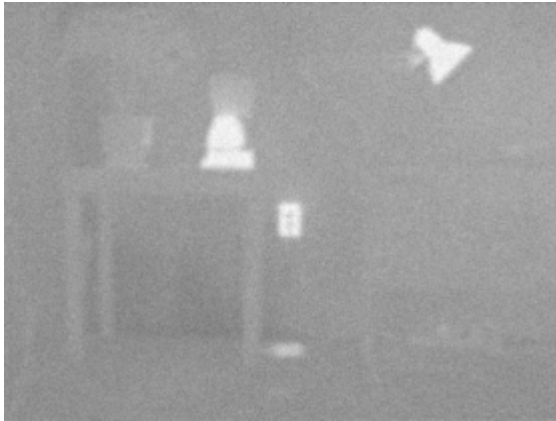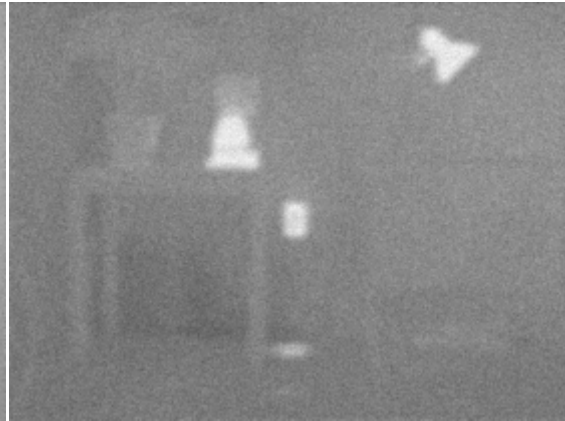
Appendix C Test Subject Background

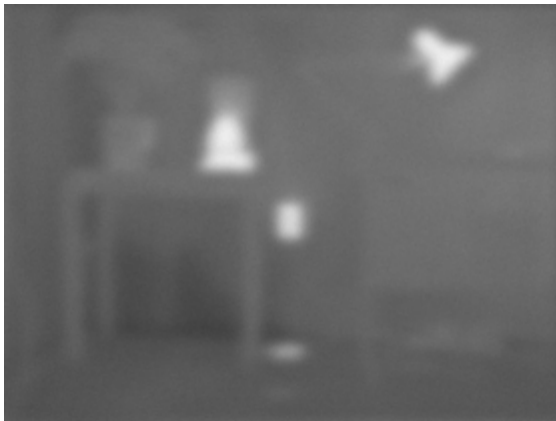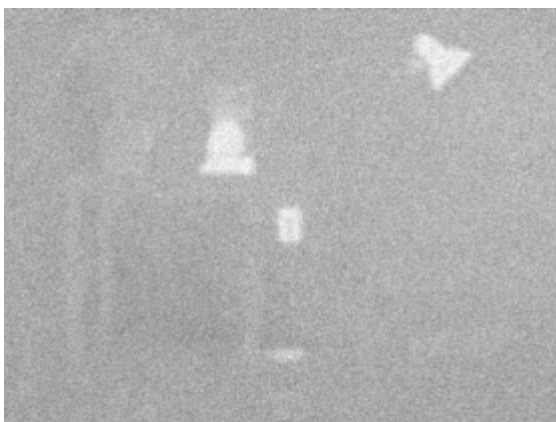| Person	Age	Years using TIC	Eyesight
A	49	8	20/20
B	51	3	20/20
C	21	3	20/20
D	43	18	20/20
E	51	4	20/70
F	24	3.5	20/20
G	41	8	20/20
H	37	9	20/20
I	45	15	20/20
J	44	7	20/30

Appendix D Example of Design Point

Design Point 1

Design Point 2

Design Point 3

Design Point 4

Design Point 5

Design Point 6
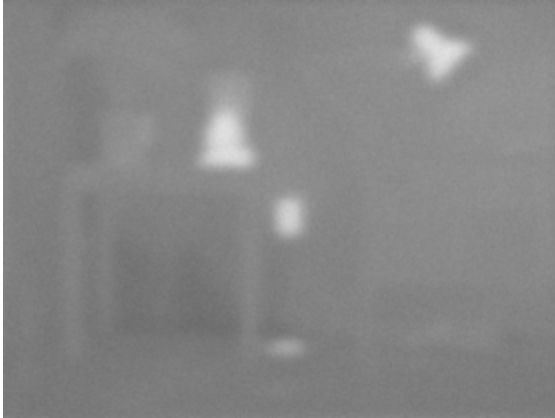
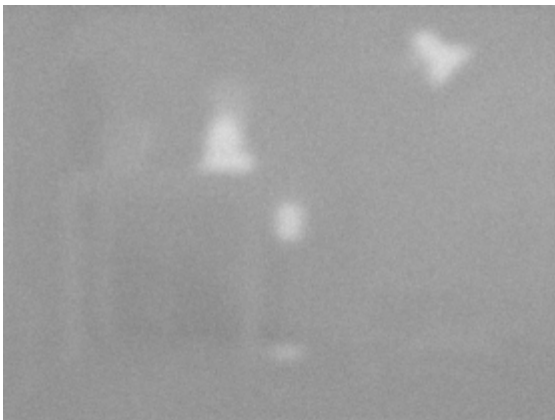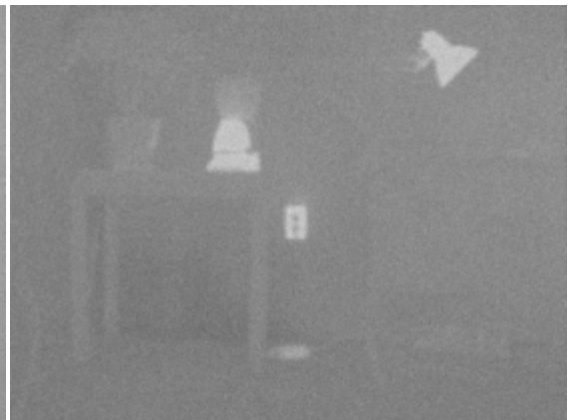Design Point 7

Design Point 8

Design Point 9

Design Point 10
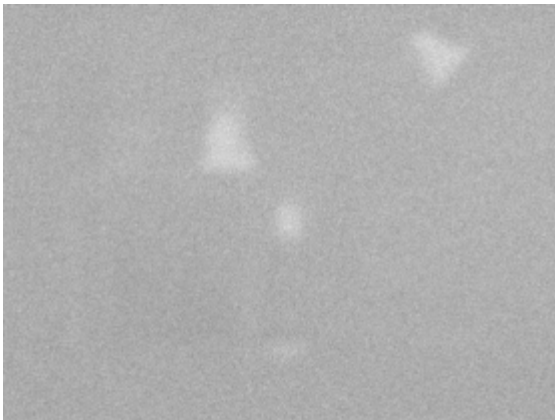

Design Point 11

Design Point 12

Design Point 13

Design Point 14

Design Point 15

Design Point 16

Design Point 17

Design Point 18
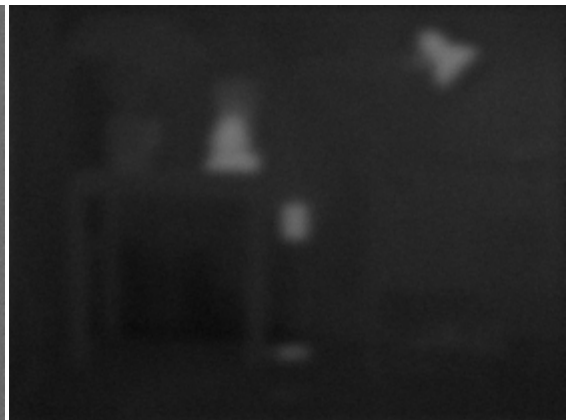
Design Point 19

Design Point 20

Design Point 21

Design Point 22

Design Point 23

Design Point 24

Design Point 25

Bibliography

Agresti, A. (1990). Categorical Data Analysis. New York: John Wiley & Sons.

Amon, F.K.; Bryner, N.P.; Hamins, A., (2005) NIST Special Publication 1040

Amon, F. K.; Bryner, N. P.; Hamins, A. (2005) NIST SP 1040; NIST Special Publication 1040.Thermal Imaging Research Needs for First Responders: Workshop Proceedings. December 9-10, 2004, Gaithersburg, MD, 70 pp, 2005.

Amon, F.K,Bryner, N.P., Hamins, A., Lock, A., (2008) NIST Technical Note 1499

Amon, F.K, Lock, A.; Bryner, N.P.; "Suite of proposed Imaging Performance Metrics and Test Methods for Fire Service Thermal Imaging Cameras."National Institute of Standards and Technology.

Bracewell, R.N. (1989). "*The Fourier Transform*". Scientific American, June 1989

Boreman, G.D. (2001). *Modulation Transfer Function in Optical and ElecroOptical Systems.*, SPIE – The International Society for Optical Engineers, Bellingham, W.A.

Cooley, J.W. and Tukey, J.W. (1965). An Algorithm for the machine calculation of complex Fourier series. Mathematics of Computation.

Dobson, A.J. (1990) An Introduction to Generalize Linear Models, Great Britain: TJ Press Ltd.

Grosshandler, W. L. (1993) "RADCAL: A Narrow-Band Model for Radiation Calculations in a Combustion Environment, NIST Technical Note 1402." National Institute of Standards and Technology.

Holst, G.C. (1998). Testing and Evaluation of Infrared Imaging Systems., SPIE Optical Engineering Press and JCD Publishing, Winter Park, FL.

Holst, G. C. (2000). Common Sense Approach to Thermal Imaging., SPIE Press and JCD Publishing, Winter Park, FL.

Kruse, P.W. (1997). "Principles of Uncooled Infrared Focal Plane Arrays." In: Uncooled Infrared Imaging Arrays and Systems, P.W. Kruse, and D.D. Skatrud, eds., Academic Press, San Diego.

ISO 12233, (2000). "Photography – Electronic still-picture cameras-Resolution measurements," International Standards Organization, Geneva, Switzerland

Lehar, S. An Intuitive Explanation of Fourier Theory

Lloyd, J.M. (1979). "Thermal Imaging Systems." Plenum, New York.

Muralt, P. (2001). "Micromachined infrared detectors based on pyroelectric thin films." *Reports on Progress in Physics*, 64(10), 1339-1388.

Neter, J., Kutner, M., Nachtsheim, C., & Wasserman, W. (1996). Applied Linear Statistics Models, Fourth Edition. Boston: McGraw-Hill

NFPA 1801, (2008). "Proposed NFPA 1801 Standard on Thermal Imagers for the Fire Service, 2009 Edition", *National Fire Protection Association*

Russ, J.C. (2002) The Image Processing Handbook Fourth Edition. CRC Press, Boca Raton, Florida

Sanchez, S.M. (2007) Work Smarter, Not Harder: Guidelines for Designing Simulation Experiments, Operations Research Department and Graduate School of Business & Public Policy Naval Postgraduate School, Montery, CA

Smith, S.W. (2007) The Science and Engineering Guide to Digital Signal Processing, California Technical, California

Theory of Thermography (2007). FLIR Systems User's Manual 249-258

Tsai, C. F., and Young, M. S. (2003). "Pyroelectric infrared sensor-based thermometer for monitoring indoor objects." *Review of Scientific Instruments*, 72(12), 5267-5273

Video Electronics Standards Association Display Metrology Committee (2001). "Flat Panel Display Measurements Standard Version 2.0".

Weeks, A.R. (1996). Fundamentals of Electronic Image Processing., SPIE – The International Society for Optical Engineers, Bellingham, WA.